Development of a lab-on-a-chip to potentially model a driver of colon carcinogenesis

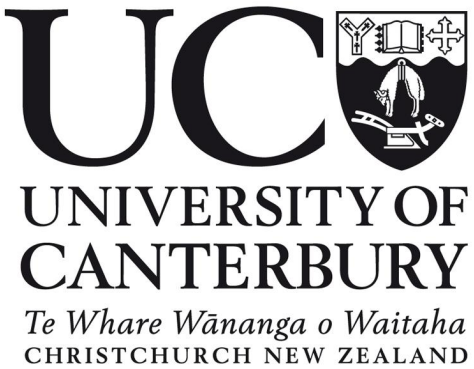

Annabella Faye Thomas

A thesis submitted in partial fulfilment of the degree of Master of Science
At the University of Canterbury, Christchurch, New Zealand
March 2020

Abstract

This thesis describes the design and fabrication of a microfluidic lab-on-a-chip (LOC) device that mimics the lumenal architecture of the human gut and was used to investigate a bacterial toxin as a driver of colon carcinogenesis. A lumen was created inside a hydrogel within a PDMS LOC device using a PDMS rod to enable adherence of human colonic HT29 cells. To enable this, the hydrophobicity / hydrophilicity of three different concentration gelatin and collagen hydrogels was investigated, by measuring the contact angle of water on the hydrogel surfaces. The morphology and metabolism of the HT29 cells was also investigated on the six different hydrogels. A 5% gelatin hydrogel was selected for the formation of lumens inside the LOC devices because it was the most hydrophilic hydrogel surface. HT29 cells formed a confluent monolayer on the hydrogel after 72 hours of incubation. The cells also adhered inside the lumens, but did not form a confluent 2D monolayer, possibly due to the initial seeding concentration being too low. The LOC device provides a template from which future work could focus on the optimisation of cell culture inside the lumen.

Due to the production of a toxin (*Bacteroides fragilis* toxin (BFT)), the carriage of enterotoxigenic *B. fragilis* (ETBF) in the colonic mucosa of humans is associated with an increased risk of colon carcinogenesis. BFT is a metalloprotease, which has been associated with the cleavage of E-cadherin adherens junctions in the intercellular space. Once cleaved, the gut epithelium becomes compromised, increasing the risk of carcinogenesis. To investigate the role of the BFT as a driver of colon carcinogenesis. BFT-treated HT29 cells grown on 5% gelatin hydrogels were exposed to BFT for 12 or 24 hours. These experiments were conducted on cells in fluorodishes and demonstrated the loss of E-cadherin and cell rounding after 12 and 24 hours. In future, these experiments should be carried out on confluent cells lining the lumen of the chip, as the work carried out in this study has provided the basis for this to be executed.

Acknowledgements

I would like to dedicate this thesis to my Grandma, Faye Patricia Glausiuss, who passed away in 2007 from bowel cancer. She has been a driving force behind my research and an inspiration to keep pursuing a career in science.

I would firstly like to thank my supervisors, Associate Professor Ashley Garrill, Associate Professor Jacqui Keenan and Associate Professor Volker Nock, who have given me endless support and guidance throughout this project. I would also like to thank Liz Dunn for her help with cell culture, Azy Hashemi for her help with nano-fabrication and Rebecca Soffe for her help with plasma ashing. I would like to thank my family and partner for their ongoing support throughout my studies. Lastly, I want to say thank you to the great friends I have made in the School of Biological Sciences over the past five years, it has been a great journey.

Table of Contents

List of Figures

List of Tables

Chapter 1

Introduction

1.1 Biological models for cell culture

1.1.1 Two-dimensional biological models

Two-dimensional (2D) cell culture models are traditionally based on the formation and growth of cellular monolayers, which adhere to a flat, horizontal, rigid surface [1, 2]. Cells grown in monolayers can be exposed to the same, or a very similar amount of growth factors and nutrients present in the culture media, which allows them to proliferate over time. Because these models are simple and easy to form, they have been widely used to investigate a variety of cellular behaviours such as differentiation, growth, migration and responses to different stimuli [3, 4, 5].

2D cell cultures have been used in cancer research to study aspects such as the regulation of cell growth and response to chemotherapeutics. There are drawbacks however, to using using 2D cell culture models. Cells grown in monolayers are generally more susceptible to the cytotoxic effect of xenobiotics in comparison to those growing in a 3D micro-environment [6]. With chemotherapeutic drug treatments, more than 80% of drug candidates for cancer treatment fail during the second and third phase clinical trials [7]. 2D cell cultures also lack the micro-environmental architecture and cellular properties that solid tumours exhibit *in vivo*. For example, cellular behaviour and morphology observed in 2D cell cultures may not represent those occurring *in vivo* [8]. To better represent the *in vivo* cellular micro-environment, 2D cell culture models have been modified

with micro-wells, micro-pillars and micro-patterned substrates. These manipulations can consequently help to better study the behaviour and morphology of cells in 2D models, by mimicking micro-structures found *in vivo* [4, 9, 10].

1.1.2 Three-dimensional biological models

In view of the problems with 2D cell culture models, three-dimensional (3D) cell culture models been developed as a more clinically relevant culture method because they can enable the creation of biologically realistic cellular environments. 3D models provide extracellular environments which enable cells to adhere and grow both horizontally and vertically, similar to how cells grow *in vivo* [1]. When cells are isolated from tissues and cultured in 2D models, different cell lines have been found to become progressively flatter, exhibiting aberrant cell division and loss of their differentiated phenotypes [1]. In contrast, when certain cells are cultured in a 3D environment, with appropriate extracellular matrix (ECM) proteins, the cells are able to regain their physiological function and form [3, 11], and in turn, cellular differentiation, proliferation, responses and survival may be more representative of those *in vivo* [1, 3, 12, 13, 14].

Various 3D cell culture methods have been used for research, such as for cancer modelling and drug discovery, and several studies have stated that the use of scaffolds which serve as ECM substrates enable cellular adherence and growth of 3D structures [15, 16, 17, 18]. For example, poly(n-isopropylacrylamide) ($_L$-pNIPAM) hydrogels were used as scaffolds to investigate the development of an *in vitro* 3D culture model of the human intestinal epithelium [18]. HT29-MTX cells cultured on the $_L$-pNIPAM gels exhibited the formation of villus-like structures, with positive expression of goblet cell and enterocyte differentiation markers. These results suggest that $_L$-pNIPAM hydrogels have potential to mimic the 3D structure of the intestinal epithelium, with the possibility for studying intestinal diseases and drug efficacy [18].

Another commonly used 3D cell culture method is the formation of multi-cellular tumour spheroids (MCTS). These can mimic the micro-environment of tissues and thus allow researchers to investigate cancer tumour structure and behaviour [12, 13]. MCTS have been used to investigate the drug efficacy of different colorectal cancer cell lines. For

example, HT29, MCT116 and SW480 colorectal cancer cell lines have been found to have differing sensitivity relative to each other, to the chemotherapeutic drug, 5-Fluorouracil. The drug was also found to have a strong impact on the cohesion of cell in MCTS, in a cell line- and 5-FU dose-dependent manner [19].

Other studies have investigated how the 3D micro-environment and extracellular matrix proteins affect MCTS formation. For example, HT29 colorectal cancer cells have been found to enhance MCTS formation on gelatin and collagen nano-scaffolds, suggesting that cells are more inclined to grow as multicellular spheroids and less subject to disaggregate [13, 19]. Although 3D cell culture models such as MCTS can help to mimic the *in vivo* micro-environment, cultivation is time-consuming and complicated, and it can be difficult to generate spheroids of uniform size [19]. These drawbacks have driven researchers to investigate the use of non-traditional 3D cell culture models, namely, microfluidic devices. These platforms have gained a large interest in the areas of cellular and molecular biology in recent years, due to the low cost and easy manipulation. Section 1.1.3 will discuss this further.

1.1.3 Microfluidic devices for biological applications

Microfluidics is a term used to describe the science and technology of systems which manipulate or process small amounts of fluids using channels. In recent years, microfluidic devices, known as "chips" or "lab-on-a-chip" ("LOC"), have been used for biological applications, such as for cell culture inside devices which can mimic *in vivo* micro-environments. Several models have been designed for various biomedical uses and applications; including drug screening, toxicology testing and drug targeting [20, 21, 22]. Cell culture within some LOC devices have enabled better observation of cancerous cell growth and action [17, 20, 23], however, most of these devices have been limited in understanding complex tumour physiology *in vivo* because of the use of planar 2D monolayer cell structures [21]. To work around such limitations, LOC devices have been designed and fabricated to replicate the 3D structure of organs and tissues [21]. These models have the potential to be used for the investigation of functions and mechanisms of human tissues, as well as the study of disease pathology [21].

Formation of lumenal structures from hydrogels

Hydrogels have been incorporated in LOC devices to create more biologically relevant models for cell culture. Hydrogels are highly hydrated, cross-linked, three-dimensional networks of hydrophilic polymers [24, 25]. Depending on their chemical composition, hydrogels can be responsive to a variety of stimuli, such as pH, light, chemicals and heat [26, 27]. ECM proteins are often used in hydrogels to facilitate cellular encapsulation, embedding and / or adherence *in vivo* [27, 28]. This helps to create cellular environments that are more similar to those found *in vivo* [18, 20, 27, 29, 30].

A commonly used protein in hydrogels is type 1 collagen. The molecule has been seen as an attractive option for hydrogel formation, likely because it is the most abundant protein in humans and plays several roles in the extracellular matrix [31]. Type 1 collagen can interact with other ECM molecules, cell surfaces and growth and differentiation factors, providing tensile strength to support the integrity of several tissues in the body [31]. Gelatin is also commonly used in hydrogel formation because it is a derivative of collagen. It forms when collagen is thermally denatured, yielding smaller peptides from the collagen fibrils [30]. This molecule is generally less expensive than type 1 collagen and other biomaterials, such as matrigel and hyaluronic acid. Gelatin therefore has potential to be used as an alternative biomaterial in LOC devices [32, 33].

Several studies have incorporated hydrogels into LOC devices to form lumenal structures. Artificial lumens have been created out of a collagen hydrogel, by placing a polydimethylsiloxane (PDMS) rod inside a LOC device, followed by injection of the hydrogel [20]. Once the gel solidified, the rod was removed, leaving a lumen inside the device. This model has been used to form artificial blood vessels using Human Umbilical Vein Endothelial Cells (HUVEC) cells [20]. Hydrogels can also be manipulated to form various lumenal structures inside LOC devices [20]. Recently, a 3D LOC device was fabricated to mimic the human colorectal tumour micro-environment *in vitro* [22] (Figure 1.1). HCT116 colorectal cancer cells were suspended in Matrigel and injected into the central device chamber [22]. The device was then used to validate the efficacy of drug-loaded nano-particles in a gradient. This suggests that LOC devices are capable of re-creating micro-environments found *in vivo* and can be used to test the effectiveness of different

therapeutics.

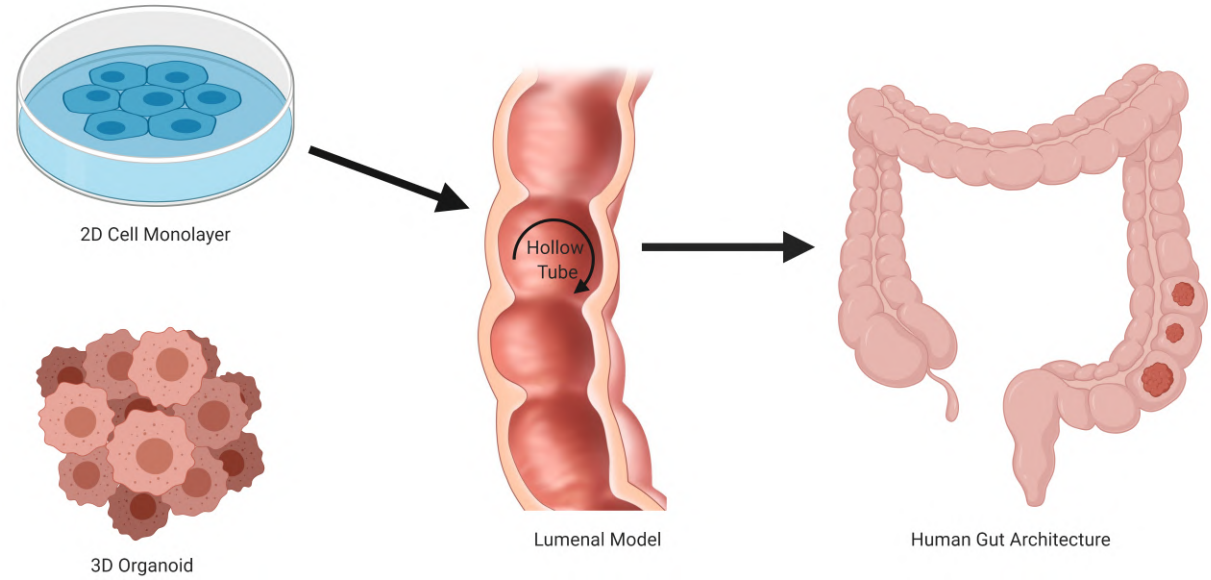

Figure 1.1: **Formation of a 2D cell monolayer inside a lumenal structure to mimic the architecture of the human gut.**

1.2 Perturbance of the normal gut: A potential influencer of colon carcinogenesis

1.2.1 Gut homeostasis

The human gastrointestinal (GI) tract is home to millions of individual bacteria. Host nutrient availability, mucosal surfaces, oxygen exposure, pH, host secretions and interactions with the immune system are thought to govern the formation of dense bacterial networks, which are metabolically active [34]. The composition of the microbiota is a primary factor, which helps to determine the type and robustness of host mucosal immune responses [35]. The *Bacteroides* genus comprises almost half the gastrointestinal faecal flora of humans. Their ability to process complex molecules plays an important role in host nutrition, as the presence of *Bacteroides* species has been found to enhance lipid and carbohydrate absorption by the host [36]. Although dynamic interactions between the host and these residing bacteria can be beneficial for host health [37], it is important to maintain intestinal homeostasis, through separation of the microbiota and immune system, to prevent an immune response to these bacteria in the gut. Several biophysical and

biochemical barriers exist, including the production of antimicrobial compounds, mucus and production of tight junctions between epithelial cells [38].

1.2.2 Cell-cell adhesion

To maintain barrier function, normal cellular architecture and morphology, endothelial and epithelial cells form intercellular adhesions through the homophilic and heterophilic interactions of cell adhesion molecules (CAMs) [39, 40]. These adhesions are crucial for the well being of multicellular organisms, because they maintain stability during tissue regeneration, wound repair and physical movement [39, 41, 42]. The cadherin super family proteins are cell surface glycoproteins that are responsible for calcium (Ca^{2+}) dependent homophilic cell-cell adhesions [42]. Four groups of cadherins exist, these are classical cadherins (further sub-divided into Type-I and Type-II), desmosomal cadherins, protocadherins and unconventional cadherins. All cadherins contain extracellular calcium-binding (EC) repeats, which vary in number depending on the specific type of cadherin [42, 43]. Classical cadherins have a similar structure and topology, with five EC repeats and an intracellular and transmembrane domain. Type-I cadherins, including neuronal (N) and epithelial (E) cadherin, have a conserved EC1 domain with five repeats (Figure 1.2). These mediate homophilic adhesions between cells and play important roles in the GI-tract, as described in Section 1.2.3 [42, 44, 45].

1.2.3 Role of E-cadherin in the gastrointestinal tract

E-cadherin is a 120kDa Type-I classical cadherin encoded by the *CDH1* gene in humans (Figure 1.2). The cytoplasmic domain is bound to β-catenin, which interacts with α-catenin and actin microfilaments, as shown in Figure 1.2 [46, 47]. E-cadherin enables epithelial monolayers to act as protective barriers against extracellular pathogens and chemicals in the GI-tract [46, 48]. Loss of E-cadherin through *CDH1* mutation, or by physical cleavage, can compromise the intestinal epithelial barrier, leading to inflammation, tissue thickening and scarring [49]. These symptoms are commonly observed in colorectal cancer (CRC) formation, contributing to the development of polyps and tumours in epithelial sheets [44, 48, 49, 50].

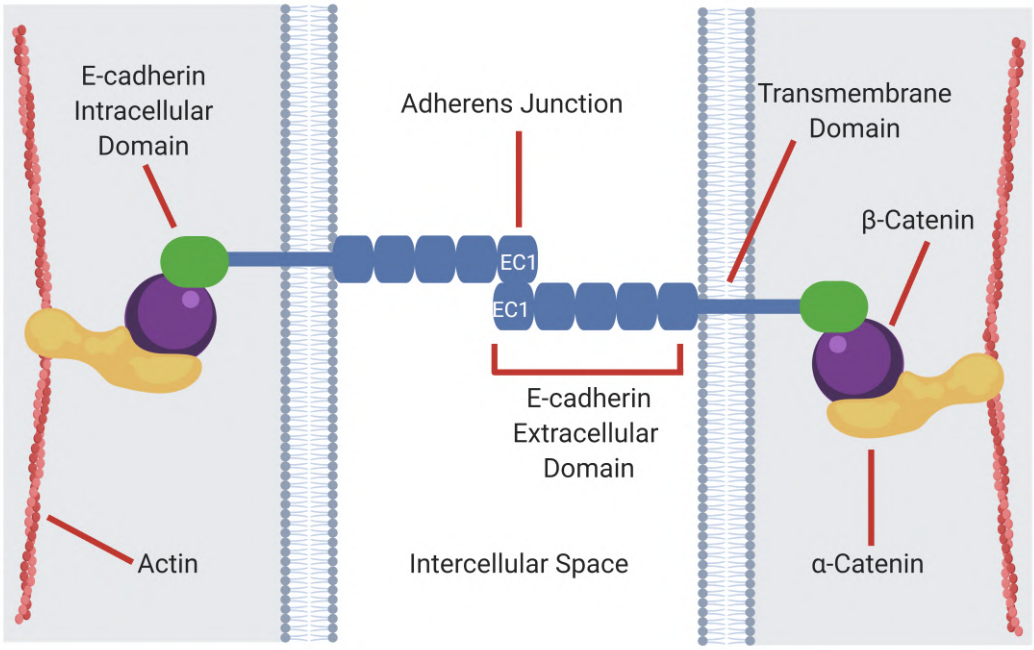

Figure 1.2: **An E-cadherin cell junction between two epithelial cells, showing the conserved EC1 domains in the intercellular space, and the binding of the intracellular domain to β-catenin.**

1.2.4 Colorectal cancer

CRC is the second most commonly diagnosed cancer in New Zealand, and its prevalence is increasing due to change of the population demographic over time [51, 52]. A small fraction of CRC cases arise due to genetic pre-disposition [53]; however, more than 85% of CRC cases are considered to be sporadic. The development of CRC is a multi-step process, by which tumour suppressor genes such as *p53* are inactivated, and oncogenes such as mutated adenomatous polyposis coli (APC), are activated, as described in Figure 1.3. Research has suggested that there are several risk factors for CRC formation, with recent studies proposing a role of human lifestyle, including diet, as potential drivers of DNA damage [54, 55, 56, 57]. Over time, damage can lead to mutations, chronic inflammation and formation of pre-cancerous tumours [58].

Figure 1.3: **The adenoma-carcinoma process, by which cells in a normal epithelium undergo several genetic mutations, leading to cancer formation.**

1.2.5 Microfluidics to model carcinogenic changes *in vitro*

2D cell culture methods and animal models have been used to study cancer formation, progression and therapeutics. These models however, may not accurately represent the tumour physiology and micro-environment in the human body [22]. Consequently, more than 80% of drug therapy candidates have anti-cancer drugs fail during the second and third phase of clinical trials [7]. Because of this, in recent years there has been an increased demand for cell culture methods which enable researchers to study cancer cells in a more biologically realistic environment. As a result, biomimetic LOC devices have been developed in an attempt to represent the micro-environments present in the human body [7, 20, 22]. LOC devices have been fabricated that contain lumenal structures, which can be used to represent the architecture of blood vessels and the GI-tract [20, 21]. These devices can therefore provide researchers with more biologically relevant platforms that have the potential to better represent and understand the complexity of carcinogenesis *in vivo* [59].

1.3 Bacterial drivers of carcinogenesis

1.3.1 Toxigenic bacteria can modulate homeostasis

Numerous studies suggest a role for the intestinal microbiota in the pathogenesis of several inflammatory diseases, such as irritable bowel disease, ulcerative colitis and CRC [60, 61, 50]. Toxins produced by bacterial strains, such as enterotoxigenic *Escherichia coli*, are thought to compromise the intestinal barrier, affect the host immune system and disturb homeostasis in the gut [62]. When homeostasis is compromised, susceptibility to intestinal inflammation and disease can increase [34, 63, 64, 65].

Bacteroides fragilis resides in the guts of most humans. It is usually passed from mother to child during birth, and colonisation by the bacterium usually promotes mucosal health in the GI-tract [66, 67]. Although colonisation by *B. fragilis* usually has a positive effect on its host, some strains are known to be enterotoxigenic. These strains have thus been grouped into a subset of the bacterial species for classification purposes. Enterotoxigenic *B. fragilis* (ETBF) produce a protein, termed *Bacteroides fragilis* toxin

(BFT), which is a 20-kDa extracellular zinc metalloprotease with three known distinct subtypes [68, 69]. It acts as a toxin in the human gut by cleaving E-cadherin cell junctions, activating immune responses that are dependent on T-cells, and compromising the GI epithelium [70, 71]. Consequently, the ETBF subset has been associated with the formation of gut-centred diseases and may play a role in colon carcinogenesis [50, 60, 61].

1.3.2 Role of ETBF in colon carcinogenesis

BFT has been found to reversibly stimulate the secretion of chloride ions and alter the function of cellular tight junctions in polarised epithelial cells of the intestine, as shown in Figure 1.4 [72]. It does not appear to directly cleave E-cadherins, but rather, binds to a specific colonic epithelial cell (CEC) receptor on the epithelial surface (Figure 1.4) [66]. This is thought to trigger the disassembly of adherens junctions and degradation of the E-cadherin proteins [46, 66, 73]. BFT is also able to modulate intracellular signalling of the Wnt signalling pathway. When E-cadherin is cleaved, nuclear signalling by β-catenin is increased, triggering cellular proliferation in the colon (Figure 1.4) [66, 72, 74, 75].

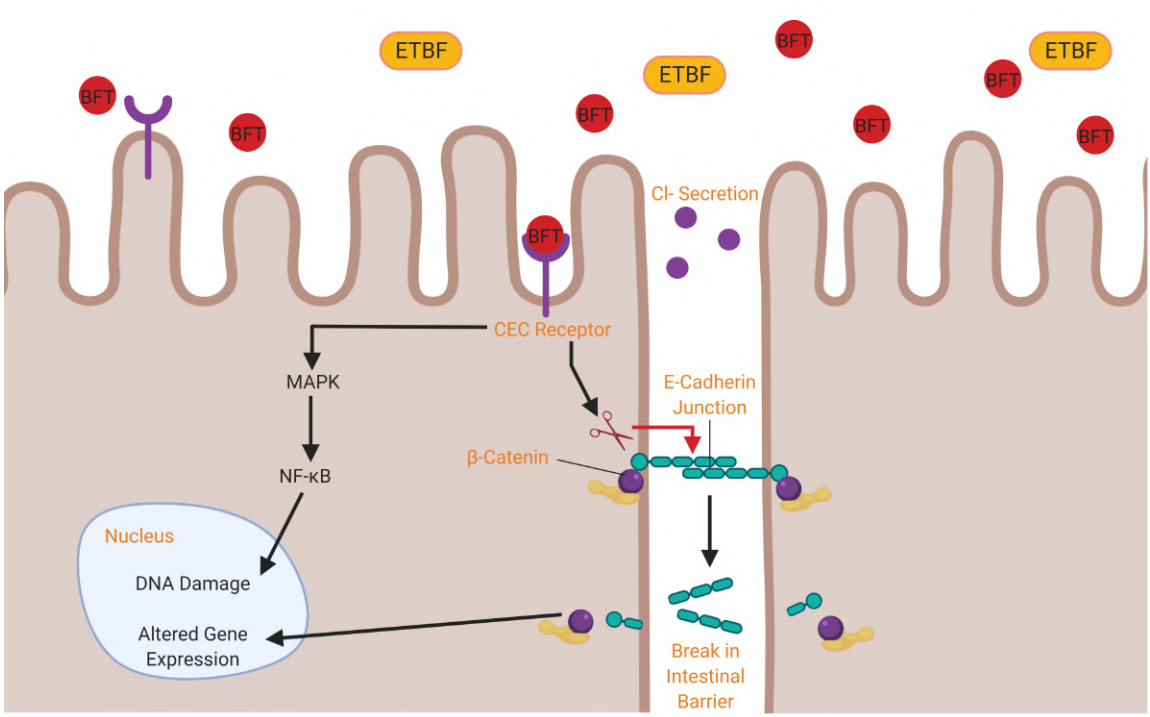

Figure 1.4: **BFT binds to an uncharacterized CEC receptor on the cell surface, triggering intracellular signal transduction, cleavage of E-cadherin, up-regulated Wnt signalling and secretion of inflammatory molecules.** These aspects contribute to ETBF-mediated DNA damage, increased intestinal barrier permeability and increased risk of CRC formation.

Carriage of ETBF is common in people with CRC and is linked to an increased risk of low-grade colonic dysplasia. The *bft* gene has also been found to be over-represented in mucosal biopsies and stool samples obtained from patients with CRC [76, 77, 78]. BFT expression has also been shown to induce prolonged colitis in mice, through the disruption of E-cadherin junctions, activation of β-catenin signalling, and secretion of inflammatory molecules such as interleukin-8 (IL-8) [46, 72].

In one clinical study investigating mucosal colonisation by ETBF and its impact on colon carcinogenesis, bacterial colonies were isolated from samples obtained from patients with colorectal neoplasia and from patients undergoing colonoscopies for CRC screening [71]. Polymerase chain reaction (PCR) was used to test for the presence of the *bft* gene [71]. A trend toward increased BFT positivity in the mucosa from early- versus late-stage CRC patients showed that the *bft* gene was associated with colorectal neoplasia, especially in cases of late-stage CRC [71]. Data also suggested that exposure of the intestinal mucosa to BFT is common in patients with CRC, suggesting that toxin exposure is a risk factor for CRC development [71]. This study supports prior research which found that detection of BFT in human stool samples was significantly higher in hospitalised CRC patients than in samples obtained from outpatient controls [76].

In another clinical study investigating the presence and relative abundance of the *bft* gene in mucosal tissue, samples from four different colonic sites were obtained from 150 patients referred for colonoscopies in New Zealand [73]. ETBF was present in all colonic sites, with an increase in ETBF positivity and abundance on the left site of the GI-tract, including the descending colon and rectum [73]. This is consistent with previous literature which reported ETBF colonisation throughout the entire gut [71, 77]. The increased abundance and positivity of ETBF was associated with early stage carcinogenic lesions in the patients tested, suggesting that ETBF has potential to be used as a marker of early stage colon carcinogenesis [73].

1.3.3 HT29 cell line to investigate colon carcinogenesis

In addition to the clinical studies described in Section 1.3.2, the effect of BFT on cultured cancer cell lines has also been investigated. The HT29 cell line was originally isolated

from a primary colorectal tumour of a 44 year old Caucasian woman [79]. The cells are able to form confluent monolayers, as shown in Figure 1.5, and are characterised by E-cadherin, denoting the formation of adherens junctions between adjoining cells. HT29 cells also have high sensitivity to BFT, which caused cleavage of E-cadherin [80, 81, 50]. The E-cadherin ecto-domain was released and the intracellular fragment was processed via γ-secretase activity, resulting in cell rounding. Evidence has shown that HT29 cells treated with 100 ng / mL (5 nM) of BFT stimulated cell rounding and loss of adherens junctions, in 100% of cells after 45 minutes [72].

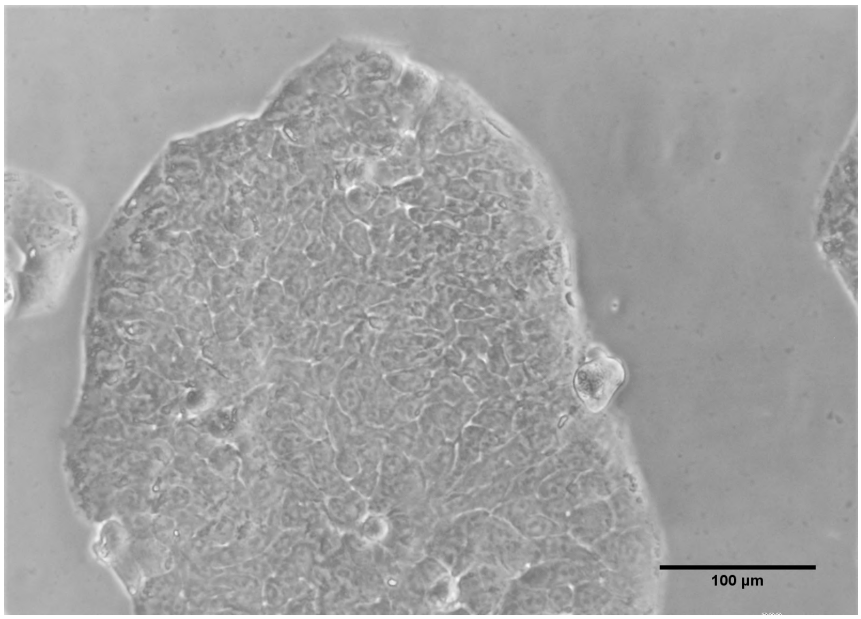

Figure 1.5: **Confluent HT29 colorectal cancer cells growing on polystyrene plastic after 72 hours of incubation at 37°C and 5% CO_2.**

1.3.4 Project aims and objectives

The purpose of this project was to provide a new model, which could potentially be used to investigate colon carcinogenesis and to show that BFT is a potential driver. Several studies have suggested an association between intestinal carriage of ETBF and increased risk of colon carcinogenesis, through the cleavage mechanism of BFT [36, 66, 71, 72]. Highly specific cleavage of E-cadherin cell junctions by BFT has been demonstrated using 2D cell culture models [72]. These models however, have been unlikely to replicate the complex gut micro-environment and architecture *in vivo*. As such, the first objective for this project was to fabricate a lab-on-a-chip device, which mimicked the lumenal architecture of the human gut. The second objective was for HT29 cells to adhere and

grow as a 2D monolayer inside the lumenal walls of the LOC device (Figure 1.1). The last objective of this study was to show that BFT was linked to the cleavage of E-cadherin, which could be detected by a morphological change. In turn, this would suggest that the LOC device could be used as a more biologically relevant model for investigating the effects of BFT on colorectal cells.

Chapter 2

Materials

Table 2.1: Cell Lines

Cell Line or Bacterial	**Description**	**Source**
HT29 (ATCC HTB-38).	Human colorectal adenocarcinoma.	Research Associate Professor Associate Professor Jacqui Keenan, University of Otago, NZ.

Table 2.2: Bacterial Strains

Bacteria	**Strain**	**Source**
Enterotoxigenic *Bacteroides fragilis*	86-5443-2-2	Associate Professor Jacqui Keenan, University of Otago, NZ.
Non-toxigenic *Bacteroides fragilis*	NCTC 9343	Associate Professor Jacqui Keenan, University of Otago, NZ.

Table 2.3: Antibodies and Cell Stains

Antibody or Cell Stain	**Source**
Anti-E-Cadherin antibody [M168] - C-terminal (ab76055), product size = 100 μL.	Abcam, AU.
Goat Anti-Mouse IgG H&L (Alexa Fluor 488) (ab150113), 500 μg.	Abcam, AU.
4,6-Diamidine-2-phenylindole dihydrochloride (DAPI), 10 mg.	Sigma-Aldrich, NZ.

Table 2.4: Buffers, Media and Solutions

Buffer, Media or Solution Name	**Components**
Phosphate Buffer Solution (PBS).	One PBS tablet (Thermo Fisher Scientific, NZ) dissolved in 100 mL DI water, autoclaved.
McCoy's Media.	McCoy's (Modified) 5A Media with L-glutamine and phenol red (Thermo Fisher Scientific, NZ), supplemented with 10% heat-inactivated fetal bovine serum (Thermo Fisher Scientific, NZ) and 1 mL of penicillin-streptomycin per 100 mL of media (10,000 U / mL) (Thermo Fisher Scientific, NZ).
Freezing Media.	900 μL of McCoy's Media and 100 μL of 10% Dimethyl Sulfoxide (DMSO) (Thermo Fisher Scientific, NZ).
Gelatin Hydrogel.	Gelatin from porcine skin Type A (Sigma-Aldrich, NZ) dissolved in 1 x PBS. Cross-linked by transglutaminase enzyme (100 U / g, Anjinomoto, JP) dissolved in 1 x PBS.
Collagen Hydrogel.	Rat tail collagen type 1 (9.04 mg / mL)(InVitro NZ Life Science), 1x PBS and NaOH (0.5 M) (Sigma-Aldrich, NZ).
1% Formaldehyde.	1 mL Formaldehyde solution (37 wt. % in H_2O, Sigma-Aldrich, NZ) and 100 mL of 1x PBS.
AZ326-MIF photo developer, 5 L.	2.38% TetraMethylAmmoniumHydroxide (TMAH) in H_2O (MicroChemicals GmbH, DE).

Propylene glycol monomethyl ether acetate (PGMEA) photo developer, 4 L.	Propylene glycol monomethyl ether acetate (>99.5%) (Sigma-Aldrich, NZ).
Trichloro(1H,1H,2H,2H-perfluorooctyl)silane (10 G).	Trichloro(1H,1H,2H,2H-perfluorooctyl)silane (97%) (Sigma-Aldrich, NZ).
Chrome etchant solution	ceric ammonium nitrate : perchloric acid : H_2O = 10.9% : 4.25% : 84.85% (Sigma-Aldrich, NZ).

Table 2.5: Consumables

Consumable Name	**Source**
Greiner 50 mL 25 cm cell culture flask with filter cap.	Lab Supply Ltd, NZ.
Invitrogen alamarBlue Cell Viability Reagent (100 mL).	Thermo Fisher Scientific, NZ.
Costar 24-Well Cell Culture Plates.	Corning Life Sciences, USA.
Costar 6-Well Cell Culture Plates.	Corning Life Sciences, USA.
Terumo Syringe, Leur Lock (5 mL, 100 units).	MediRay, NZ.
Gelatin from porcine skin (1 Kg).	Sigma-Aldrich, NZ.
Axygen 1.7 mL MaxyClear Snaplock Microcentrifuge Tubes (Polypropylene, Clear, Nonsterile).	Corning Life Sciences, USA.

Axygen 0.6 mL MaxyClear Snaplock Microcentrifuge Tubes (Polypropylene, Clear, Nonsterile).	Corning Life Sciences, USA.
Nunc OmniTray Single-Well Plate (OmniTray Cell Culture Treated, with Lid, Sterile, PS).	Thermo Fisher Scientific, NZ.
Falcon Collagen I (rat tail, 100 mg).	InVitro NZ Life Science.
Tefzel (ETFE) tubing (1 / 16" OD x .040" ID, 1517 XL Tub Tfzl Nat 1 / 16 x.040 x 100 ft)	IDEX Health and Science, USA.
FluoroDish Cell Culture Dish (35 mm, 23 mm well, 100 units).	World Precision Instruments, USA.
Negative-tone dry film resist (SUEX300).	DJ MicroLaminates, USA.
4-inch silicon wafers (prime grade single-side polish).	WaferPro, USA.
Polydimethylsyloxane (PDMS Sylgard 184 silicone elastomer kit).	Electropar, NZ.
TE Series 14-gauge needle (1 / 2", 50 pack).	Techcon, USA.
Terumo blunt 18-gauge needle (1.5", 1.2 x 38 mm, 100 pack).	McFarlane, AU.
Terumo hypodermic 20-gauge needle (1", 0.90 x 25 mm, 100 pack).	Universal Specialities Limited, NZ.
TE series 21-gauge needle (1 / 2", 50 pack).	Techcon, USA.
Tubing tygon (1.6 x 32 mm, 50 ft).	Thermo Fisher Scientific, NZ.
P-733 PEEK shut-off valve.	IDEX Health and Science, USA.

1 / 4-28 flangless fitting nut, Short (XP-218 x Flangeless Fitting for 1 / 16” OD Tubing – 10 pack).	IDEX Health and Science, USA.
XP-200 x flangless blue ferrules (Standard 1 / 16”– 10 pack).	IDEX Health and Science, USA.
P-671 PTFE threaded adapter (0.040” thru-hole).	IDEX Health and Science, USA.
Microfluidic Fittings (1 / 4"-28 Kit to 1 / 16" OD & 3 / 32" ID).	IDEX Health and Science, USA.

Chapter 3

Methods

3.1 Lab-on-a-chip (LOC) fabrication

3.1.1 Mask writing and development

The computer program L-edit (Version 8.03) was used to create three separate designs for the lab-on-a-chip, based on the design by Beebe et al., (2016) [20]. Each of these were etched into three separate glass photomasks (masks). Each file was saved as a *.dxf* file and a laser mask writer (Heidelberg μPG101 mask writer) was used to transfer each design onto three separate masks. The masks came pre-coated with a layer of chrome and a layer of AZ1518 photo-resist. Lithography was carried out in a yellow-lit room to prevent alterations of the features by UV light. The masks were individually loaded into the mask writer, and once aligned correctly, a laser was used to selectively expose the photo-resists to UV light, transferring the uploaded designs onto the masks. Two of the designs were combined and used to produce a wafer that comprised of two layers, forming the base layer of the LOC, as shown in Figures 3.1 and 3.2. The third design was used to create a wafer with a single layer, forming the top layer of the LOC, as shown in Figure 3.3.

Once all three masks were written, they were individually placed in a petri dish containing AZ326-MIF photo developer (MicroChemicals GmbH, DE) for one minute. Following this, the masks were rinsed with DI water and dried with a nitrogen gun; thus removing photo-resist in the areas of the masks which were exposed to UV light. Lastly, each design was observed using a light microscope (Nikon Eclipse Ts2) at 4 x magnifica-

tion (NA 0.10) to make sure the patterns were fully developed. Full development was characterised by the sharpness of the edges of the etched patterns, as shown in Figure 3.4.

To etch the features out of the chrome layers on each of the three masks, chrome etching was carried out. The developed masks were placed one at a time in a tray in an acid fume-hood. Masks were immersed in chrome etchant solution (ceric ammonium nitrate : perchloric acid : H_2O = 10.9% : 4.25% : 84.85%) (Sigma-Aldrich, NZ) and were gently shaken for one minute. Etchant was poured back into the bottle and the masks were washed with DI water and dried with an air gun. Masks were checked under a microscope at 4 x magnification (NA 0.10) to make sure all features had been etched out. Lastly, the masks were washed with acetone, methanol and isopropyl alcohol to strip the remaining photo-resist layers (Fig. 3.4).

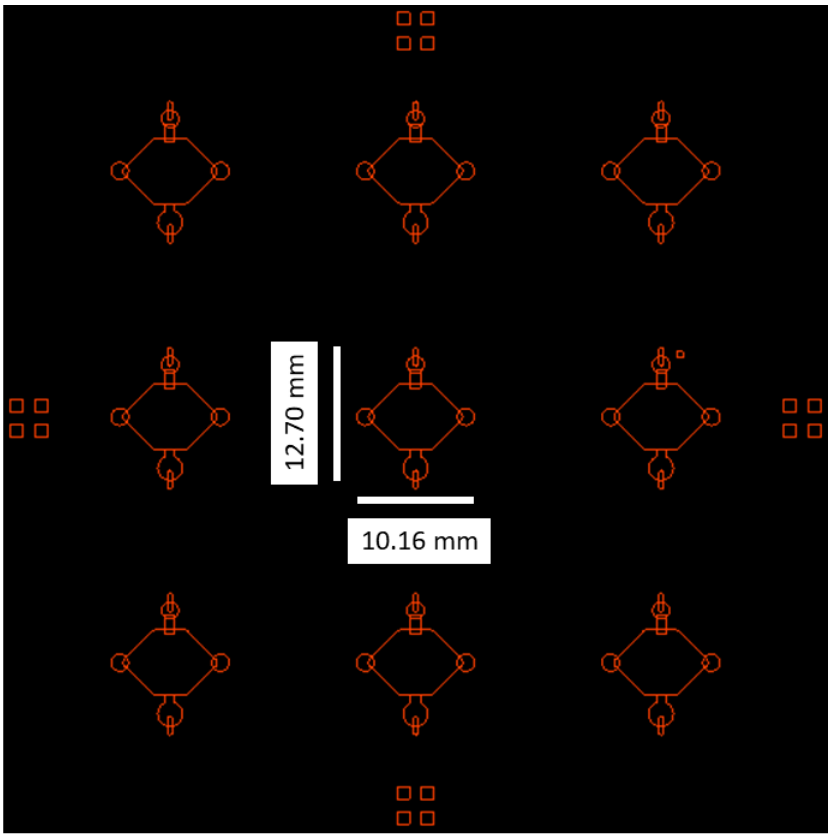

Figure 3.1: **Design of the first layer which was used to form half of the base of each LOC device. The design was physically raised so that a negative imprint would be obtained when moulding the actual devices.**

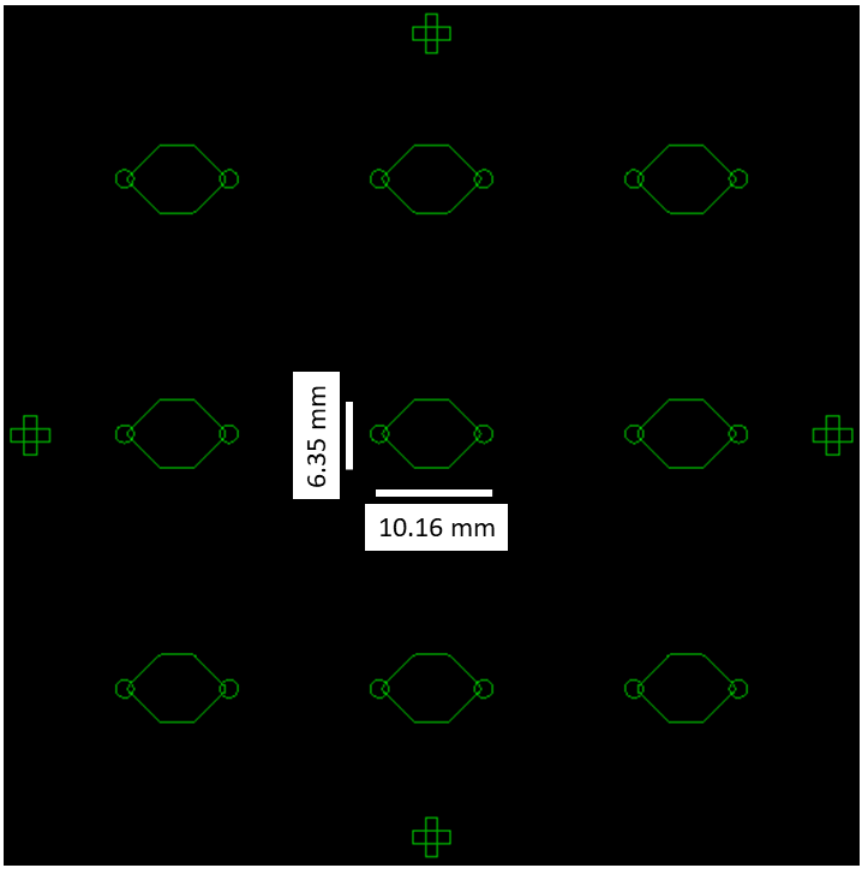

Figure 3.2: **Design of the second layer which was used to form the second half of the base of each LOC device. The design was physically raised so that a negative imprint would be obtained when moulding the actual devices.**

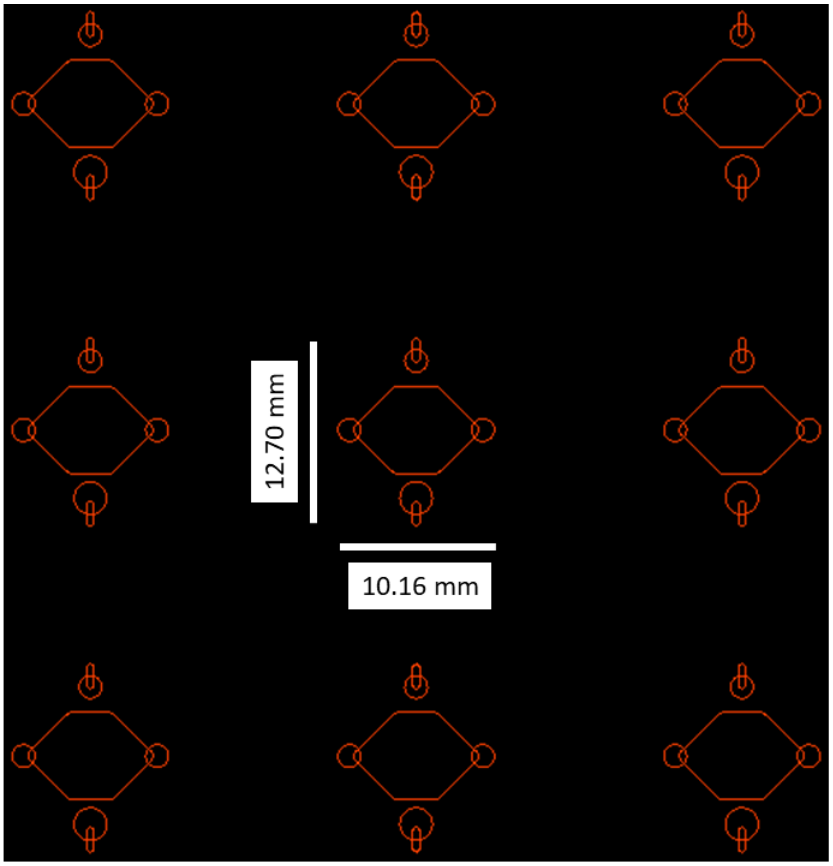

Figure 3.3: **Design of the top layer which was used to form the top part of each LOC device. The design was physically raised so that a negative imprint would be obtained when moulding the actual devices.**

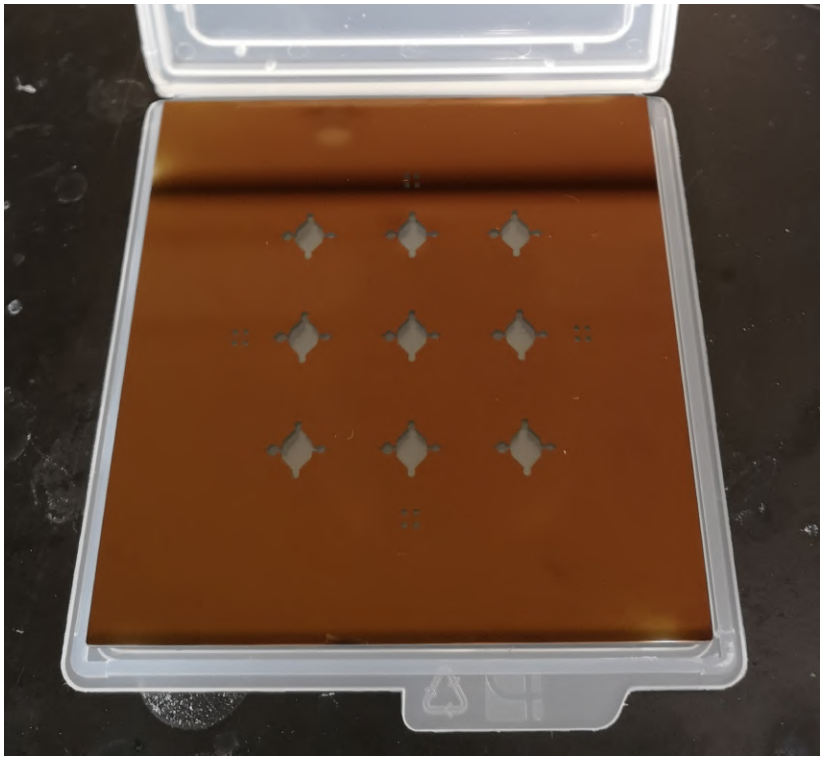

Figure 3.4: **A fully developed photo mask after chrome etching.**

3.1.2 Wafer lamination

A 4-inch silicon wafer (prime grade single-side polish, WaferPro, USA) was removed from a 180°C oven and cooled to room temperature. The wafer was placed in a plasma asher in preparation for plasma cleaning (PIE Scientific Tergeo plasma asher). The pulse ratio was set to 50, oxygen was 5 sccm, power was 100 W and ashing time was one minute. Meanwhile, the photoresist laminator (Sky-335R6) was set to a measured temperature of 65°C. Once the temperature had stabilised, the rollers were switched on. An aluminium sheet with a defined wafer holder was cleaned using methanol. Double-sided tape was attached just above the holder and two transparent polyethylene (PE) sheets were placed on the aluminium sheet, affixing one to the tape. The wafer was placed into the wafer holder by aligning the flat edge of the wafer with the holder, as seen in Figure 3.5. The lower PE sheet was moved so that it was approximately 10 mm below the flat edge of the wafer. A negative-tone dry film resist (SUEX300, DJ MicroLaminates, USA) with a thickness of 300 μm was selected for lamination.

The protective layer of the resist was peeled away to reveal 10mm of the dry film. The

dry film was aligned to the flat edge of the wafer and was gently pressed onto the wafer. Once in place, the protective layer was fully peeled away, allowing the film to rest on the lower PE sheet. The aluminium sheet was placed at the edge of the rollers and carefully fed through the laminator. As the sheet moved in, the lower PE was pulled back so that the dry film came in full contact with the wafer over time. Lastly, the laminated wafer was baked on a hotplate at 65°C for 15 minutes and the film was peeled off the top side of the wafer.

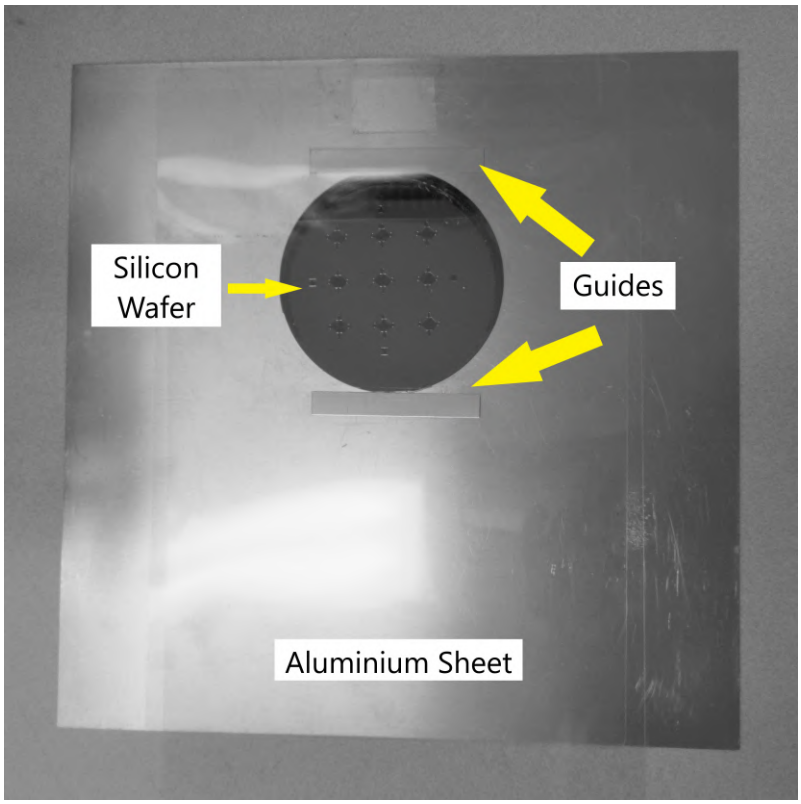

Figure 3.5: **Placement of a wafer in the designated slot of the aluminium sheet.**

3.1.3 Mask alignment

To align the etched masks and laminated wafers for the transfer of the design to the wafers, a mask aligner (Karl Suss MA-6) was used. The mask aligner was switched on and the light source was left to stabilise for 30 minutes. After this, the UV exposure intensity of the light was measured using a UV intensity meter (Suss microtech UV, model 100 with the p365nm sensor). The measured intensity value was 2.6 mW / cm^2. Because the dry film thickness on the wafer was 300 μm, the filtered dose (mJ / cm^2 at 365 nm) was set to 1750 mJ / cm^2 based on the SUEX Epoxy thin film preliminary data sheet (DJ MicroLaminates). To calculate the total time of exposure, the filtered dose was

divided by the measured UV intensity, obtaining a total exposure time of 673 seconds. To minimise thermal stress in the resist, the mask aligner was set to carry out 45 rounds of 15 second exposures, with a one minute rest between each exposure round. The mask with the pattern for the first layer of the base of the LOC device was placed mirror side down on the mask holder. The mask holder was then slotted into the mask aligner slot. Transparent sheets were placed around the mask and the ZJB360 glass filter slide was placed on top (Fig. 3.6). The wafer was placed in the wafer holder in the open drawer (Fig. 3.7). Suction was turned on to prevent the wafer from moving, then the drawer was shut. The mask aligner was run at a filtered dose of $1750\,\mathrm{mJ\,/\,cm^2}$ for 45 rounds of 15 second exposures.

Once the exposure process had finished, the wafer was removed and baked using a hotplate (Torrey). The ramp setting in the hotplate was used, which meant that the hotplate would cool down by the stated temperature every hour, until it had reached the final desired temperature. The first bake was at 65°C for 5 minutes, (ramp 100°C / hr), then at 95°C for 20 minutes (ramp 100°C / hr) and lastly at 20°C for 20 minutes (ramp 15°C / hr). Once baked, the wafer was laminated again using a new SUEX 300μm dry film (Section 3.1.2), and placed on a hotplate at 65°C for 15 minutes. The baked wafer was then placed in the mask aligner drawer. The second mask for the base of the LOC device was placed on the mask holder, then inserted into the mask aligner. The filtered dose for the second layer exposure ($\mathrm{mJ\,/\,cm^2}$ at 365 nm) was $3500\,\mathrm{mJ\,/\,cm^2}$ because the film thickness had doubled since the first exposure. To calculate the total time of exposure, the filtered dose was divided by the measured UV intensity, thus obtaining a total exposure time of 1346 seconds. The aligner again was used to carry out rounds of 15 second exposures, with a one minute rest between each exposure round to reduce thermal stress. Once the existing first layer resist features had been aligned with the new mask, the mask aligner was run at a filtered dose of $3500\,\mathrm{mJ\,/\,cm^2}$ for 90 rounds of 15 second exposures.

Once exposure had finished, the wafer was placed in a mesh holder in a 5-inch Petri dish with the feature side down, as shown in Figure 3.8. PGMEA photo-developer (Sigma-Aldrich, NZ) was poured over the wafer and it was left for one hour to develop both

layers simultaneously. The wafer was then washed with isopropyl alcohol and dried using a nitrogen gun. A final hard-bake was carried out on a hotplate at the following temperatures: 125°C for one hour (ramp 100°C / hr) and then 20°C for 20 minutes (ramp 15°C / hr), which completed the first mould. The lamination process was repeated on a second wafer to form the second mould (Section 3.1.2). For this, the third photomask with the pattern for the top layer of the LOC device was used, as described above. After photo-development and baking, the mould for the top layer of the LOC device was finished.

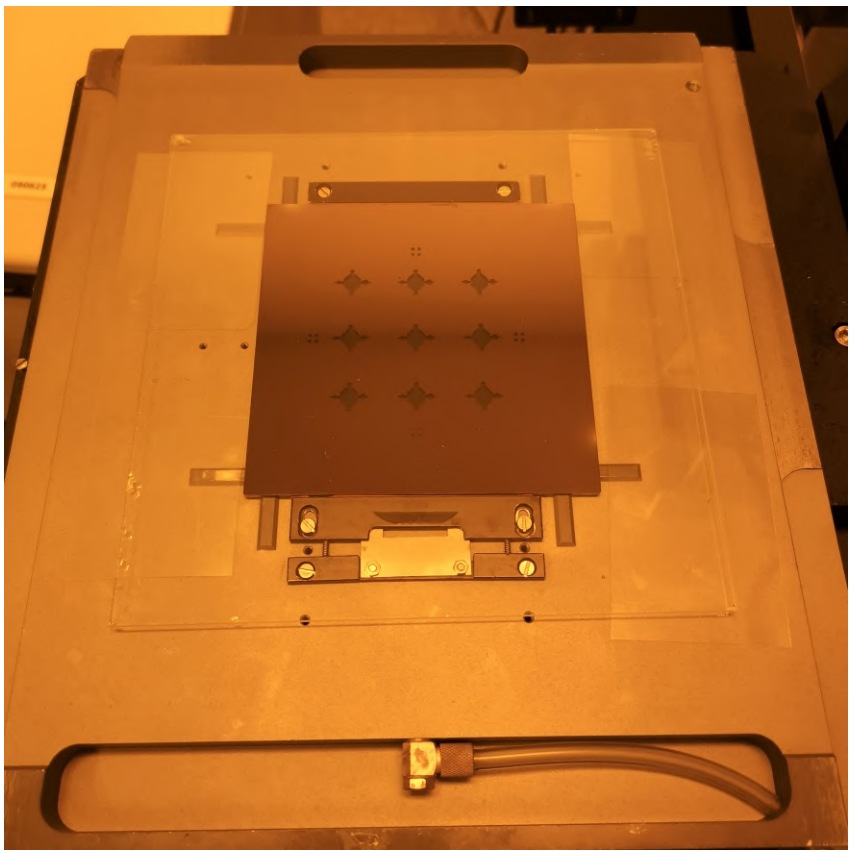

Figure 3.6: **Placement of the mask holder in the mask aligner, followed by placement of the transparent sheets and glass filter slide.**

Figure 3.7: **Placement of a 4-inch silicon wafer on the mask aligner wafer holder of a Suss microtech mask aligner.**

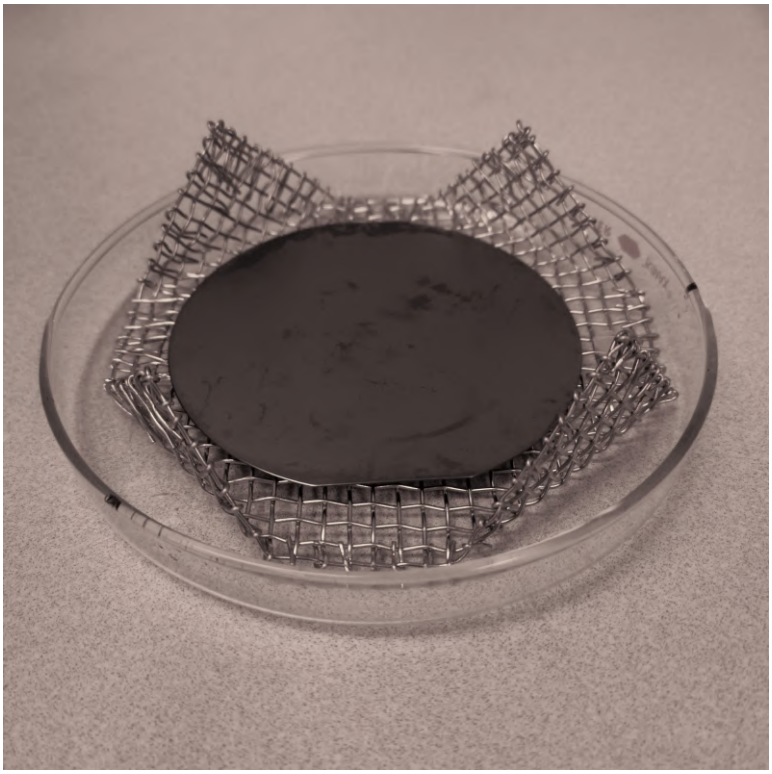

Figure 3.8: **A wafer placed face-down in a mesh holder in a 5-inch petri dish, ready for PGMEA photo-developer to be poured over it. Feature-side down developement aided the removal of un-exposed photoresist.**

3.1.4 Soft lithography

The developed wafer was pre-treated with vapour of trichloro(1H,1H,2H,2H-perfluorooctyl) silane (Sigma-Aldrich, NZ) in a vacuum desiccator. The silane was used as it forms a thin layer on the wafer, allowing easy detachment of PDMS from the photo-resist. A single drop of silane was transferred into a small open bottle, which was then placed in the desiccator, along with the silicon wafer, photo-resist side up. A vacuum pump was applied for 30 minutes to aid silane evaporation. Next, a polydimethylsyloxane (PDMS Sylgard 184 silicone elastomer kit, Electropar, NZ) was used for moulding. PDMS pre-polymer and its curing agent were mixed in a plastic container at a 10 : 1 (w / w) ratio and the mixture was degassed in a vacuum desiccator for one hour to remove air bubbles.

A clean PE sheet was placed on a square shaped flat piece of metal. The wafer was then placed on top, followed by placement of a plastic ring with a diameter 0.5 cm smaller than that of the wafer. Use of a ring smaller than the wafer helped to restrict PDMS to the inside of the ring. Liquid PDMS was poured into the ring onto the wafer, covering the features (Fig. 3.9a). A second PE sheet was placed on top of the ring, as well as a heavy metal lid to prevent leakage of the PDMS in-between the ring and the wafer (Fig. 3.9b). The set-up was placed in a desiccator for one hour to remove any air bubbles formed during casting, and was then placed on a hotplate at 80°C for two hours to cure the PDMS. Once cured, the PDMS was removed from the ring using a scalpel and was gently peeled off the wafer. It was then placed between two PE sheets and baked for another two hours at 80°C to complete cross-linking. This process was carried out for both wafers each time new LOC devices needed to be made. The devices were then cut using a craft guillotine.

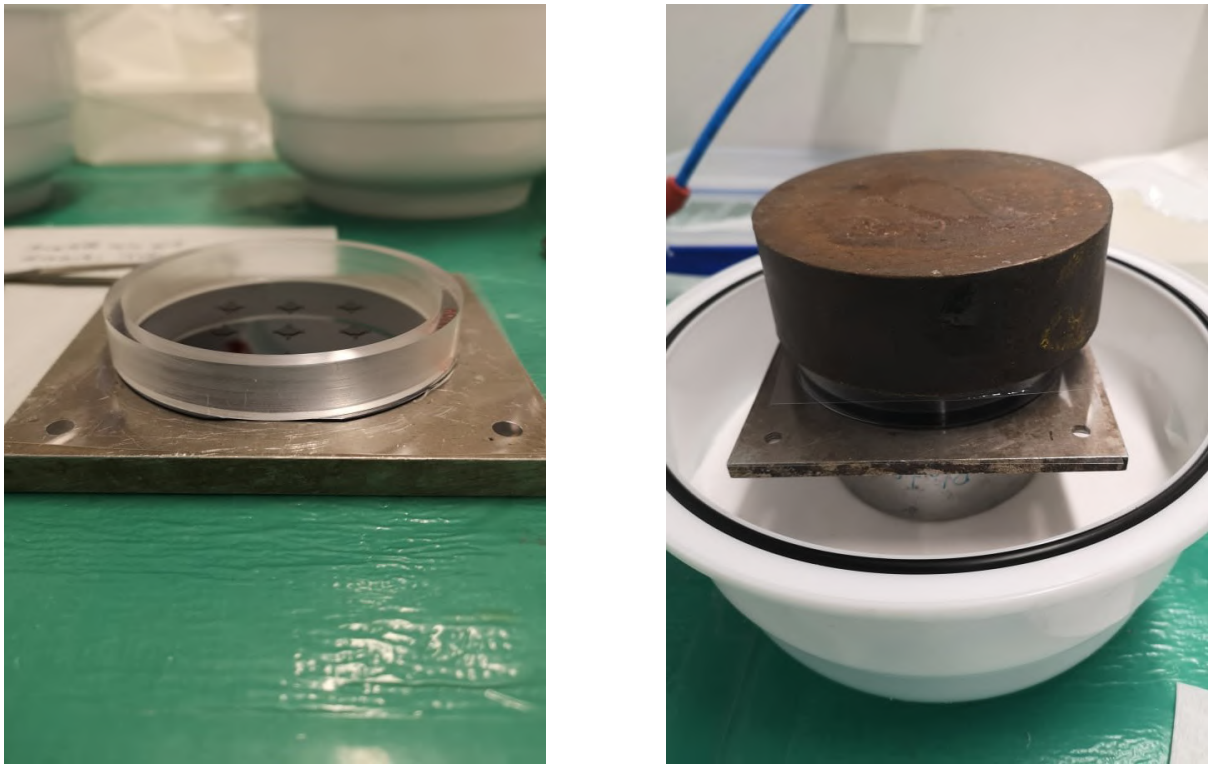

(a) (b)

Figure 3.9: **Liquid PDMS moulding using the patterned wafer.** (a) Placement of a plastic ring on the wafer to prevent liquid PDMS from leaking out between the ring and the wafer. (b) The flat metal plate containing the wafer and ring placed under a weight in the base of a desiccator.

3.1.5 PDMS rod fabrication

To form straight rods for use inside the LOC devices, an 18-gauge flat ended needle was inserted into excess PDMS, as shown in Figure 3.10a. Once removed from the PDMS, a pair of tweezers was used to pull the rod out from inside the needle, as shown in Figure 3.10b. Rods were cut to size to fit across the base layer of the LOC devices.

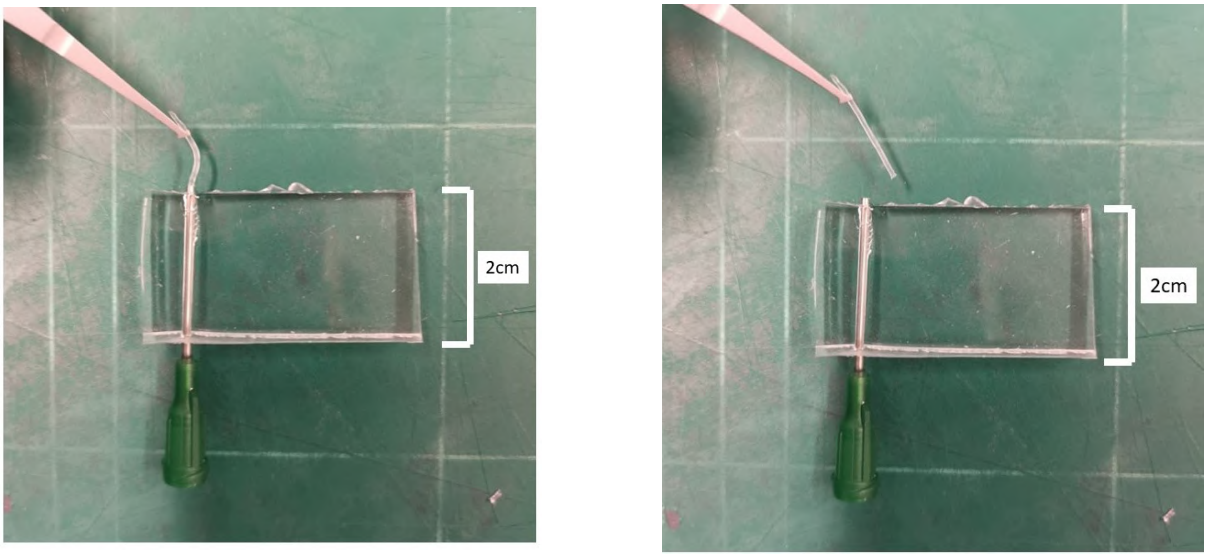

(a) (b)

Figure 3.10: **Formation of PDMS rods for use in LOC devices.** (a) Insertion of an 18-gauge flat-ended needle into cast PDMS. (b) Removal of the PDMS rod from the needle using a pair of tweezers.

3.1.6 Plasma bonding of LOC

To prepare the LOC devices for plasma bonding, 1 mm and 2 mm hole punches were used to create holes either side of each main LOC body, as shown in Figure 3.11. The 1 mm holes were punched vertically and the 2 mm holes were punched at a 45 degree angle to facilitate rod removal. To bond the top and bases of the LOC devices together, they were placed on a piece of PE sheet and put in the plasma asher. The pulse ratio was set to 50, oxygen was set to mixed gas at 7,3 sccm, power was 15 W and the ashing time was one minute. Once treated, the PDMS rods were placed on the base layers, as seen in Figure 3.11, followed by placement of the top layers on the base layers. The inner rods did not bond to the rest of the LOC because they had not been plasma treated prior to LOC bonding. This meant that the surface energy of the base and top of the LOC devices were not the same as the surface energy of the rods, allowing rod removal after bonding. The flat end of a pair of tweezers was then used to press the layers together, ensuring even bonding. The LOC devices were baked on a hotplate at 80°C for two hours to aid bonding.

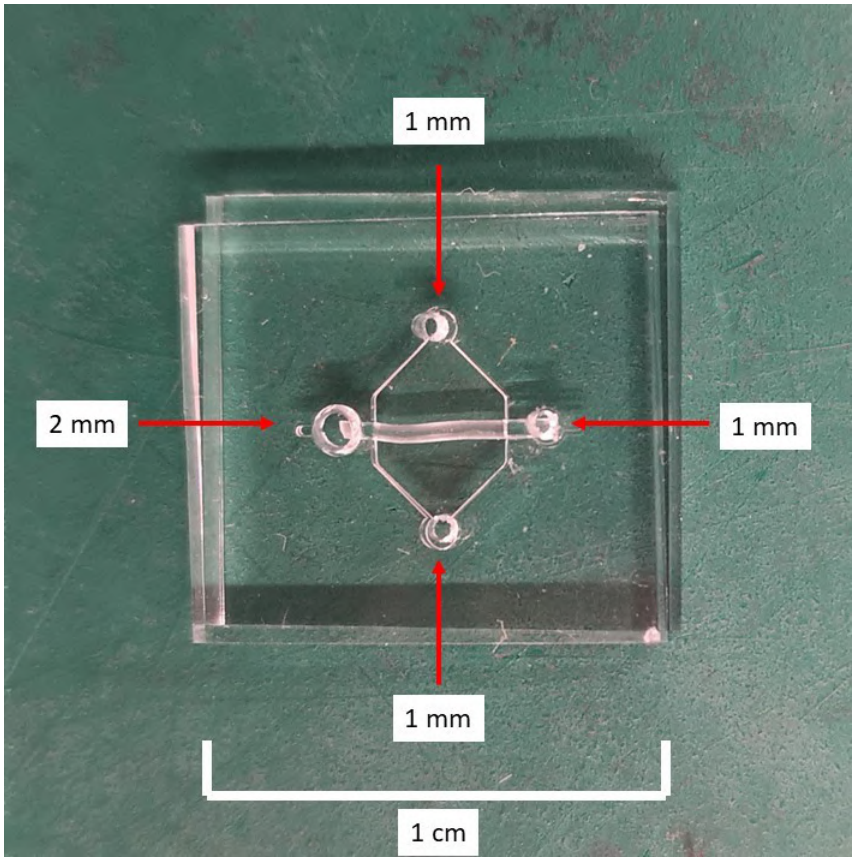

Figure 3.11: **Holes were punched in the top layer of a LOC device using 1.5 mm and 1 mm hole punches. A rod was placed on the base layer, then the top layer was pressed on top, forming a LOC device.**

3.2 Hydrogel formation

3.2.1 Collagen hydrogel formation

To investigate the formation of collagen hydrogels for potential use in the LOC devices, 3%, 5% and 7% concentration collagen hydrogels were made on ice by mixing 80 μL of collagen (10 mg / mL) (In Vitro Technologies, NZ) and 3 μL of 0.5 M NaOH in 0.6 mL Eppendorf tubes. PBS was then added to each solution to adjust the concentrations. Following this, 40 μL of each collagen solution was pipetted into the bottom of nine wells of a 96-well plate (Nunc, ThermoFisher, NZ). The plate was left at room temperature for ten minutes, followed by incubation at 37°C and 5% CO_2 for ten minutes to solidify the gels.

3.2.2 Gelatin hydrogel formation

To investigate the formation of gelatin hydrogels for potential use in the LOC devices, 1%, 2%, 3%, 4%, 5% and 10% concentration gelatin hydrogels were formed. Firstly, the required amount of gelatin powder was added to 100 mL of PBS. The solutions were then heated on a hotplate at 65°C until the gelatin had dissolved. Following this, 0.1 g of transglutaminase (TG) enzyme (100 U / g) (Anjinomoto, JP) was dissolved in 1 mL of PBS and added to the 1% gelatin solution. Next, 0.2 g, 0.3 g, 0.4 g and 0.5 g of TG were dissolved in 2.5 mL of PBS and added to their respective gelatin solutions. Lastly, 1 g of TG enzyme was dissolved in 10 mL of PBS and was added to the 10% gelatin solution. Once mixed, 4 mL of solution from the three containers was transferred to all wells of three PS 6-well culture plates (Fig. 3.12). The plates were placed in an incubator at 37°C for 5 hours and then cooled down to 4°C in a fridge. 1 mL of PBS was then pipetted onto each well to coat the gels. Plates were heated on a hotplate for 30 minutes at 65°C to heat-inactivate the remaining enzyme [82]. Excess PBS was removed from the wells using a Pasteur pipette. Hydrogels were then observed to determine which concentrations formed solid hydrogels suitable for cell culture, as shown in Figure 3.12.

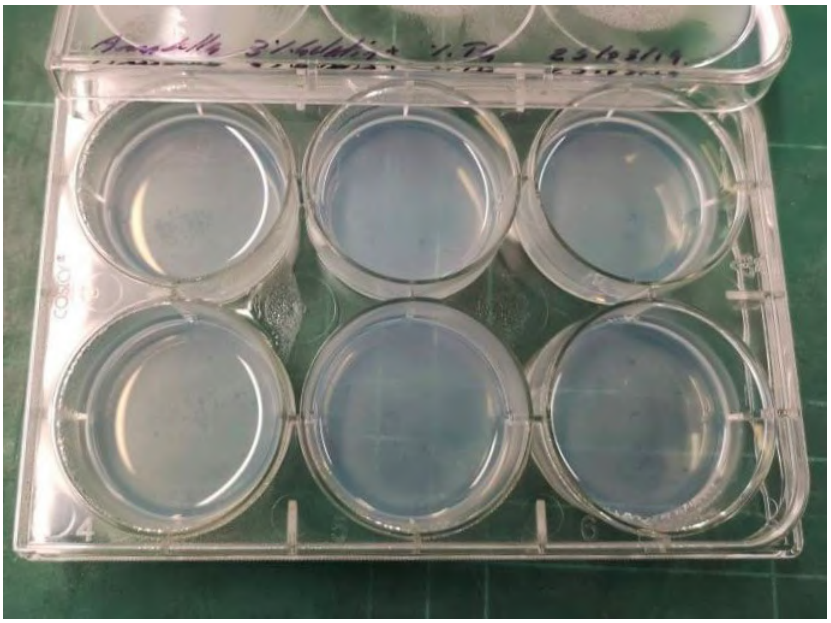

Figure 3.12: **Set 3% concentration gelatin hydrogels in a 6-well cell culture plate after baking, cooling and heat-treatment.**

3.3 Formation of lumens inside LOC devices

To form lumens inside the bonded LOC devices, the devices were placed in a single-welled omnitray (Nunc, ThermoFisher, NZ) and desiccated for one hour to remove oxygen from the PDMS. Meanwhile, 10 mL of 5% gelatin hydrogel was made according to Section 3.2.2. The space inside the LOC devices around the rods were filled with 0.1 mL of hydrogel by inserting a 21-gauge flat-headed needle attached to a 1 mL syringe through one of the 1 mm holes in the top LOC layer. Next, 2 mL of phosphate buffer solution (PBS, Gibco) was pipetted into the omnintray around the LOC devices using a 1 mL pasteur pipette to prevent evaporation of the hydrogels while baking. The devices were incubated for 5 hours at 37°C, and were then cooled at 4°C overnight. A pair of tweezers was used to gently pull the rods out of the devices through the 2 mm holes to form individual lumens within the gels inside the devices, as shown in Figures 3.13 and 3.14. The LOC devices were then sterilised under UV light in a laminar flow cabinet for one hour.

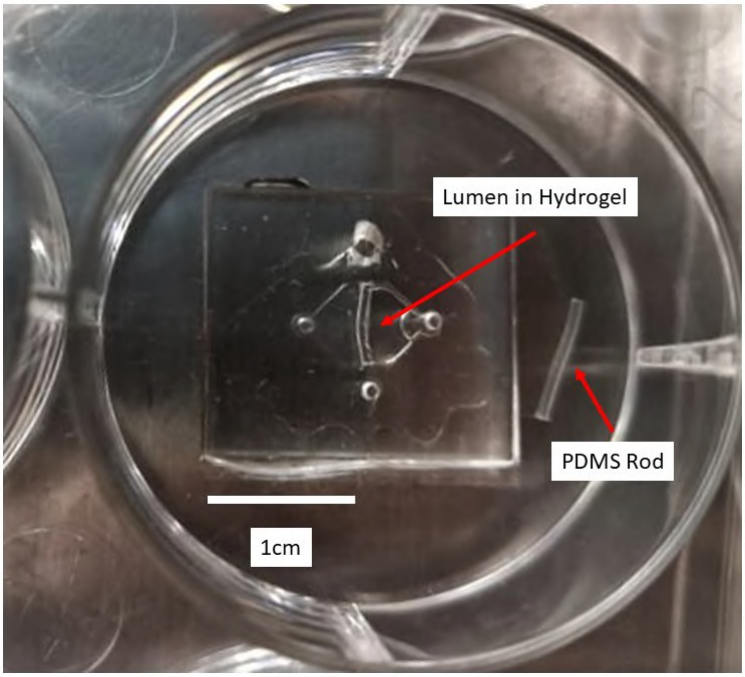

Figure 3.13: **Top view of a lumen formed in a 5% gelatin hydrogel within the LOC. The removed PDMS rod can be seen to the right of the LOC device.**

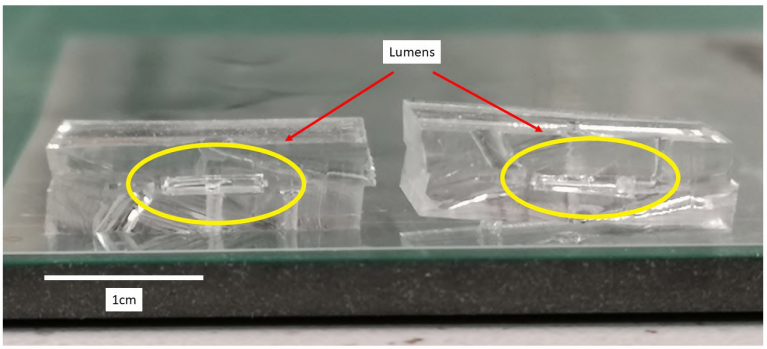

Figure 3.14: **Cross-section of a lumen running horizontally through a 5% gelatin hydrogel within a LOC, as circled in yellow.**

3.4 HT29 cell culture and counting

The HT29 colonic epithelial cell line (ATCC HTB-38) was used to model the human colorectal epithelium *in vitro*. Cells were grown in McCoy's 5A Medium (Gibco, NZ) supplemented with 10% Fetal Bovine Serum (FBS) (Gibco) and 1% Penicillin / Streptomycin (Gibco) at 37°C and 5% CO_2. For maintenance, the cells were grown in 25 mL Greiner flasks (Lab Supply, NZ), with the media replaced every two to three days. To lift the cells, the media was first removed and the cells were washed with 10 mL PBS (Gibco) before the addition of 1 mL of TrypLE Express (Gibco). The flask was incubated at 37°C and 5% CO_2 for ten minutes (to enable the trypsin to lift the adherent cells from the base of the flask). Media (9 ml) was added to the flask to neutralise the TrypLE. To subculture the cells, 1 mL of this cell suspension was transferred to a new flask containing 9 mL of McCoy's media.

To count the cells, 15 μL of cell suspension and was mixed with 15 μL of Trpyan blue dye (0.5% w / v) (Sigma-Aldrich, NZ) to give a 1 : 1 dilution. An aliquot was placed on a haemocytometer and cells were counted in each of the four outer corners using a light microscope (Nikon Eclipse Ts2). These counts were averaged, then multiplied by two (to account for the dilution in trypan blue) and multiplied by 10^4 to give the number of cells per mL in the suspension.

3.5 HT29 cell growth on polystyrene, PDMS and gelatin thin films

PDMS was prepared at a 10 : 1 ratio, by mixing 35 g of PDMS with 3.5 g of PDMS curing agent in a plastic cup, which was then placed in a vacuum desiccator for 30 minutes to remove air bubbles. A 1 mL syringe was used to add 0.4 mL volumes of PDMS to wells of a 24-well polystyrene (PS) well plate (Fig. 3.15 and 3.15). The plates were placed in a vacuum desiccator for 30 minutes, followed by a four hour hard bake on a hot plate at 80°C. To prepare gelatin thin films, 0.23 g of gelatin powder from porcine skin (Sigma-Aldrich, Auckland, NZ) was mixed with 200 mL of PBS and heated at 60°C until the gelatin had dissolved. One mL volumes of gelatin were used to coat untreated (polystyrene) wells, as well as wells that were already coated with PDMS. Both plates were sterilised under UV light in a laminar flow cabinet for one hour. Excess gelatin was removed from the coated plate using a Pasteur pipette, leaving a thin film coating the wells. Plates were sealed with parafilm to maintain sterility until use.

Cells were counted, as described in Section 3.4 and diluted using McCoy's media to a concentration of 5×10^4 per mL. Each experimental replicate consisted of seeding 1 mL of cell suspension in each of three PDMS coated wells and three non-coated PS wells in the first plate (Rows A and B, Columns 1, 2 and 3) (Fig. 3.15). In the second plate, the same volume of cell suspension was added to three wells coated with both PDMS and gelatin, and three gelatin thin coated wells (Rows A and B, Columns 1, 2 and 3) (Fig. 3.16). Both plates were incubated at 37°C for 24, 48 and 72 hours at 5% CO_2. The supernatant in one of the three wells was collected after 24, 48 and 72 hours incubation respectively and non-adherent cells were pelleted by centrifugation (three minutes at 1000 rpm). The supernatant was removed and the cell pellet was re-suspended in 100μL of media before being counted (Section 3.4).

To collect the adherent cells in the corresponding wells, PBS was used to wash the cells before the addition of 500μL of TrypLE express. Following a ten minute incubation at 37°C, 500μL of McCoy's media was added to neutralise the trypsin before the cells were transferred to an Eppendorf tube for counting. This process was carried out twice

more (on different days) in the remaining wells to a total of three experimental replicates. To investigate HT29 cellular morphology, images were taken prior to trypsinisation on the polystyrene, PDMS and gelatin-coated surfaces using a light microscope (Magnification 10x, NA 0.25) (Nikon Eclipse Ts2) after 72 hours of incubation. To identify whether trypsinisation had lifted all of the cells from the gelatin-coated surfaces, images were also taken after trypsinisation.

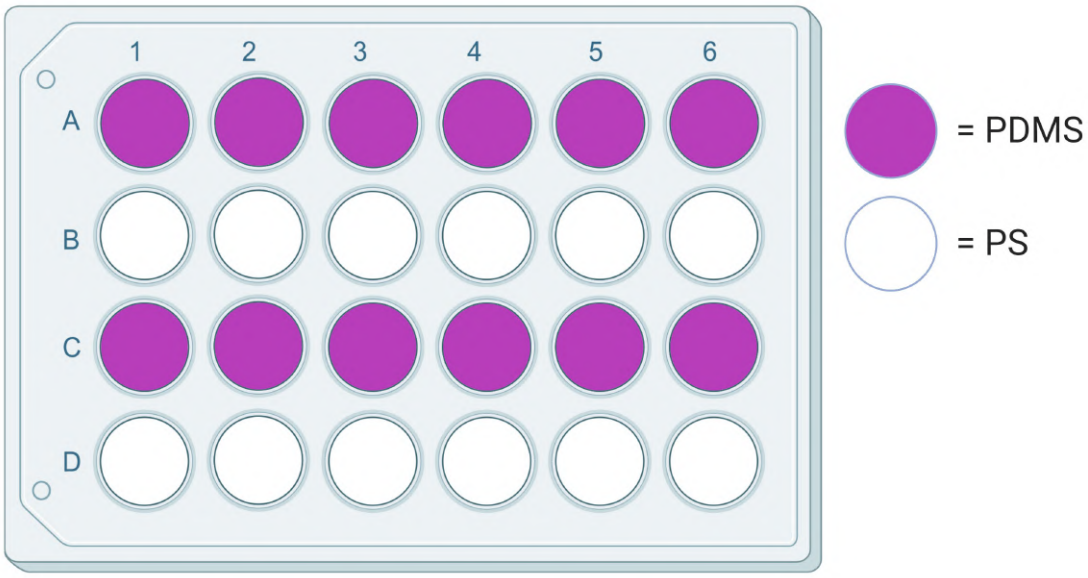

Figure 3.15: **12 wells of a PS 24-well plate were coated with PDMS and the remaining wells were left uncoated.**

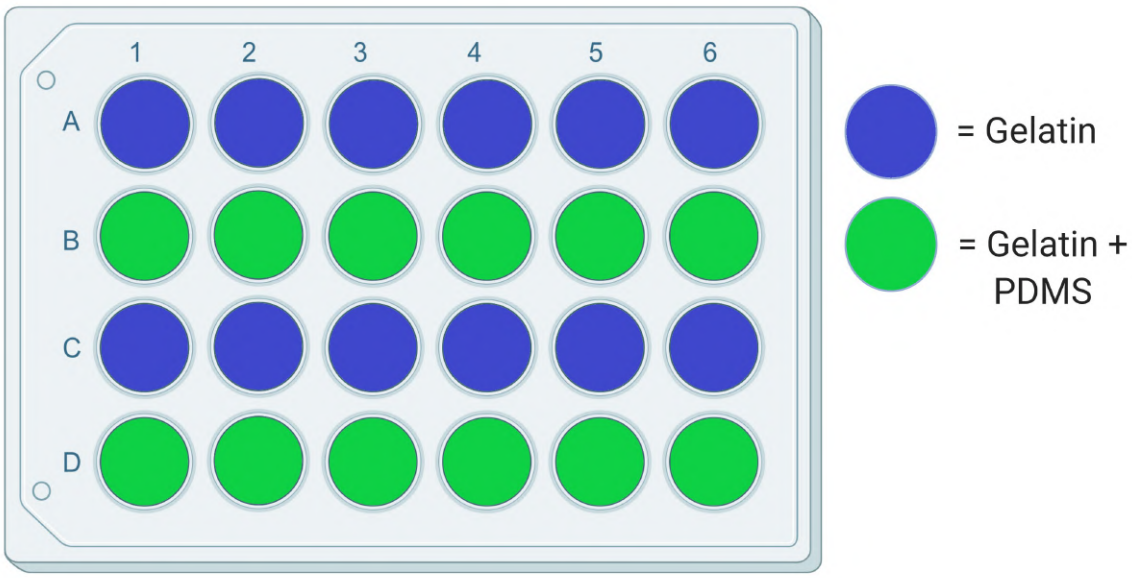

Figure 3.16: **All 24 wells of a PS 24-well plate were coated with PDMS, and 12 wells were then also coated with gelatin thin films.**

3.6 HT29 cell growth on gelatin hydrogels

To measure HT29 cell growth on gelatin hydrogels at 24, 48 and 72 hours, 3%, 5% and 10% gelatin hydrogels were prepared in three PS 24-well plates, as described in Section 3.2.2. Cells were then seeded at $5 \text{x} 10^4$ per mL, as shown in Figure 3.17. The plates were placed in an incubator at 37°C and 5% CO_2 for 24 hours. Images were taken using a light microscope (Magnification 10 x, NA 0.25) (Nikon Eclipse Ts2). The supernatant was removed and cells were collected according to Section 3.5. Adherent cells were trypsinised using TrpyLE. Non-adherent and adherent cells were then counted according to Section 3.4. This process was repeated at 48 and 72 hours of incubation.

3.7 HT29 cell metabolism on collagen and gelatin hydrogels

To identify how metabolically active HT29 cells were on collagen and gelatin hydrogels, the alamarBlue cell viability reagent was used. The active ingredient, resozurin (blue in colour), is converted to highly fluorescent resorufin (red in colour) by the redox power of living cells. The fluorescence can then be measured and is proportional to the number of living cells respiring in a sample. The aim of this experiment in this study was to identify whether there was a significant effect of hydrogel type and concentration on HT29 cell metabolic activity over a 72 hour time period.

To prepare collagen hydrogels for cell seeding and the alamarBlue assay, 3%, 5% and 7% collagen hydrogels were made up according to Section 3.2.1. The collagen recipe ratio was increased to a total of 480 μL of collagen solution per gel concentration. 40 μL of each collagen gel solution was transferred to 12 wells of a 96-well plate and incubated at 37°C and 5% CO_2 (Section 3.2.1). Once the gels had set, 100 μL of McCoy's media was pipetted onto the gels and incubated for 24 hours to allow the gels to equilibrate with the media. The media was then removed and discarded.

To prepare gelatin hydrogels for cell seeding and the alamarBlue assay, 3%, 5% and 10% gelatin hydrogels were prepared in 18 wells of three 24-well plates, as described in

Section 3.2.2 (Fig. 3.17). Next, 1 mL of McCoy's media was pipetted onto the gels for 24 hours to permeate the gel with the media. HT29 cells were seeded in nine of the wells at a density of $5 \text{x} 10^4$ cells per mL. The other gels were not seeded and were instead used as controls to correct for any changes in media colour (Fig. 3.17). Next, nine wells of a second plate were seeded with cells to use as a PS control. The plates were incubated at 37°C and 5% CO_2 for 20 hours.

Because the different gel concentrations could potentially alter the media colour, 200 μL of media was transferred from the three 20 hour replicate wells of the 3%, 5%, 10% plates and control gels to a 96-well plate to take into account the effect of the media on the fluorescence reading. A further 600 μL was removed from the wells and discarded, leaving 200μL in the wells. Following this, 20 μL of alamarBlue reagent (Invitrogen, USA) was added to the wells. It was used as an indicator of metabolic function and cellular health. Plates were incubated for four hours at 37°C and 5% CO_2. Lastly, 200 μL were transferred from the plates to the 96-well plate. The plate reader (Molecular Devices SpectraMax M5) was set to read fluorescence at 530 nm excitation and 590 nm emission and the plate was read. This process was repeated at 48 and 72 hours of incubation.

HT29 cells were seeded at $5 \text{x} 10^4$ per 200 μL in nine wells containing gel in each plate. Nine wells without gel were also seeded to use as polystyrene controls. Lastly, 200 μL of McCoy's media was pipetted onto three wells of each gel concentration, as well as three wells of plain PS. After 20 hours incubation, 20 μL of alamarBlue cell viability reagent was added to the first three wells of each gel concentration, the PS control and the wells with plain media. The plate was incubated for four hours and then 200 μL of media was transferred from the wells to a new 96-well plate. The fluorescence of the new plate was read at 37°C using the plate reader, at 530 nm excitation and 590 nm emission. The above process was repeated at 40 and 60 hours, with the plate being read at 48 and 64 hours of incubation.

To statistically analyse the fluorescent reading data, the data was log transformed using the equation Y = Log2(Y); therefore, increasing the distance between small values and decreasing the distance between large values in the dataset. A two-way repeated

measure analysis of variance (2-way RM ANOVA) was carried out on the transformed data. This determined whether there was a significant difference between the mean cellular metabolism of HT29 cells on different concentration gelatin and collagen hydrogels over a 72 hour time period. Cellular metabolism was based on the relative fluorescent units (RFUs) obtained during experimentation. Lastly, a Tukey's multiple comparison test was carried out to determine whether there were any significant differences between the mean cellular metabolism of HT29 cells on specific collagen and gelatin hydrogels.

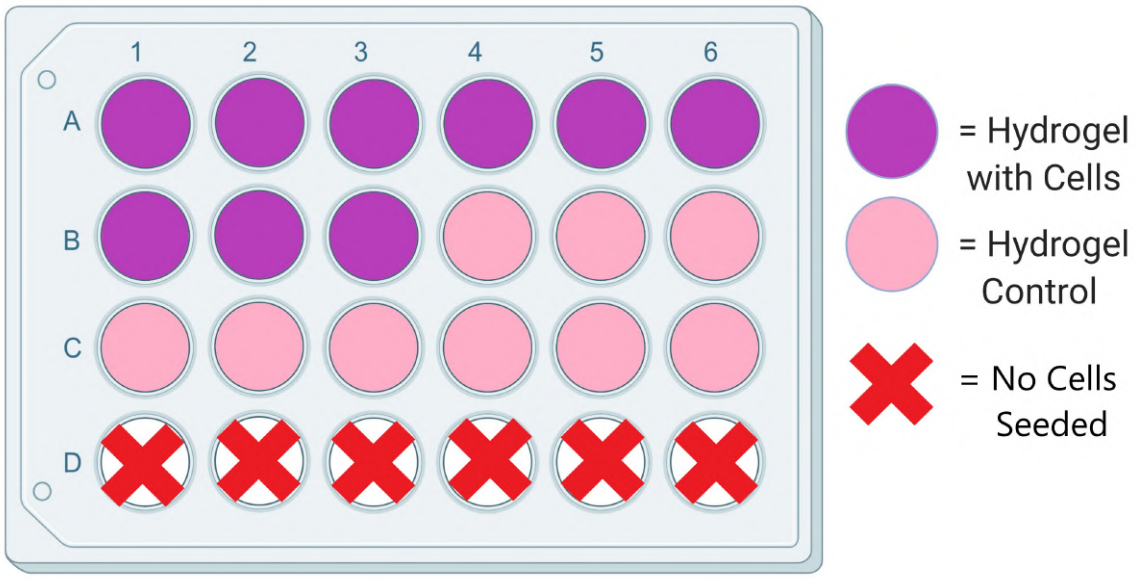

Figure 3.17: **Set up of hydrogels and cells in a PS 24-well plate.**

3.8 HT29 cellular morphology on collagen and gelatin hydrogels

To investigate cellular morphology of HT29 cells on the hydrogels, 3%, 5% and 7% collagen hydrogels were prepared according to Section 3.2.1. Next, 3%, 5% and 10% gelatin hydrogels were prepared and sterilised under UV, according to Section 3.2.2. Following this, 3 mL of each gel was transferred using a 5 mL syringe and 21-gauge needle into three 35 mm by 23 mm fluorodishes (World Precision Instruments, USA), to a total of 18 separate dishes. The gels were carefully spread across the glass dish surfaces using the slanted needle head. Cells were then sub-cultured according to Section 3.4 and were seeded at $5 \text{x} 10^4$ cell per mL into three dishes with gels and one PS dish as a control. Dishes were incubated at 37°C and 5% CO_2 for 24 hours. Cell morphology was then vi-

sualised without any cell stains using the phase contrast setting of a confocal microscope (Leica TCS SP5) at 24 and 72 hours of incubation. The 20 x dry lens (NA 0.50), 40 x dry lens (NA 0.75) and 63 x oil immersion lens (NA 1.40) were used.

3.9 Contact angle of water on hydrogels

The contact angle (CA) (denoted θ) is the angle between a solid surface and a liquid-vapour interface, and describes the wettability of the solid surface [83]. Measurements of CA are achieved through the application of a liquid, most often water, to a surface. At a specific pressure and temperature, a given solid surface has a unique CA. In this thesis, CA was used as a measure of the level of hydrophobicity or hydrophilicity of collagen and gelatin and hydrogels. This was used to determine which gel would be most appropriate as a cell substrate. Studies have suggested that polymers with a water CA between 45° and 75° show optimal cellular adherence [83].

3.9.1 Contact angle of water on collagen hydrogels

PDMS was made, as described in Section 3.1.4 and was poured into an Omnitray. Once cured, the PDMS was cut into 2 x 2 cm squares using a guillotine. Following this, 3%, 5% and 7% collagen gels were made, as described in Section 3.2.1. Next, 2 x 2 cm PDMS squares were treated in the plasma asher to reduce the surface hydrophobicity. The pulse ratio was set to 50, oxygen was supplied at 5 sccm, power was 255 W and ashing time was one minute. Once treated, 200 μL of each gel concentration was pipetted on top of each PDMS square and spread out using the pipette tip to form an even layer. Squares were left at room temperature for ten minutes, followed by a ten minute incubation period in an incubator at 37°C and 5% CO_2.

A telescopegoniometer (CAM 2008, KSV) was used to measure the water CA of the hydrogels. It was calibrated using a 4 mm metal ball, followed by the placement of a PDMS square on the telescopegoniometer stage. All measurements were made using the static, sessile drop mode. The frame interval was set to three seconds and the number of frames was set to 30 frames. A small droplet of DI-water was dropped onto the hydrogel surface and the tangent of the sessile drop profile was aligned using a camera and the

CAM 2008 software package. The CA was measured by geometrically measuring the angle between the water droplet and the surface of the hydrogel on both sides of the droplet. The CA was measured for all three collagen hydrogels by measuring the CA of three separate gel disks three times each.

3.9.2 Contact angle of water on gelatin hydrogels

To measure the CA of gelatin hydrogels, 3%, 5% and 10% gelatin hydrogels were prepared in 85 x 128 mm cell culture omnitrays, as described in Section 3.2.2. A 14 mm metal holepunch was used to cut disks in the gels. The telescopegoniometer was calibrated using a 4 mm metal ball, followed by the placement of a gelatin disk on a glass slide, which was then placed on the telescopegoniometer stage (Fig. 3.18). Measurements were taken, as described above, and the tangent of the sessile drop profile was aligned using a camera and the CAM 2008 software package (Fig. 3.19). The CA was measured for all three gelatin hydrogels by measuring the CA of three separate gel disks three times each. While each gel was expected to have a unique CA, data was collated to check whether CA measurements converged to a specific angle range for each gel. The same measurement process was also used to find out the CA of water on the PDMS control.

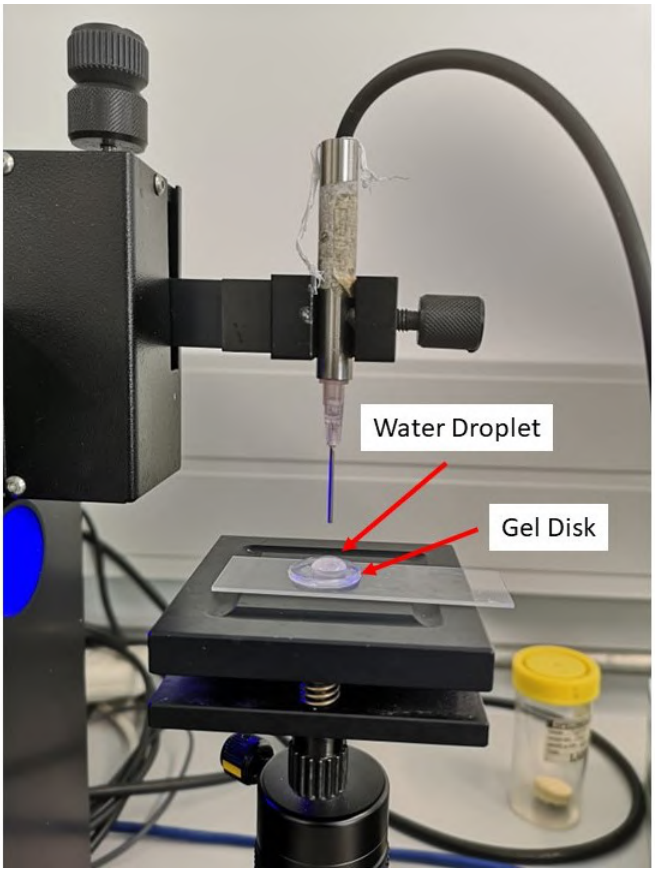

Figure 3.18: **Contact angle measurement set up, with the placement of the needle directly above the centre of a gel disk.**

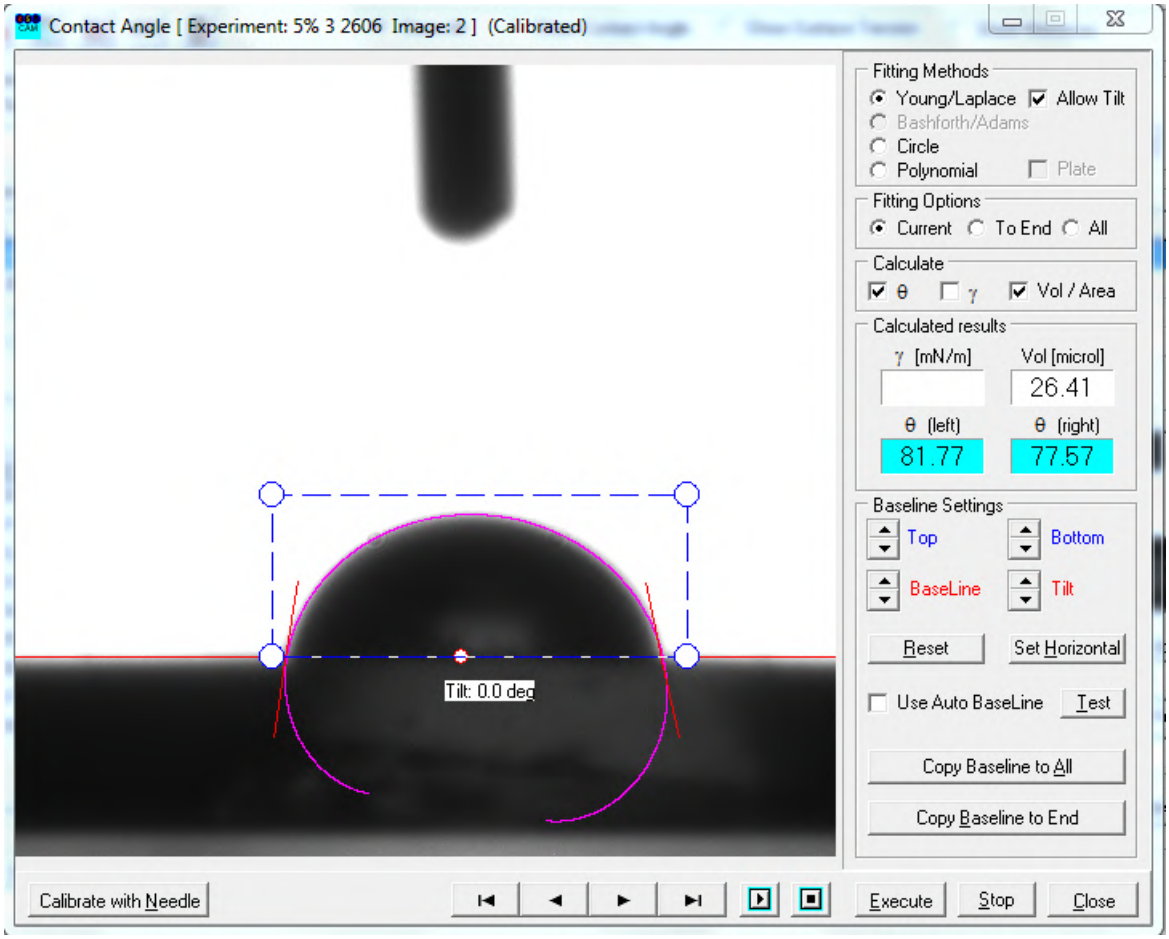

Figure 3.19: **Measurement of the contact angle of water on a 10% gelatin hydrogel, using CAM2008 software. The left CA (θ_L) was 81.77° and right measured CA (θ_R) was 77.57°, as denoted in the right panel in blue.**

3.10 Seeding HT29 cells in LOC devices

HT29 cells were counted, as described in Section 3.4, and diluted to a concentration of $5 \text{x} 10^4$ per mL. Next, sterilised LOC devices were placed in a plastic container, and 5 μL of the diluted cell suspension was seeded into each lumen of each device (250 cells total in 5 μL media) and immediately incubated at 37°C for 25 minutes. The LOC devices were then flipped upside down to achieve a uniform coating of cell in the lumens. Flipping was repeated twice for each side.

3.11 Pump system for media flow through LOC devices

To set up the pump system that was used to provide fresh, supplemented media to cells growing inside a LOC device, a small lathe with a circular saw attachment was

used to cut the plastic Luer-locks off a blunt-ended 14-gauge needle (inner diameter = 1.6 mm) (Techcon, USA) and a blunt-ended 18-gauge needle (inner diameter = 0.838 mm) (Terumo, Mcfarlane, AU), leaving the straight cut metal components. Next, a 1 mL syringe was placed in the holder of a syringe pump (NE-4000 Two Channel Syringe Pump Multi-Phaser). A threaded adapter (0.040-inch) (IDEX Health and Science, USA) was used to attach 15 cm of Tefzel tubing (Kinesis, AU) to the syringe. The end of the tubing was attached to a flangless fitting nut (IDEX Health and Science, USA) with a blue ferrule (1 / 16-inch) (IDEX Health and Science, USA) and was twisted into a shut off valve (IDEX Health and Science, USA), as shown in Figure 3.20.

On the other side of the shut off valve, another fitting nut with blue ferrule was attached to a new 10 cm piece of Tefzel tubing, which was run from the other end of the shut off valve into a 3 cm piece of thicker flexible tubing (Tygon, Thermo Fisher, NZ) (Fig. 3.20). This tubing was used as a sleeve to hold the 14-gauge needle in one end of the LOC device through the 2 mm hole that had been made with the holepunch, as shown in Figure 3.20. On the other side of the device, the 18-gauge needle was held in the 1 mm hole using the same sleeve set up. Another shut off valve was attached to a fitting nut and blue ferrule, with a 10 cm piece of Tefzel tubing. The tubing ran into a fourth fitting nut and blue ferrule, which was twisted in to a threaded adapter (0.040-inch) (IDEX Health and Science, USA). The adapter was then attached to a microfluidic Eppendorf reservoir (Elveflow, Darwin Microfluidics, FR) and the tubing was run into the bottom of the 1.5 mL Eppendorf containing supplemented McCoy's media (Fig. 3.20).

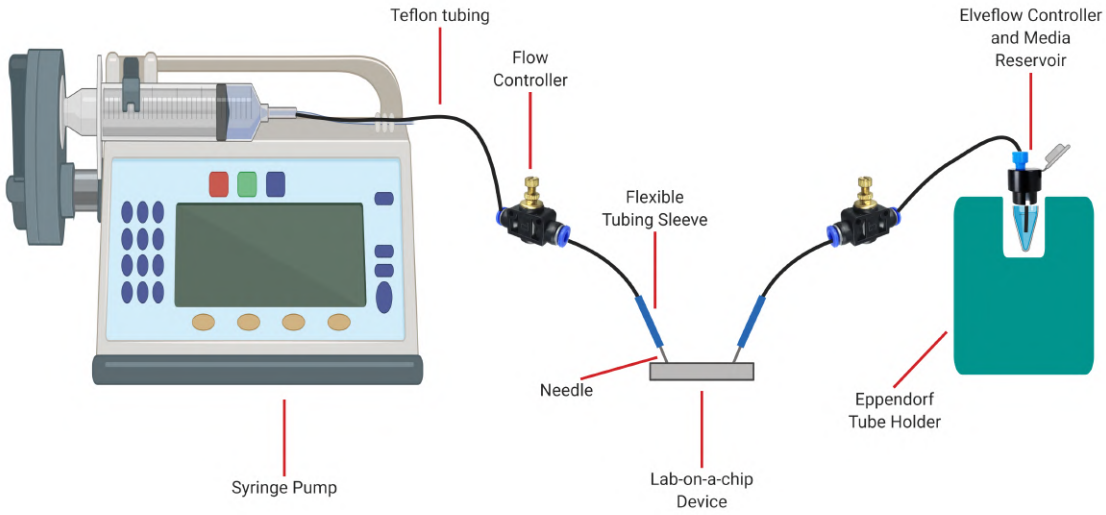

Figure 3.20: **Set-up of pump system to deliver fresh media to cells growing in the LOC device.**

3.11.1 Flow rate of media through the LOC lumens

The optimum flow rate of McCoy's media was found by testing different flow rates through the lumens of LOC devices which had been seeded with HT29 cells. Cells were seeded in the devices according to Section 3.10 and then the pump system was set up, as described above. Media was drawn from the reservoir, through the lumen and into the syringe at flow rates of 3, 4, 5, 6, 7, and 8 μL per hour. Each flow rate was tested in a new LOC for a total of three hours each, and the devices were checked under a light microscope (Magnification 10 x, NA 0.25) (Nikon Eclipse Ts2) to observe whether cells had been dislodged from the inner lumen surface by the sheer stress of the media. The optimum flow rate was found to be 5 μL per hour. The pump system was run in reverse to draw media through the channel from the reservoir, at 1 mL per minute until the media had filled the tubing up to the device. The rate was then lowered to 5 μL per hour so that the cells inside the lumen of the LOC device would not be disturbed by shear stress of the media flowing through the channel.

3.12 *Bacteroides fragilis* toxin (BFT)

To obtain the toxin, *B. fragilis* strain 86-5443-2-2 cells, which express the *bft-2* toxin isotype were grown for three days in 200 mL of broth medium (brain heart infusion base containing yeast extract, vitamin K, hemin and L-cysteine in a microaerobic environment at 37°C [84]. The resultant cultures were centrifuged at 2330 rpm for ten minutes to pellet cells. The supernatant was subjected to a second round of centrifugation and passed through a 0.22 μm filter to remove any residual bacteria, before the addition of solid $(NH_4)_2SO_4$ at full 60% (w / v) saturation. After gentle mixing at 4°C for 90 minutes, the solution was centrifuged at 3000 rpm for 40 minutes. The resulting pellet was dissolved in PBS and any residual insoluble material was removed by centrifugation at 10,000 rpm for ten minutes at 4°C [85]. BFT activity in the precipitated protein was confirmed by adding serial dilutions in cell culture media with the addition of 1% FBS to HT29 cells, with greater than 50% cell rounding over time used to indicate the toxigenic effect [86]. As a negative control, the supernatant from non-toxigenic *B.fragilis* (NTBF) grown in broth culture was collected.

3.13 Immunostaining for E-cadherin in HT29 cells

For immunostaining, HT29 cells (5×10^4 per mL) were grown in glass fluorodishes and in fluorodishes coated with 5% gelatin hydrogels for 96 hours. The cells were then fixed with 1% formaldehyde in PBS for 15 minutes at room temperature. The fixative solution was discarded and the cells in each dish were washed three times with ice cold PBS, with five minutes per wash. The cells were then incubated with 1 mL of blocking buffer (100 μL of 1% bovine serum albumin (BSA) dissolved in 900 μL of PBS-Tween (1% BSA + 0.1% Tween)) for one hour at room temperature. The buffer was then discarded.

For staining, the primary antibody (Anti-E Cadherin antibody [M168]-C-terminal) (Abcam, AU) was diluted at a 1 / 100 ratio (5 μL diluted in 500μL of 1% BSA). Cells were incubated with 500 μL of antibody solution and 200 μL of PBST at 4 °C overnight. The next day, the antibody solution was discarded from the fluorodishes and they were washed on a tilt shaker at 30 rpm (Heidolph Instruments Duomax 1030) three times for five minutes each with ice cold PBS. The secondary antibody (Goat Anti-Mouse IgG

H & L, Alexa Fluor 488) (Abcam, AU) was diluted at a 1 / 250 ratio in 1% BSA (5 μL diluted in 1250μL of BSA). Cells in each dish were incubated with the antibody solution for one hour in the dark at room temperature. Following this, the antibody solution was discarded from each dish and the cells were washed three times on a tilt shaker at 30 rpm for five minutes each with ice cold PBS. Lastly, 1 mL of PBS was pipetted on to the cells to prevent them from drying out. To visualise the location and presence of E-cadherin, stained HT29 cells were observed using the 63 x oil immersion lens and 20 x dry lens of a confocal microscope (Leica TCS SP5), with the emission bandwidth (beginning to end) set to 486 nm - 576 nm.

3.14 Observation of cell rounding in BFT-treated HT29 cells

The toxigenic effect of BFT is associated with a detectable change in cell morphology, identified as cell rounding. Cells were grown in plain glass fluorodishes and in fluorodishes coated with 5% gelatin hydrogel for 48 hours. Cells were then rinsed once with PBS to remove all traces of supplemented media. BFT-rich supernatant from an enterotoxigenic *B. fragilis* (ETBF) was diluted in McCoy's 5A media without the addition of FBS, at a 1 : 35 ratio. BFT was then added to half of the dishes and incubated for three and a half hours. The concentrated supernatant from a non-toxigenic *B. fragilis* (NTBF) was similarly added to the other half of the dishes as the control, and was incubated for three and a half hours. Light microscopy (Magnification 20 x, NA 0.45) (Nikon Eclipse Ts2) was used to determine if approximately 50% toxin-mediated cell rounding was evident in this time frame.

3.15 Detection of HT29 cell rounding and loss of E-cadherin after application of BFT

To observe any cell rounding and the loss of E-cadherin after 12 and 24 and hours of incubation with BFT-rich supernatant, HT29 cells were grown on 5% concentration gelatin hydrogels for 48 hours, followed by treatment with BFT-rich supernatant for both 12

and 24 hours at 37°C and 5% CO_2, as described in Section 3.14. Following this, the cells were then fixed and stained for E-cadherin, as described in Section 3.13. To obtain a better visualisation of the cells before and after the application of BFT-rich supernatant, the cell nuclei were then stained using DAPI ($2\,\mu$g / mL of 0.1% PBS-tween), by adding 1 mL of DAPI solution to the dishes. The cells were left to incubate for one hour at room temperature and the stain was then discarded and the cells were washed three times with ice cold PBS on a tilt shaker at 30 rpm, five minutes each wash. The fixed cells were then imaged using the 20 x dry lens (NA 0.50) and 63 x oil immersion lens (NA 1.40) a confocal microscope (Leica TCS SP5) to identify any loss of E-cadherin in the samples treated with BFT-rich supernatant. The emission bandwidth of the microscope (beginning to end) was set to 420 nm - 493 nm. As a control, HT29 cells that were grown for 48 hours were then treated with concentrated supernatant from NTBF for 12 and 24 hours, followed by staining for E-cadherin and nuclei and visualisation using a confocal microscope.

Chapter 4

Results

4.1 Adherence of HT29 cells on polystyrene, PDMS and gelatin thin films

The ability of HT29 cells to adhere to PDMS (used as the main body of the LOC devices in this study) and polystyrene (PS) was compared to the ability of cells to adhere to PDMS and PS coated with a 0.1% gelatin solution over time. Paired t-tests were carried out to investigate whether there were significant differences in the means of adherent and non-adherent cells on the four different surfaces over a 72 hour incubation period.

HT29 cells readily adhered to the PS surface and remained adherent after 72 hours of incubation, with cell numbers increasing over time. There was a significant difference between adherent and non-adherent cells on the PS surface (p-value = 0.033), as shown in Figure 4.1a. In contrast, a 0.1% gelatin thin film appeared to affect HT29 cell adherence over time. Whereas all cells were adherent at 24 hours of incubation, counts revealed that 63% of the cells were no longer adherent at 72 hours of incubation, as shown in Figure 4.1b). A paired t-test indicated no significant difference in the means of adherent and non-adherent cells grown on PS coated with gelatin after 72 hours of incubation (p-value = 0.079) (Fig. 4.1b).

In contrast, HT29 cells cultured on PDMS failed to adhere after 72 hours, as shown in Figure 4.2a. On the contrary, 75% of cells added to PDMS coated with a 0.1% gelatin

thin film were adherent after this period of time, as shown in Figure 4.2b). A paired t-test indicated no significant difference between the means of adherent and non-adherent cells grown on PDMS coated with 0.1% gelatin thin films over 72 hours (p-value = 0.77).

Images taken after trypsinisation showed that some cells were still adherent to both the PS and PDMS surfaces that were coated with 0.1% gelatin thin films, as shown in Figures 4.3a and 4.3b). While this observation suggested that adherent cell numbers were likely to be artificially low, it also clearly showed that a thin film of gelatin appeared to facilitate the adherence of HT29 cells to the PDMS surface over time.

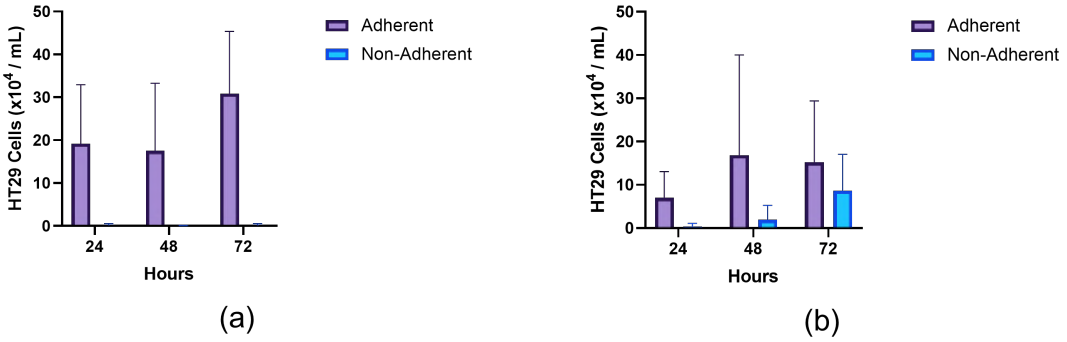

Figure 4.1: **Mean cellular adherence of HT29 cells on (a) PS and (b) PS coated with a 0.1% gelatin thin film over a 72 hour time period.**

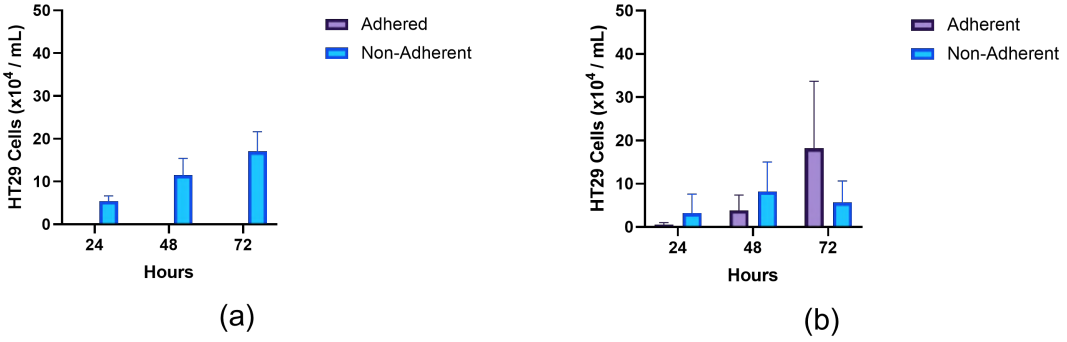

Figure 4.2: **Mean cellular adherence of HT29 cells on (a) PDMS and (b) PDMS coated with a 0.1% gelatin thin film over a 72 hour time period.**

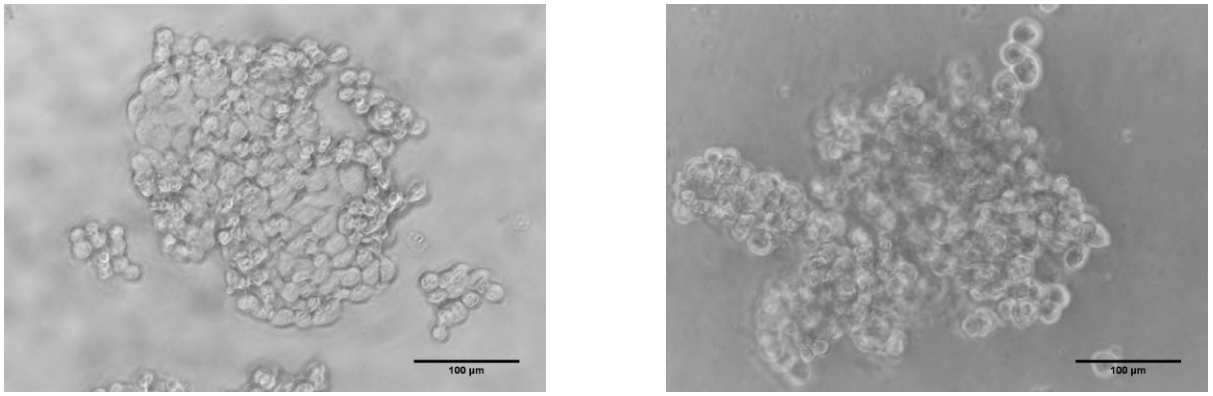

(a) (b)

Figure 4.3: **HT29 cells grown on (a) PS coated with a 0.1% gelatin thin film and (b) PDMS coated with a 0.1% gelatin thin film were observed to have remained adherent after trypsinisation, using the 10 x objective lens (NA 0.25) of a light microscope.**

4.1.1 Cell morphology on polystyrene, PDMS and gelatin thin films

HT29 cells grown on PS and on PS coated with gelatin thin films showed evidence of confluency after 72 hours of incubation, as shown in Figure 4.4a and 4.4b. In contrast, HT29 cells grown on PDMS and PDMS coated with gelatin thin films appeared to form rounded, three-dimensional cell clusters over the same period of time. The cell clusters on PDMS were observed to be non-adherent, as shown in Figure 4.5a. Cells grown on PDMS coated with a 0.1% gelatin thin film were observed to have a mixed population of adherent and non-adherent cells, as shown in Figure 4.4b.

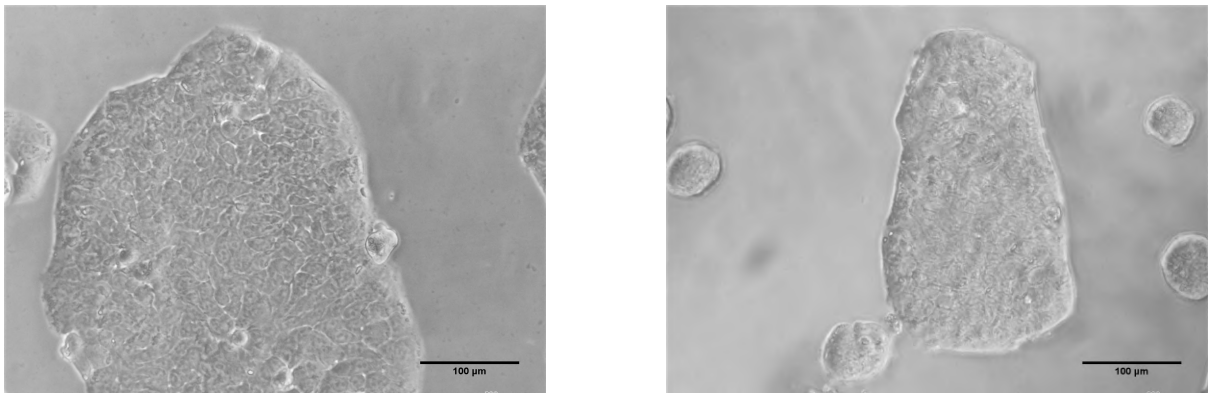

(a) (b)

Figure 4.4: **HT29 cells had formed large, adherent, confluent layers when they were observed on (a) PS and (b) PS coated with gelatin after 72 hours of incubation.** Cells were observed using the 10 x objective lens (NA 0.25) of a light microscope.

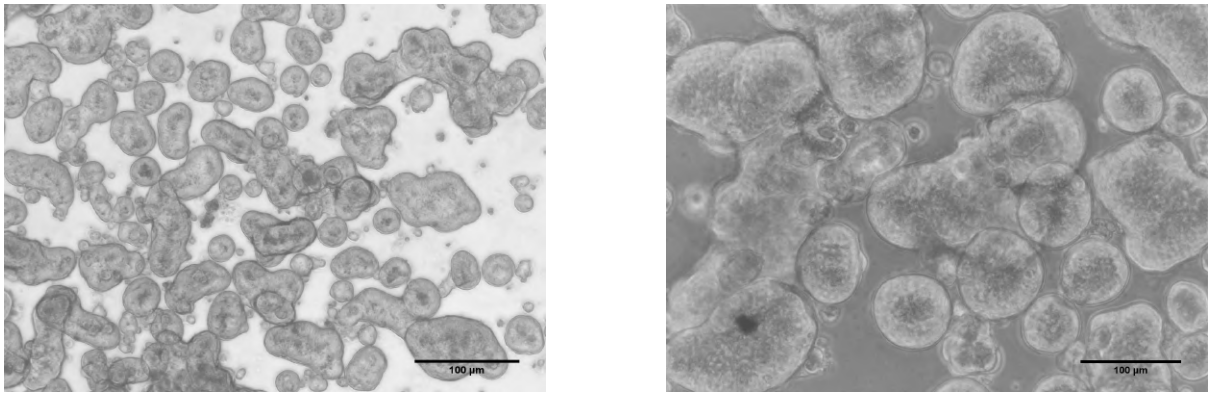

(a) (b)

Figure 4.5: **HT29 cells had formed rounded, clustered morphologies after 72 hours when they were observed on (a) PDMS and (b) PDMS coated with 0.1% gelatin thin films.** Cells were observed using the 10 x lens (NA 0.25) of a light microscope.

4.2 Investigation of collagen and gelatin hydrogel formation for potential use in LOC devices

The objective in creating the PDMS LOC devices was to mimic the tubular architecture of the human gut and so HT29 cells were needed to adhere around the periphery of the lumen inside the devices. Because collagen is an abundant protein in the human gut and has been shown to facilitate cellular adhesion, it was thought that a collagen hydrogel could be used to facilitate HT29 cellular adhesion in the LOC devices [87]. Gelatin is an irreversibly hydrolysed form of collagen, which has also been found to aid cellular adhesion, as described in Section 4.1. It was therefore thought that a gelatin hydrogel could also be used to fill the LOC devices, form lumenal structures and facilitate HT29 cell adhesion.

As described in Section 3.2.1, 3%, 5% and 7% collagen hydrogels were made. All three wells of each different concentration formed solid hydrogels, and the 7% hydrogel was the most solid in comparison to the other two. This was expected because the 7% hydrogel contained the most collagen fibrils. The 1%, 2%, 3%, 4%, 5% and 10% concentration gelatin hydrogels in this study were made according to Section 3.2.2. The 3%, 4%, 5% and 10% solutions formed solid hydrogels, whereas the 1% and 2% solutions did not form solid hydrogels. To determine which gelatin hydrogel would be most appropriate to use

in the LOC devices, HT29 cell metabolism and morphology was investigated on the 3%, 5% and 10% concentration hydrogels, as described in Sections 4.3.2 and 4.5.

4.3 Alamar blue assay of HT29 cellular metabolism on collagen and gelatin hydrogels

To identify how metabolically active HT29 cells were on collagen and gelatin hydrogels, the alamarBlue cell viability reagent was used. Cells grown in the wells of a 96-well plate reduced resozurin (blue in colour) to highly fluorescent resorufin (red in colour) by redox power over a four hour time period. The fluorescence of the media in the wells of the plate was then measured using a plate reader, with an excitation between 530–560 nm and an emission at 590 nm. The intensity of the measured fluorescence was proportional to the number of living cells respiring in each well [88].

4.3.1 HT29 cellular metabolism on collagen hydrogels

The log transformation, as described in Section 3.7, resulted in an even distribution of residual values, as shown in Figure 4.6. A 2-way RM ANOVA indicated that the combination of incubation time and collagen hydrogel concentration had no significant effect on the mean cellular metabolism of HT29 cells after 72 hours of incubation (p-value = 0.57) (Fig. 4.7). The test indicated a significant effect of time on mean cellular metabolism of HT29 cells (p-value = 0.014), and no significant effect of hydrogel concentration on mean cellular metabolism (p-value = 0.94). A Tukey's multiple comparison test indicated no significant difference between the mean cellular metabolism of HT29 cells on all combinations of collagen hydrogel types at 24, 48 and 72 hours incubation (p-value $>$ 0.05), as shown in Figure 4.7.

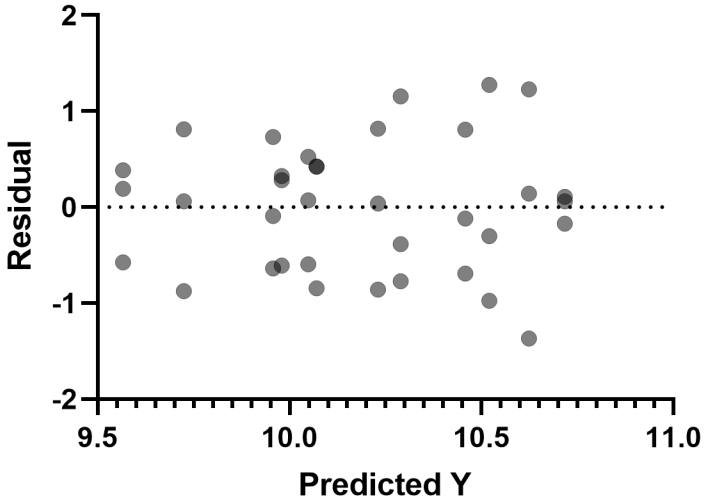

Figure 4.6: **Residual plot of transformed relative fluorescence values of HT-29 cells on different concentration collagen hydrogels over a 72 hour time period.**

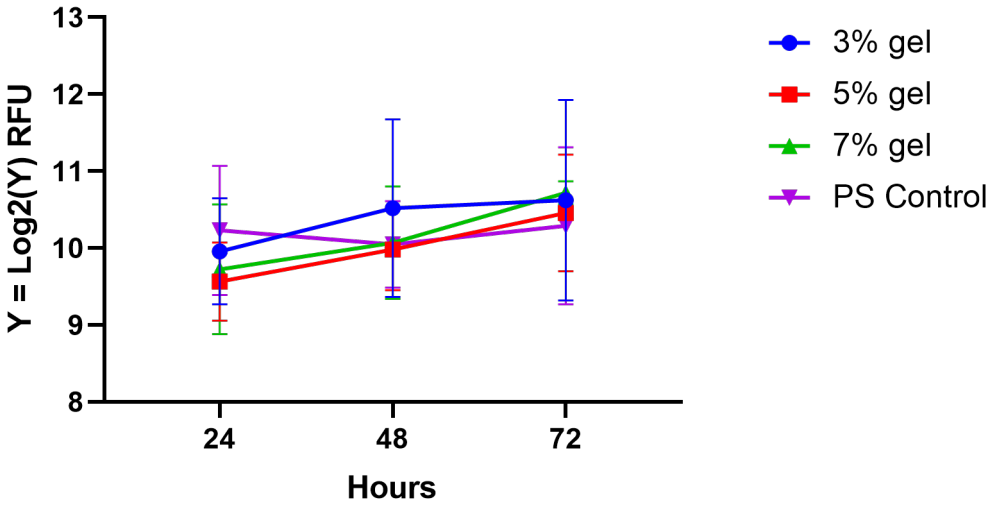

Figure 4.7: **Mean cellular metabolism of HT29 cells on 3%, 5% and 7% collagen hydrogels and PS control over a 72 hour time period.**

4.3.2 HT29 cellular metabolism on gelatin hydrogels

The log transformation, as described in Section 3.7, resulted in an even distribution of residual values, as shown in Figure 4.8. A 2-way RM ANOVA indicated that the combination of incubation time and gelatin hydrogel concentration had no significant effect on the mean cellular metabolism of HT29 cells after 72 hours of incubation (p-value = 0.73) (Fig. 4.9). The test indicated a significant effect of time on mean cellular metabolism

of HT29 cells (p-value = 0.0003), and no significant effect of hydrogel concentration on mean cellular metabolism (p-value = 0.22). A Tukey's multiple comparison test indicated no significant difference between the mean cellular metabolism of HT29 cells on all combinations of gelatin hydrogel types at 24 and 48 hours incubation (p-value > 0.05), as shown in Figure 4.9.

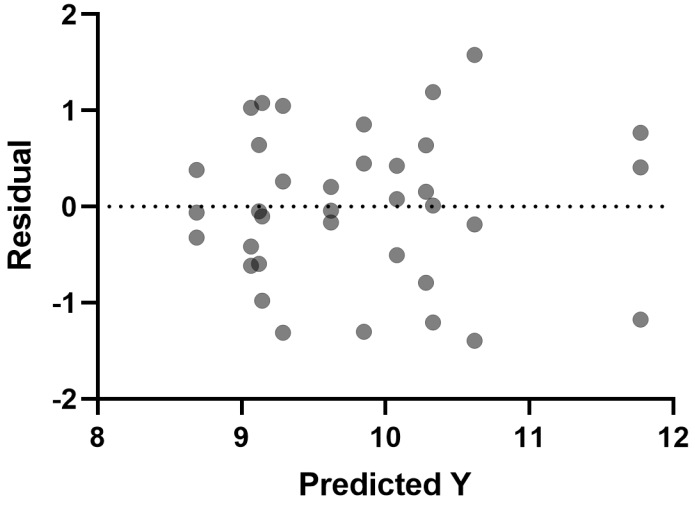

Figure 4.8: **Residual plot of transformed relative fluorescence values of HT-29 cells on different concentration gelatin hydrogels over a 72 hour time period.**

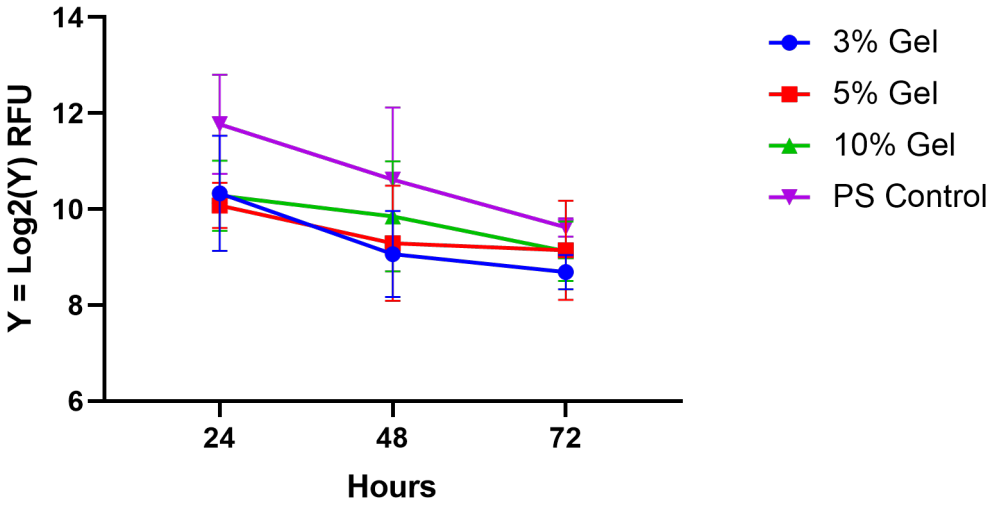

Figure 4.9: **Mean cellular metabolism of HT29 cells on 3%, 5% and 10% gelatin hydrogels and PS control over a 72 hour time period.**

4.4 Contact angle measurements of water on collagen and gelatin hydrogels

The contact angle (CA) (denoted θ) is the angle between a solid surface and a liquid-vapour interface. In this study, the CAs of 3%, 5% and 7% concentration collagen hydrogels, as well as 3%, 5% and 10% concentration gelatin hydrogels, were measured. This was to identify the level of hydrophobicity or hydrophilicity of each hydrogel surface, which was used to determine which gel would be most appropriate as a substrate for HT29 cells. As mentioned in Section 3.9, previous studies suggested that polymers with water CA between 45° and 75° show optimal cellular adherence [83]. In this study, the CA of water on gelatin and collagen hydrogel surfaces were calculated from the measured angles. An ordinary one-way analysis of variance (ANOVA) was carried out to determine whether there were significant differences between the mean CA of DI water on both gelatin and collagen hydrogel surfaces. A Brown-Forsythe test was used to investigate whether the variation within the different hydrogel groups and PDMS control were equal or not. Lastly, a Tukey's multiple comparison test was carried out to determine whether there were any significant differences between the mean CA of DI water on specific hydrogels in the two analyses.

4.4.1 Contact angle of water on collagen hydrogels

The 3% collagen hydrogel had a mean CA of 34.9°, the 5% hydrogel had a mean CA of 32.2° and the 7% hydrogel had a mean of 43.9°, as shown in Figure 4.11. An ANOVA indicated a significant difference in the mean CA of DI water on the 3%, 5%, 7% collagen hydrogels and the PDMS control (p-value < 0.0001). The R^2-value was 0.91; therefore, 90% of the variation between the mean contact angle of DI water on the different collagen hydrogels can be explained by this test. A Brown-Forsythe test showed no significant difference in the variance between the groups (p-value $= 0.19$). Therefore, the standard deviations were the same for the different groups (p-value < 0.05).

A Tukey's multiple comparison test was carried out to investigate whether there was a significant difference between the mean CA of DI water on specific hydrogels in the analysis. It indicated no significant difference between the mean CA of the 3% and 5%

collagen hydrogels (p-value = 0.93), no difference between the mean CA of the 3% and 7% collagen hydrogels (p-value = 0.22) and no significant difference between the mean CA of the 5% and 7% hydrogels (p-value = 0.066). However, there were significant differences in the mean CA between all three collagen hydrogels and the PDMS control (p-value $<$ 0.0001) (Fig. 4.11).

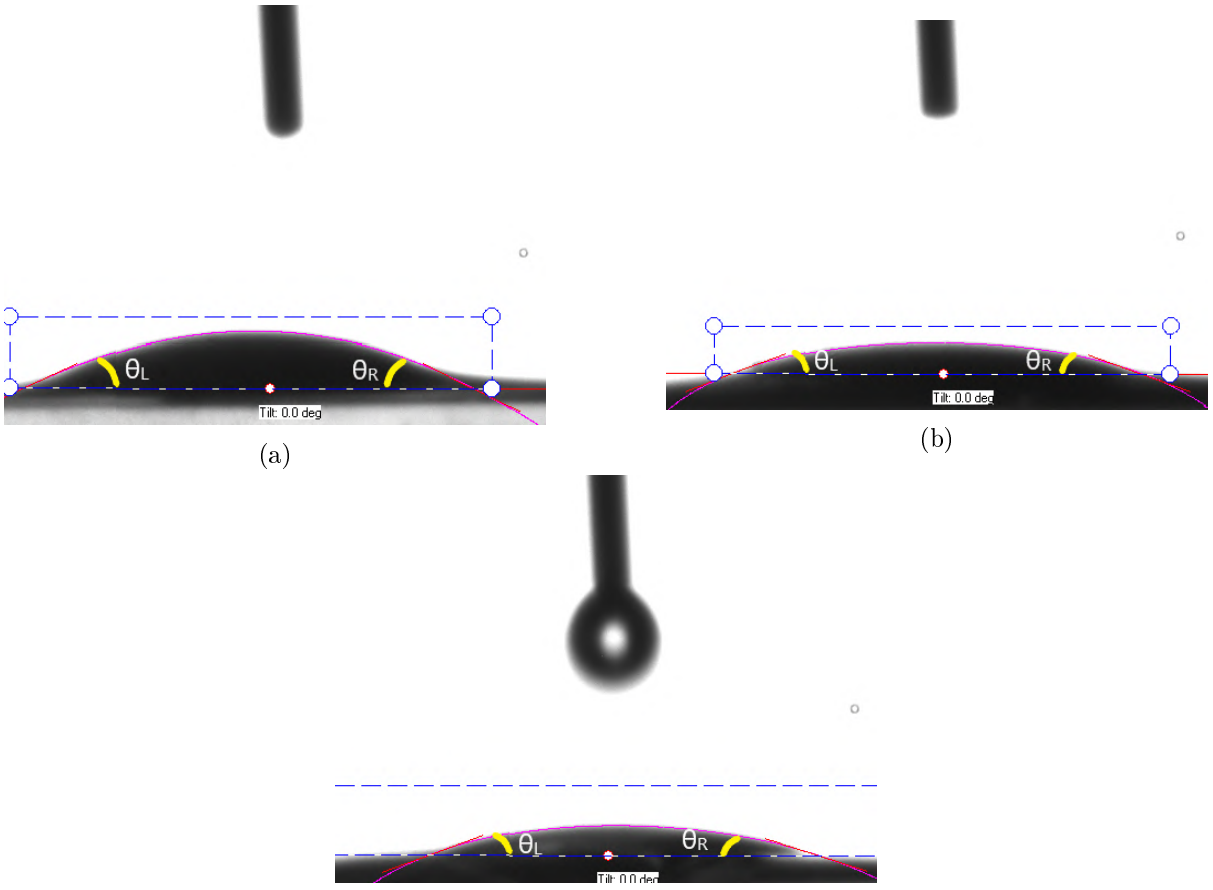

Figure 4.10: **DI water droplets on different concentration collagen hydrogels and a PDMS control were used to calculate the CA (denoted in yellow) of each hydrogel surface.** (a) CA of water on a 3% collagen hydrogel. $\theta_L = 24.4°$. $\theta_R = 26.6°$. (b) CA of water on a 5% collagen hydrogel. $\theta_L = 20.4°$. $\theta_R = 19.5°$. (c) CA of water on a 7% collagen hydrogel. $\theta_L = 20.2°$. $\theta_R = 17.3°$.

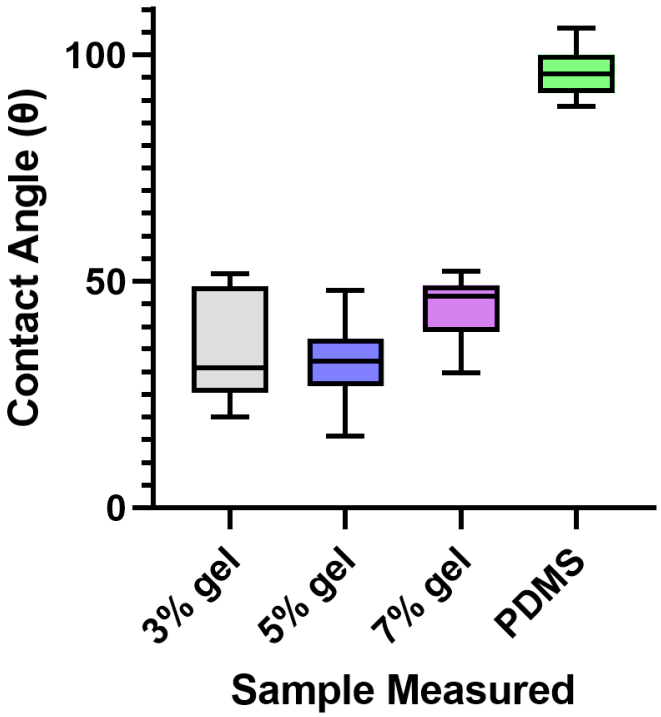

Figure 4.11: **Mean contact angle of DI water on PDMS, 3%, 5% and 7% collagen hydrogels, and PDMS control.**

4.4.2 Contact angle of water on gelatin hydrogels

The 3% gelatin hydrogel had a mean CA of 77.2°, the 5% hydrogel had a mean CA of 64.4° and the 10% hydrogel had a mean of 75.1°, as shown in Figure 4.13. An ANOVA indicated a significant difference in the mean CA of DI water on the 3%, 5%, 10% gelatin hydrogels and the PDMS control (p-value < 0.0001). The R^2-value was 0.55; therefore, 55% of the variation between the mean contact angle of DI water on the different gelatin hydrogels can be explained by this test. A Brown-Forsythe test showed no significant difference in the variance between the groups (p-value $= 0.14$). Therefore, the standard deviations were the same for the different groups (p-value < 0.05).

A Tukey's multiple comparison test indicated no significant difference between the mean CA of the 3% and 5% hydrogels (p-value $= 0.12$), no difference between the mean CA of the 3% and 10% hydrogels (p-value $= 0.98$) and no significant difference between the mean CA of the 5% and 10% hydrogels (p-value $= 0.24$). However, there was a significant difference in the mean CA between the 3% hydrogel and PDMS (p-value $=$

0.01), the 5% hydrogel and PDMS (p-value < 0.0001) and between the 10% hydrogel and PDMS (p-value $= 0.0042$) (Fig. 4.13).

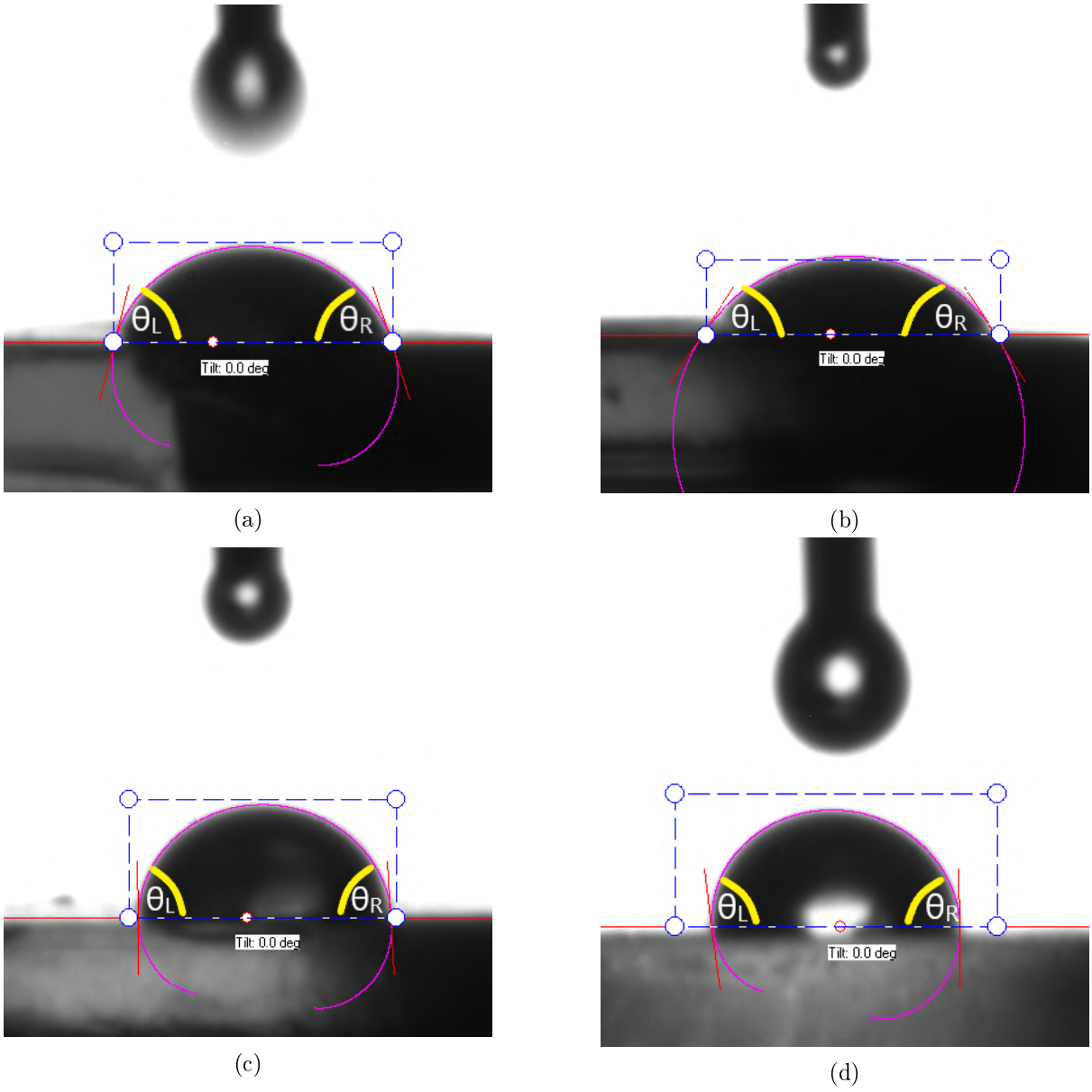

Figure 4.12: **DI water droplets on different concentration gelatin hydrogels and a PDMS control were used to calculate the CA (denoted in yellow) of each hydrogel surface.** (a) CA of water on a 3% gelatin hydrogel. $\theta_L = 75.8°$. $\theta_R = 71.7°$. (b) CA of water on a 5% gelatin hydrogel. $\theta_L = 56.3°$. $\theta_R = 56.3°$. (c) CA of water on a 10% gelatin hydrogel. $\theta_L = 90.6°$. $\theta_R = 86.5°$. (d) CA of water on PDMS. $\theta_L = 92.6°$. $\theta_R = 88.0°$.

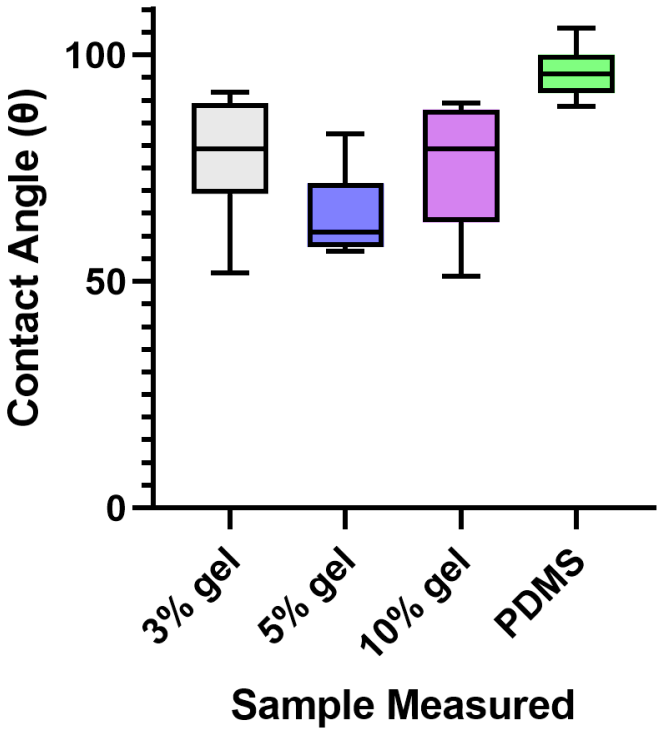

Figure 4.13: **Mean contact angle of DI water on PDMS, 3%, 5% and 10% gelatin hydrogel disks, and PDMS control.**

4.5 HT29 cell morphology on collagen and gelatin hydrogels

Confocal microscopy was used to observe the morphology of HT29 cells grown on collagen and gelatin hydrogels and compared to HT29 cells grown on glass. After 24 hours of incubation, cells grown on the glass control formed tight, confluent clusters, as shown in Figure 4.14a.

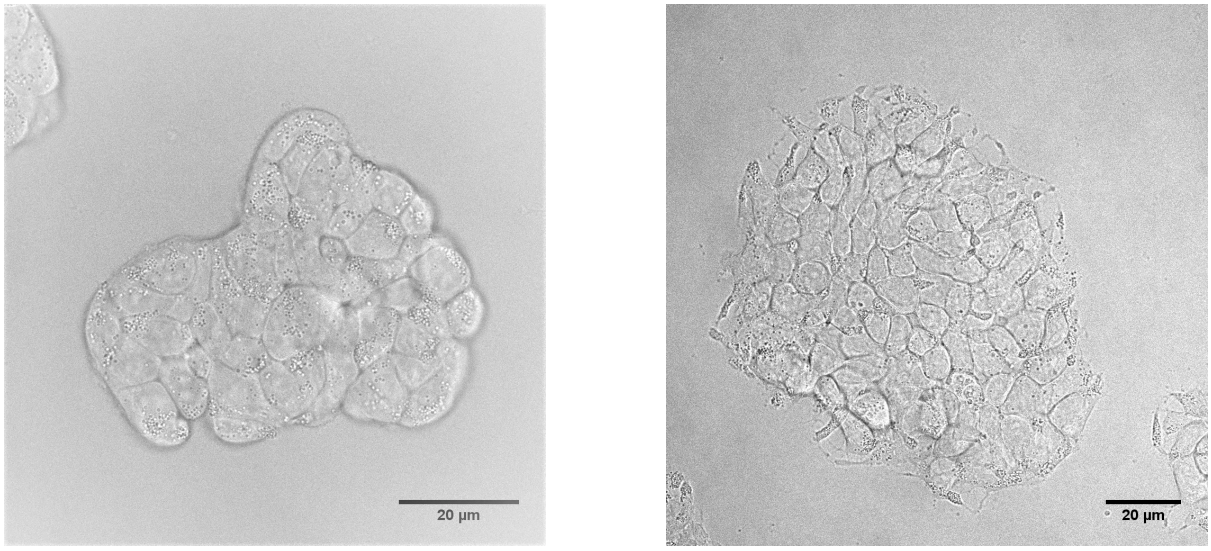

(a) (b)

Figure 4.14: **HT29 cellular morphology was observed on glass controls after (a) 24 hours and (b) 72 hours of incubation. Cells were observed using the 63 x oil immersion objective lens (NA 1.40) of a confocal microscope.**

After 24 hours of incubation, HT29 cells on both the 3% and 5% collagen hydrogels exhibited spherical cell morphology and formed sparse clusters across the hydrogel surfaces (Fig. 4.15a and 4.15b). HT29 cells on the 7% collagen hydrogel also appeared to exhibit spherical shaped morphology and appeared to be starting to form a confluent layer across the hydrogel surface (Fig. 4.15c). After 72 hours of incubation, the cells continued to exhibit spherical morphology on both the 3% collagen hydrogel (Fig. 4.16a) and the 7% collagen hydrogel (Fig. 4.16c). Cells on both hydrogels formed dense clusters and cells were observed to be on top of each other. HT29 cells on the 5% collagen hydrogel exhibited a more normal epithelial morphology, where cells had started to form a confluent layer across the hydrogel (Fig. 4.16b).

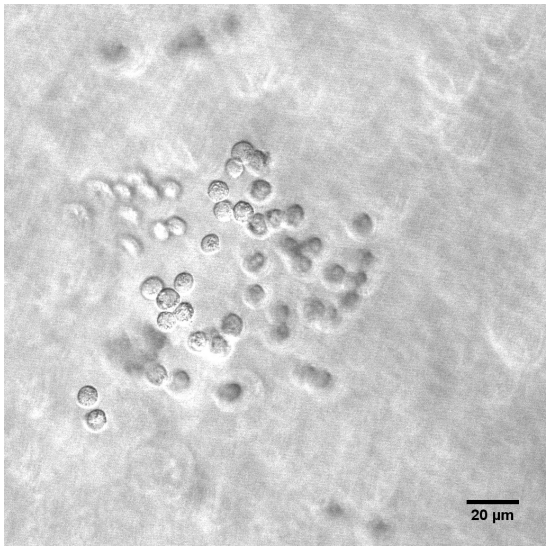

(a)

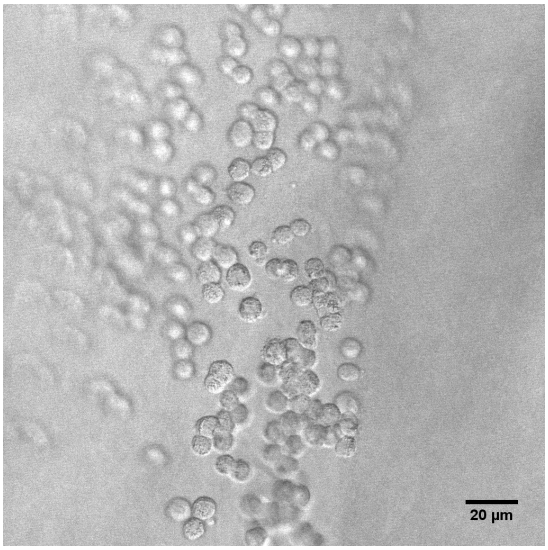

(b)

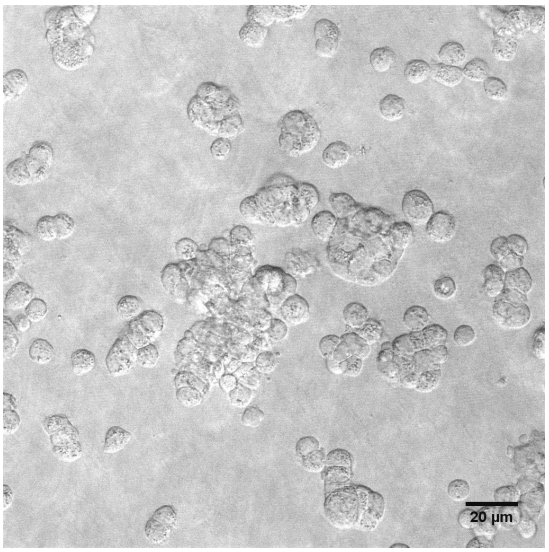

(c)

Figure 4.15: **HT29 cellular morphology was observed after 24 hours on (a) a 3% collagen hydrogel, (b) a 5% collagen hydrogel and (c) a 7% collagen hydrogel, using the 20x oil immersion objective lens (NA 0.70) of a confocal microscope.**

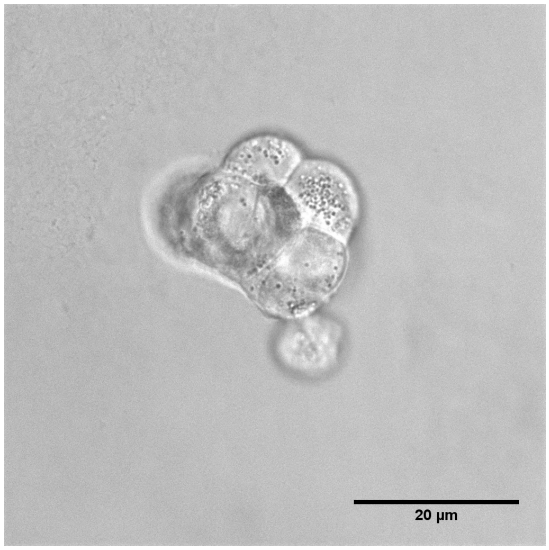

(a)

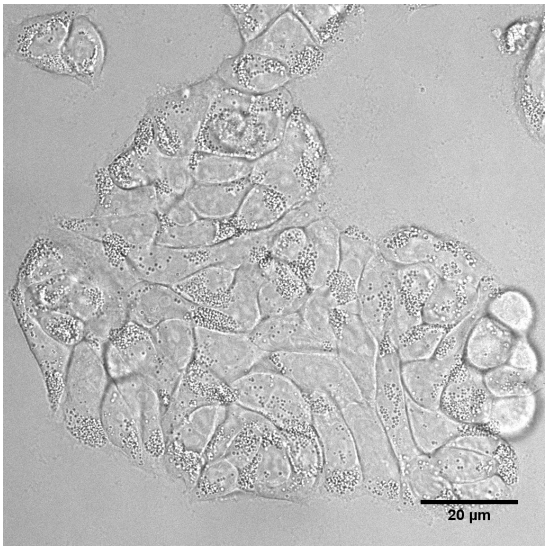

(b)

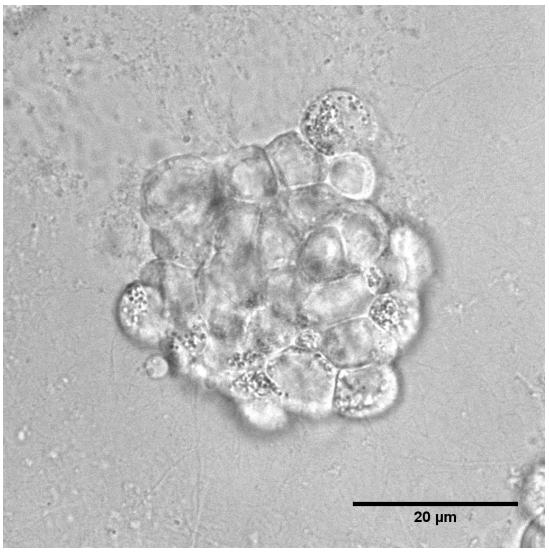

(c)

Figure 4.16: **HT29 cellular morphology was observed after 72 hours on (a) a 3% collagen hydrogel, (b) a 5% collagen hydrogel and (c) a 7% collagen hydrogel using the 63x oil immersion objective lens (NA 1.40) of a confocal microscope.**

Cells that were grown on the 3% and 5% hydrogels appeared to have formed small, confluent clusters with cell-cell contacts (Fig. 4.17a and 4.17b). Cells grown on the 10% hydrogel appeared to be more dispersed across the surface, and some cells had formed filopodia to connect to each other, as shown in Figure 4.17c. After 72 hours of incubation, cells that were grown on glass had formed confluent clusters, as shown in Figure 4.14b). After 72 hours, cells that were grown on the 3%, 5% and 10% gelatin hydrogels appeared to have formed large, confluent clusters across the surfaces, as shown in Figures 4.18a, 4.18b and 4.18c. The filopodia observed on the 10% gelatin hydrogel had dissapeared by

this time point, as shown in Figure 4.18c.

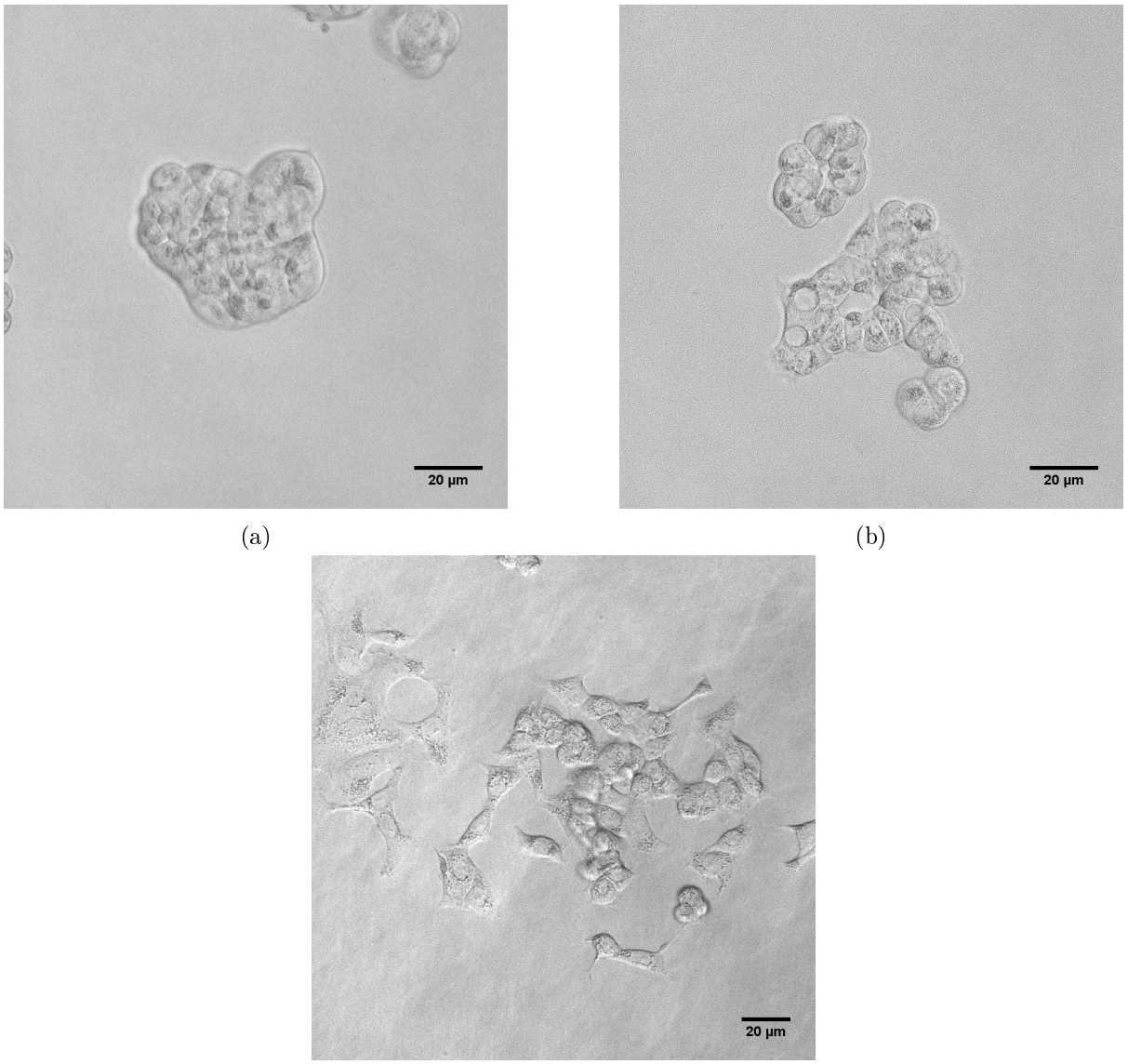

(a) (b)

(c)

Figure 4.17: **HT29 cellular morphology was observed after 24 hours on (a) a 3% gelatin hydrogel using the 40 x dry objective lens (NA 0.75), (b) a 5% gelatin hydrogel using the 40 x dry objective lens (NA 0.75) and (c) a 10% gelatin hydrogel using the 20 x oil immersion lens (NA 0.70) of a confocal microscope.**

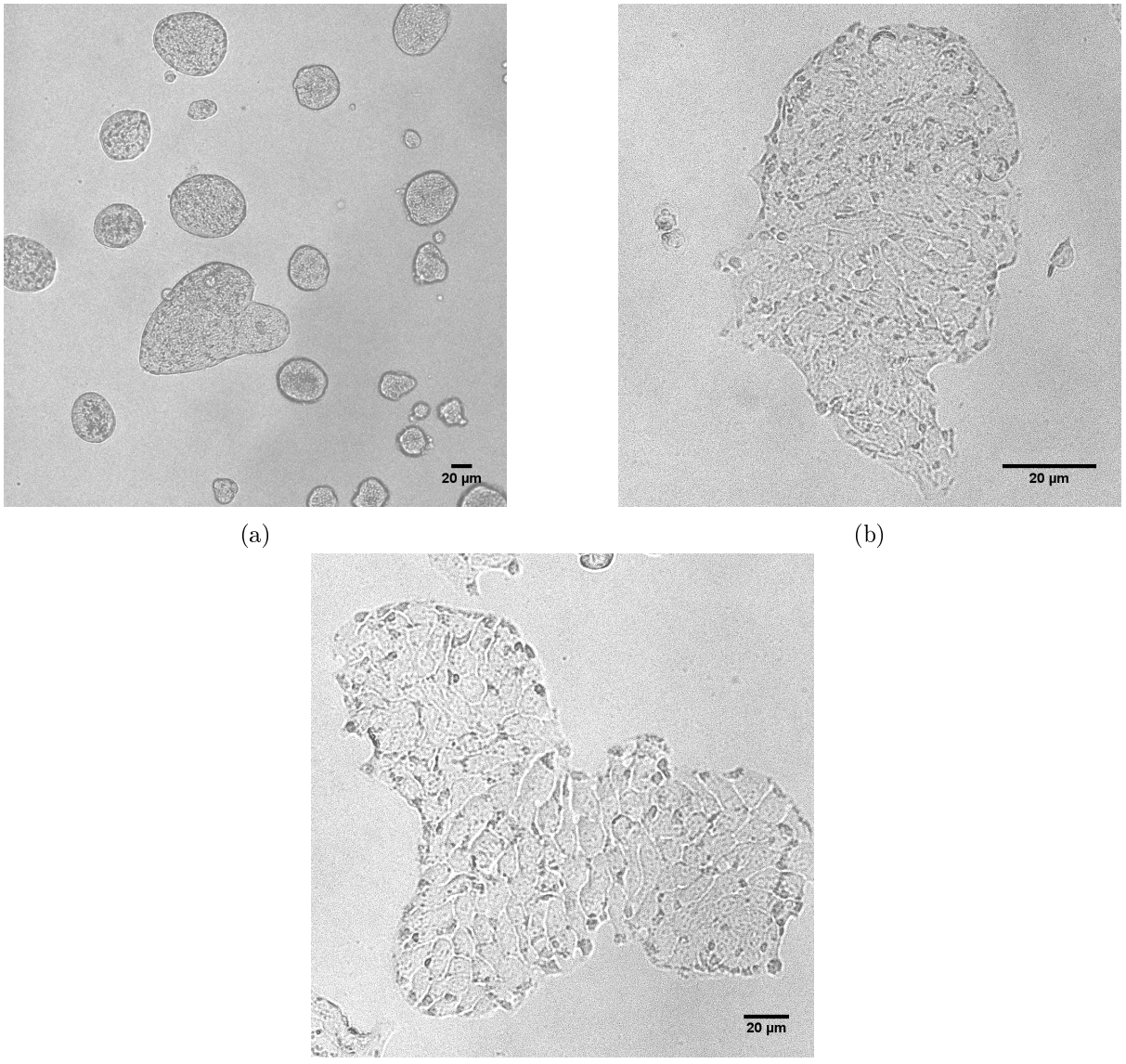

(a) (b)

(c)

Figure 4.18: **HT29 cellular morphology was observed after 72 hours on (a) a 3% gelatin hydrogel, (b) a 5% gelatin hydrogel and (c) a 10% gelatin hydrogel using the 20 x dry objective lens (NA 0.50) of a confocal microscope.**

4.6 Fabrication of LOC devices

LOC devices were fabricated from PDMS, as described in Section 3.1. After plasma bonding of the bottom and top layers of the chip parts with the PDMS rods inside, the devices were filled with a 5% gelatin hydrogel. Once the hydrogels had set, the rods were successfully removed from the 2 mm hole-punched hole in the top chip layers. This left hollow lumens for cell culture, as shown in Figure 3.13.

4.7 Cell seeding in LOC devices and flow rate optimisation

Cells were seeded and grown inside the 5% gelatin hydrogel lumens of LOC devices in an attempt to form a confluent layer which coated the entire inner lumen surface. After two hours of incubation, HT29 cells had adhered to the gelatin inner lumen surface inside the LOC devices, as shown in Figure 4.19. The pump system was then set up, as described in Section 3.11, to provide fresh media to the growing cells. Media flow rates through the lumen of 8 μL per hour or higher led to the dislodgement of all cells from the lumen wall. Flow rates of 6μL and 7 μL per hour had dislodged less cells. The optimum media flow rate was 5 μL per hour because the sheer stress of media passing through the lumen was not enough to dislodge any of the cells, and because enough nutrients was still being provided to the cells each hour in order for them to grow.

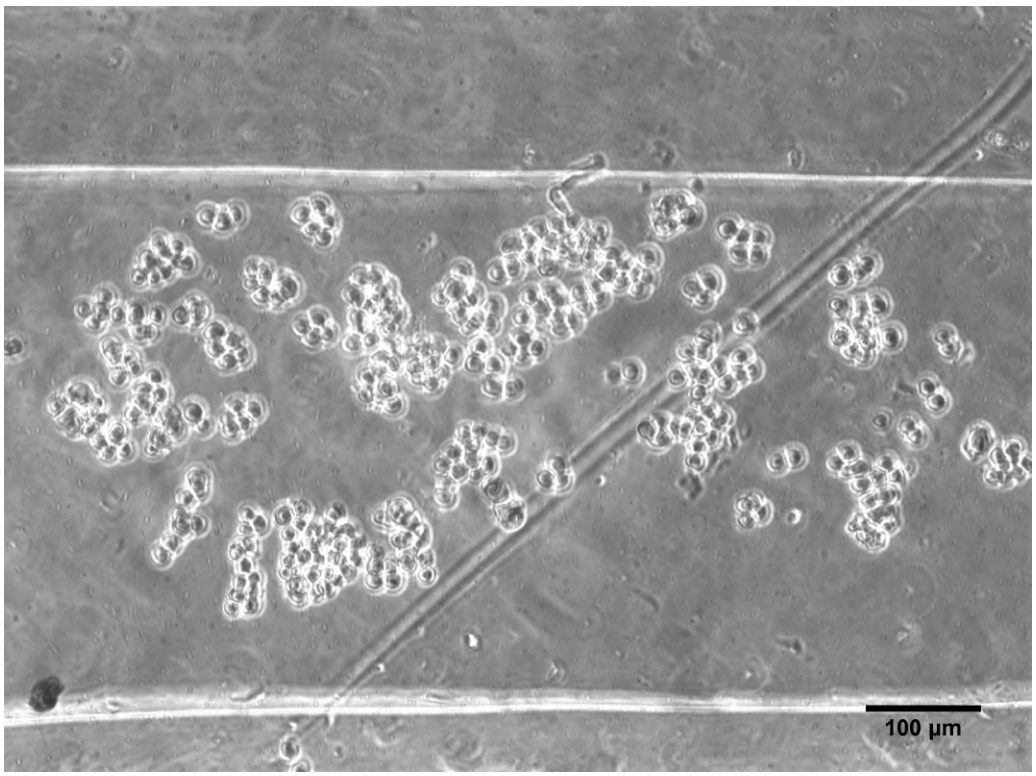

Figure 4.19: **HT29 cells were observed to be adhered to the 5% gelatin hydrogel lumen surface within a LOC device after two hours of incubation.** Cells were observed using the 10 x objective lens (NA 0.25) of a light microscope.

4.8 Localisation of E-cadherin in HT29 cells

To investigate the presence and location of E-cadherin in HT29 cells grown on glass and on 5% gelatin hydrogels, cells were fixed and permeabilised prior to being immunostained with a mouse anti-E-cadherin monoclonal antibody. E-cadherin was detected using an Alexa fluor 488-labelled secondary antibody (green), and was observed around the periphery of HT29 cells grown on glass, as shown in Figure 4.20a and on 5% gelatin hydrogels, as shown in Figure 4.20b. The E-cadherin staining was overlayed on the bright field images, which also showed that E-cadherin was located at the cell peripheries of cells grown on glass (Fig. 4.21a) and on a 5% gelatin hydrogel (Fig. 4.21b).

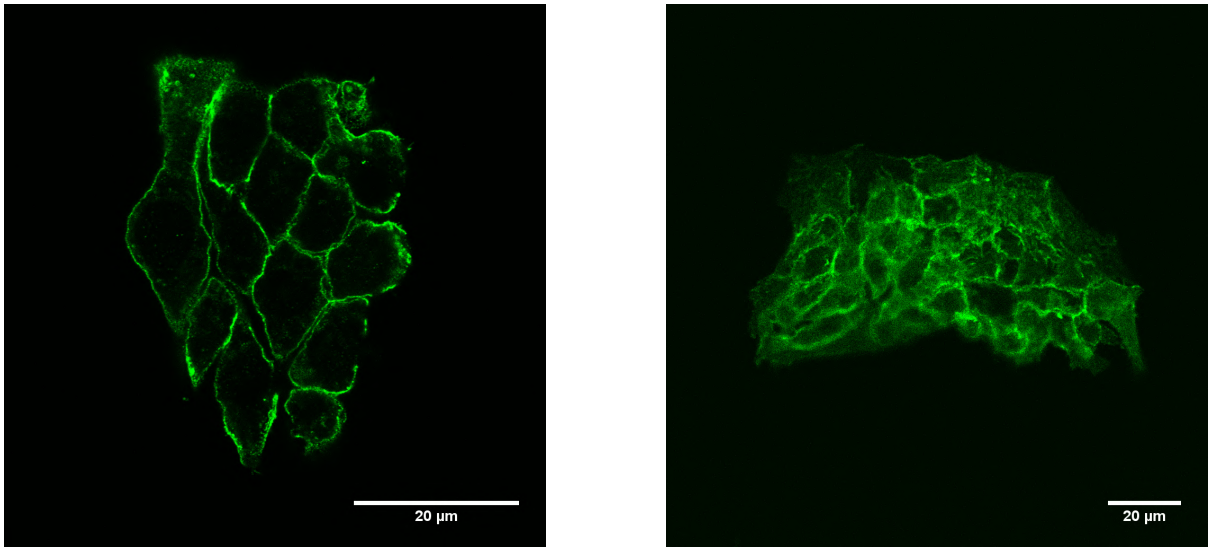

(a) (b)

Figure 4.20: **Localisation of E-cadherin (green) in HT29 cells was observed at the peripheries of cells grown on (a) glass using the 63 x oil immersion objective lens (NA 1.40), and (b) 5% gelatin hydrogels using the 20 x dry objective lens (NA 0.50) of a confocal microscope.** Different lenses were used because the hydrogel thickness affected the distance that the lens could see through the sample.

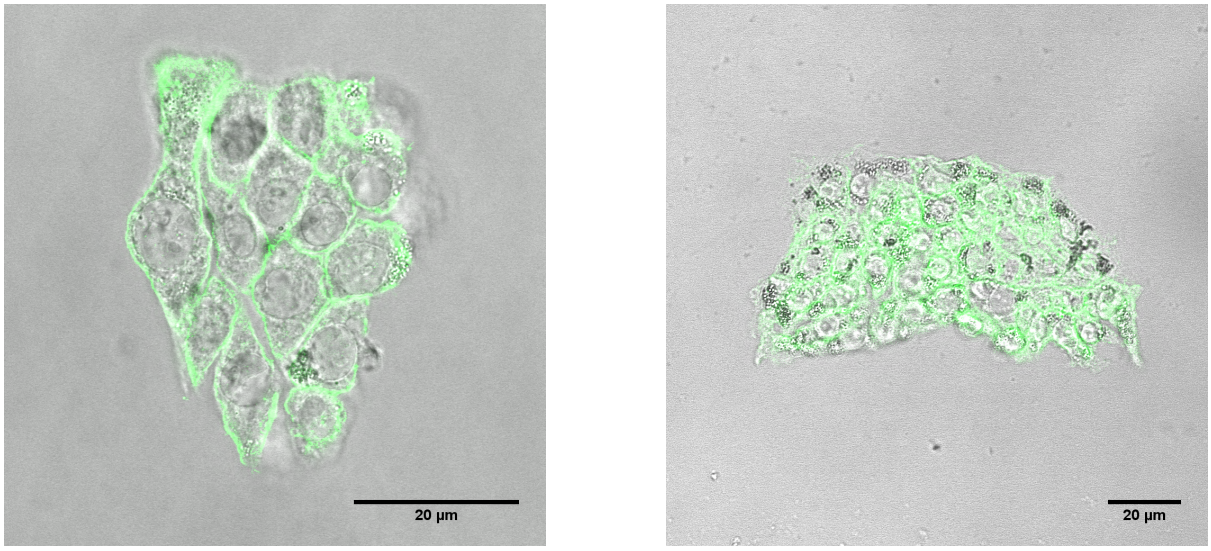

(a) (b)

Figure 4.21: **Localisation of E-cadherin (green) in HT29 cells was over-layed on the bright field images. E-cadherin was observed at the peripheries of cells grown on (a) glass using the 63 x oil immersion objective lens (NA 1.40), and (b) 5% gelatin hydrogels using the 20 x dry objective lens (NA 0.50) of a confocal microscope.** Different lenses were used because the hydrogel thickness affected the distance that the lens could see through the sample.

4.9 Effect of BFT on HT29 cells

To investigate whether BFT would lead to cell rounding, HT29 cells were incubated with BFT-rich supernatant for three and a half hours. Approximately 50% of cells exhibited rounding on glass and on 5% gelatin hydrogels, as seen in Figure 4.22. The concentrated supernatant derived from a nontoxigenic *B. fragilis* (NTBF) was used as a control and HT29 cells grown on glass or a 5% gelatin hydrogel showed no morphological changes after three and a half hours of incubation with the supernatant derived from NTBF, as seen in Figure 4.23.

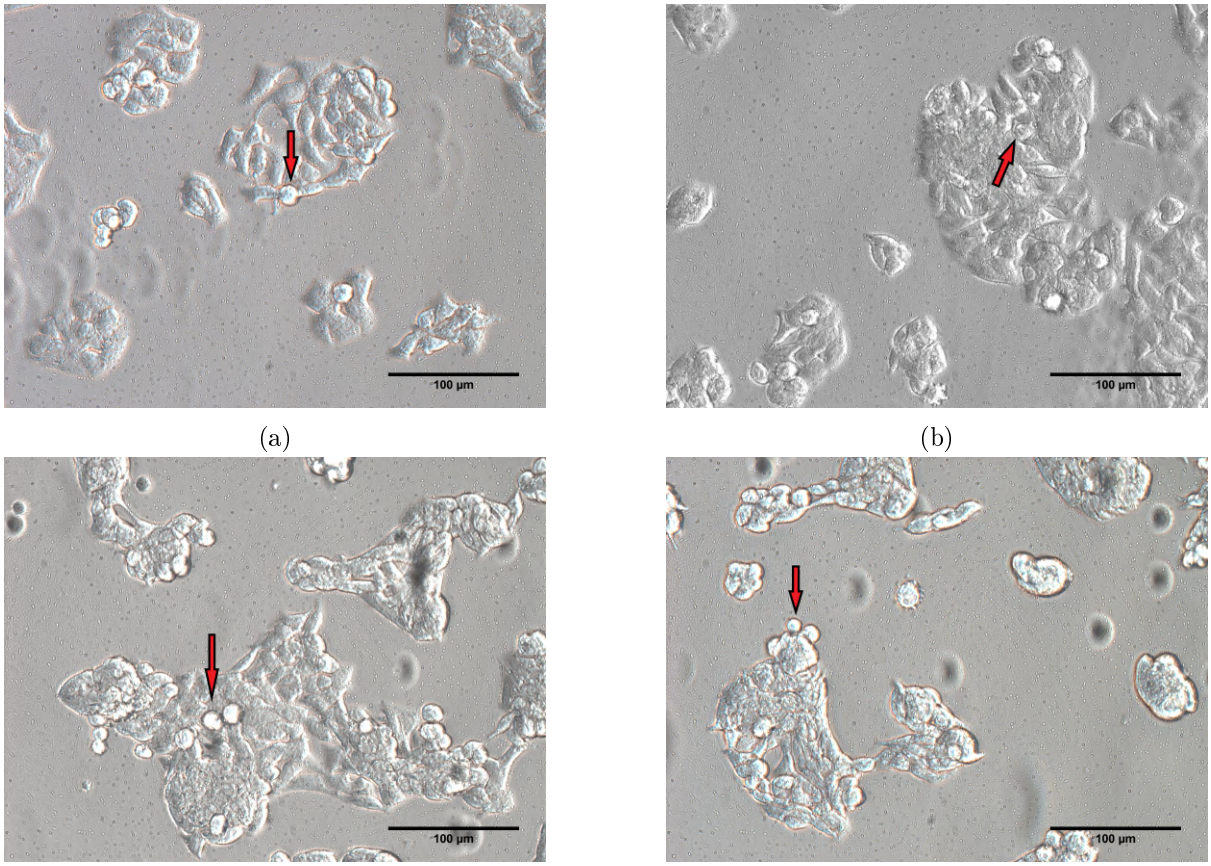

(a) (b)

(c) (d)

Figure 4.22: **Cell rounding, as indicated by red arrows, was observed after infection with BFT-rich supernatant for 3.5 hours. (a,b) Infected HT29 cells grown on glass. (c,d) Infected HT29 cells grown on 5% gelatin hydrogels.** Images are representative of three separate experiments and were taken by using the 20 x dry objective lens (NA 0.50) of a confocal microscope.

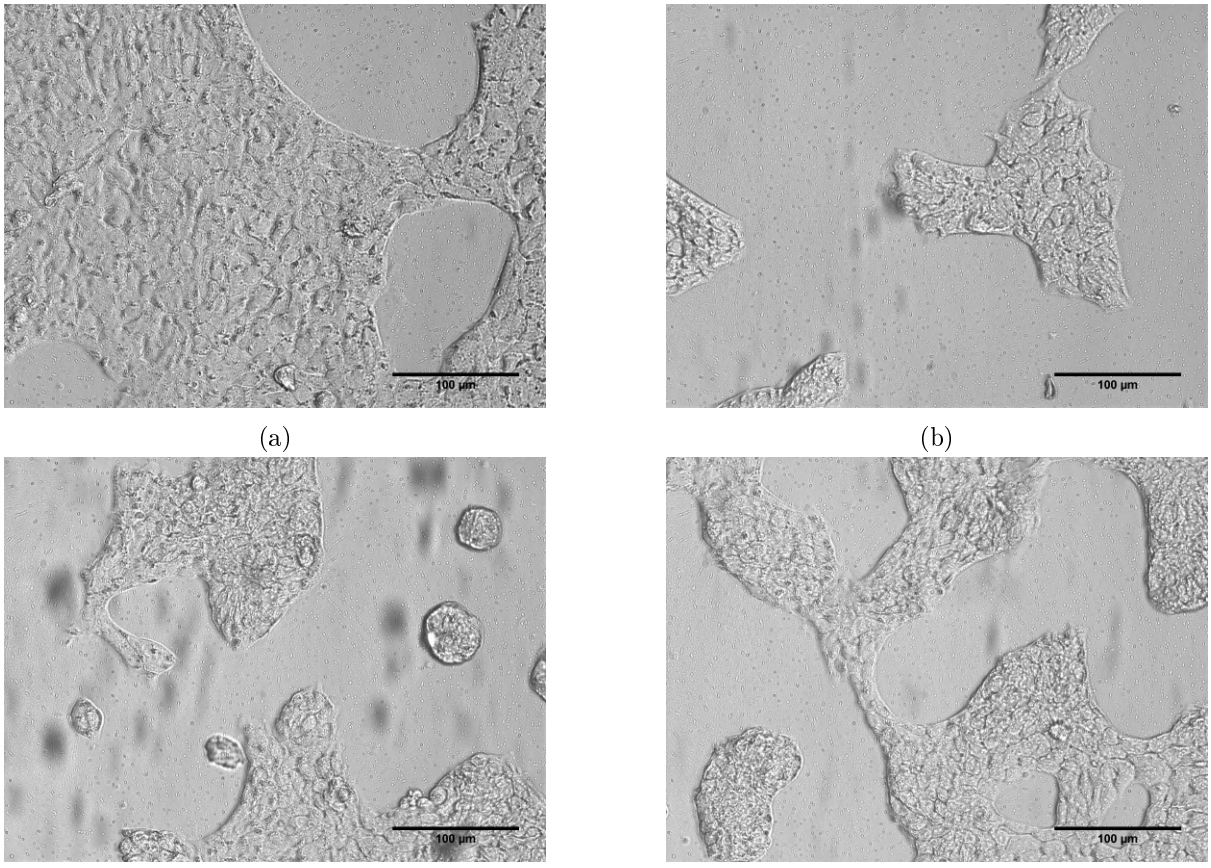

(a) (b)

(c) (d)

Figure 4.23: **No morphological changes were observed in HT29 cells grown on (a,b) glass and (c,d) 5% gelatin hydrogels, which were treated with concentrated supernatant derived from NTBF.** Images are representative of three separate experiments and were taken by using the 20 x dry objective lens (NA 0.50) of a confocal microscope.

Cell staining for E-cadherin (green) was carried out on BFT-treated HT29 cells and on HT29 cells that were treated with supernatant derived from NTBF. This was to identify whether BFT was involved with the loss of E-cadherin over time. Nuclear staining (blue) was also carried out to present a better visualisation of the cells before and after the application of BFT-rich supernatant and concentrated supernatant derived from NTBF. HT29 cells on glass and 5% gelatin hydrogels were incubated with BFT and supernatant derived from NTBF for 12 and 24 hours, followed by fixation and staining, and immunofluorescent confocal microscopy, as described in Section 3.15.

After 24 hours, BFT-treated HT29 cells that were grown on glass and 5% gelatin hydrogels exhibited cell rounding and the loss of E-cadherin. This was evident due to the lack of green staining at the cell peripheries, as shown in Figures 4.24a and 4.24b. In contrast, HT29 cells treated with supernatant derived from NTBF, that were grown on

glass and 5% gelatin hydrogels, had staining of E-cadherin at the cell peripheries after 24 hours of incubation (Fig. 4.24c and 4.24d). Nuclei were observed in the cytosol of all cells, as shown in Figures 4.24 and 4.26.

To better visualise the exact location of E-cadherin and nuclei in the HT29 cells that were treated with BFT and supernatant derived from NTBF for 24 hours, the E-cadherin and nuclear stain images were lay on top of the original bright field images. As shown in Figures 4.25a and 4.25b, BFT-treated HT29 cells on glass and 5% gelatin hydrogels did not show the presence of E-cadherin at the cell peripheries. In contrast, HT29 cells treated with supernatant derived from NTBF, that were grown on glass and 5% gelatin hydrogels, showed the presence of E-cadherin at the cell peripheries. This was confirmed by the location of the cell membranes in the bright field images, as shown in Figures 4.25c and 4.25d.

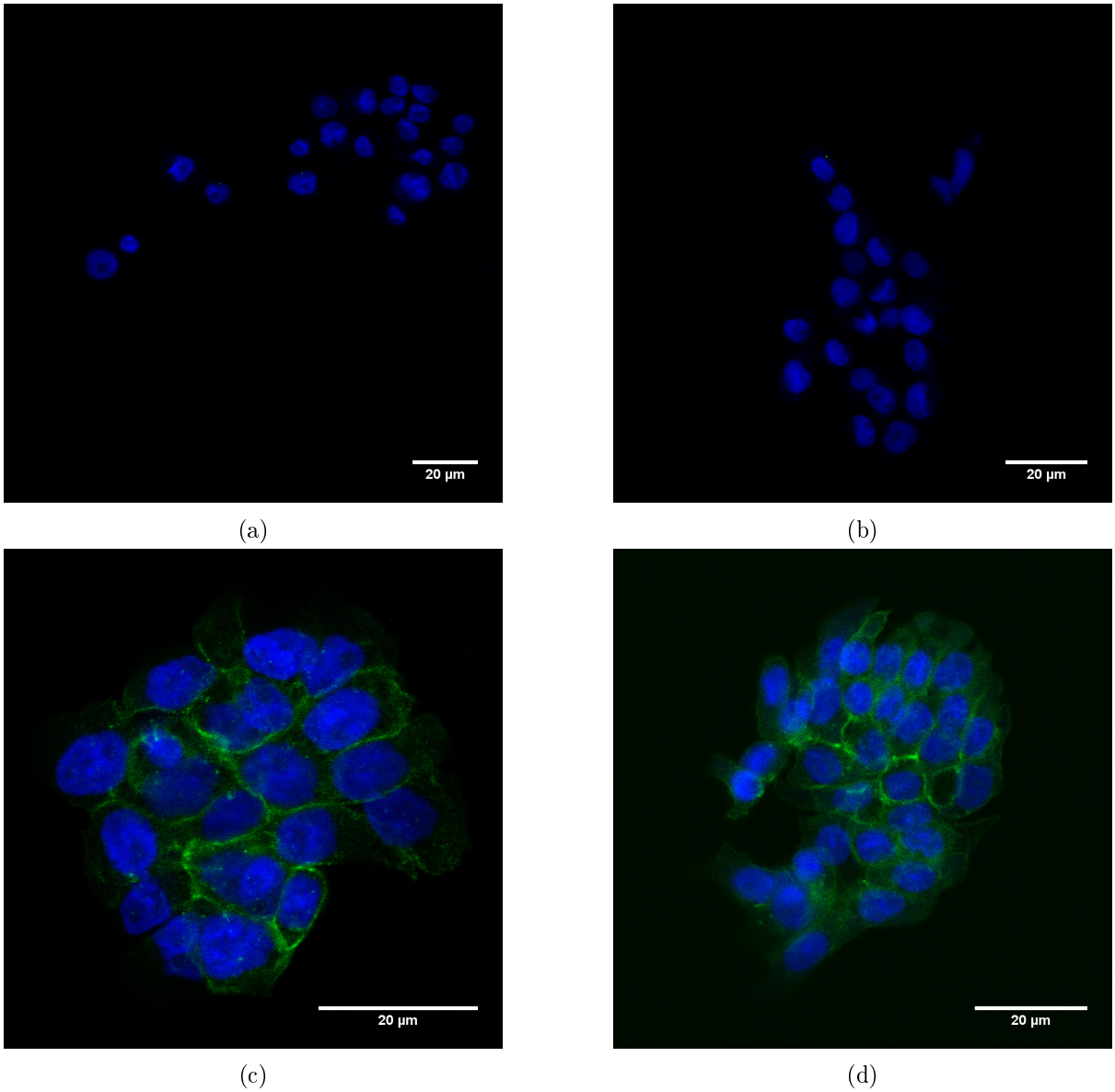

(a) (b)

(c) (d)

Figure 4.24: **After 24 hours, E-cadherin (green) was not present in BFT-treated HT29 cells grown on (a) glass and (b) a 5% gelatin hydrogel. E-cadherin was localised at the cell peripheries of HT29 cells grown on (c) glass and (d) 5% gelatin hydrogel, which were treated with concentrated supernatant derived from NTBF. Nuclei (blue) were observed to be present in the cytosol of cells treated with BFT (a,b) and concentrated supernatant derived from NTBF (c,d).** Images are representative of three separate experiments and were taken using the 20 x dry objective lens (NA 0.50) of a confocal microscope.

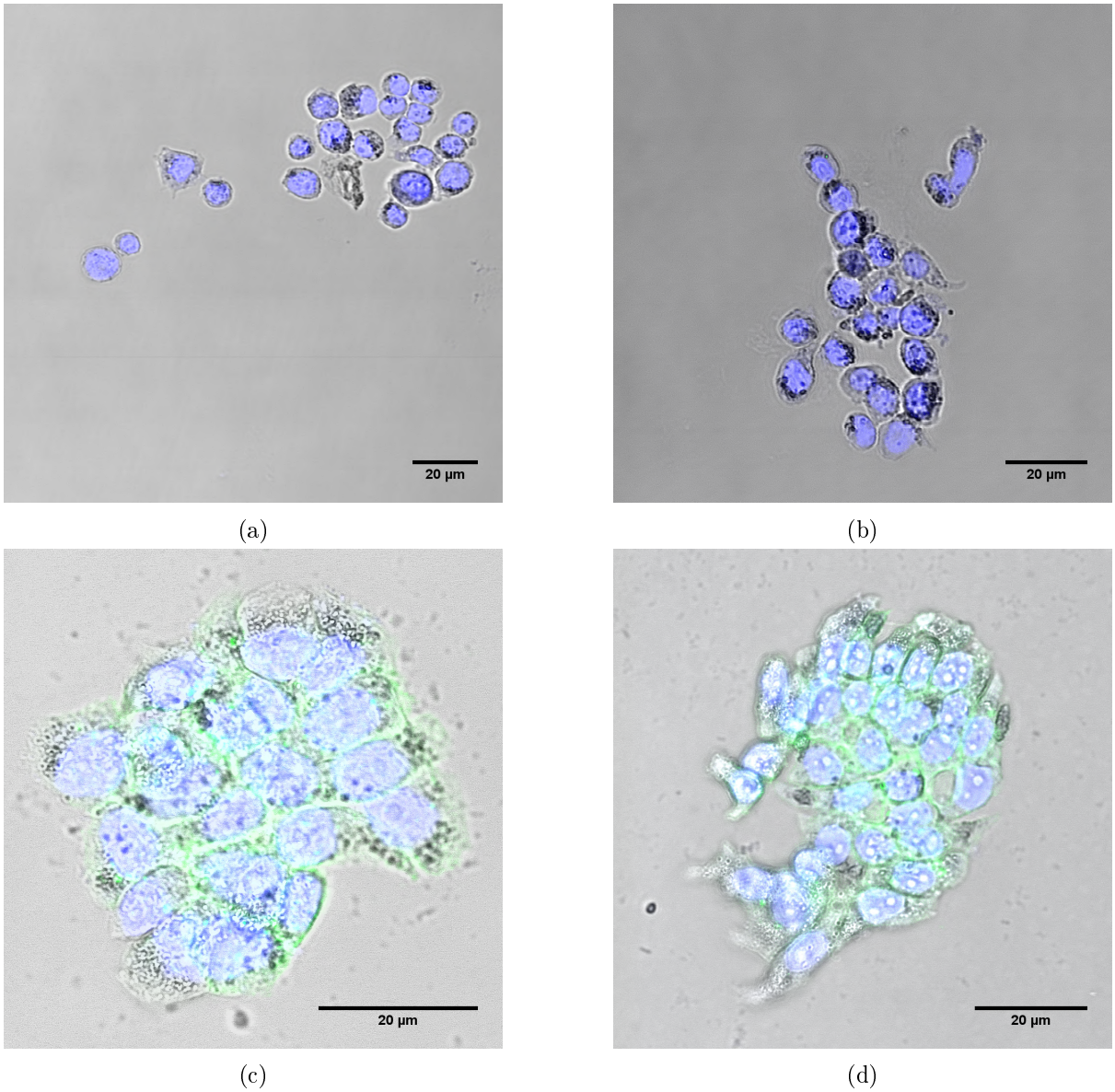

(a) (b)

(c) (d)

Figure 4.25: **After 24 hours, the localisation of E-cadherin (green) and nuclei (blue) were over-layed on the bright field images. E-cadherin was not present in BFT-treated HT29 cells grown on (a) glass and (b) a 5% gelatin hydrogel. E-cadherin was localised at the cell peripheries of HT29 cells grown on (c) glass and (d) 5% gelatin hydrogel, which were treated with concentrated supernatant derived from NTBF. Nuclei were observed in the cytosol of cells treated with BFT (a,b) and concentrated supernatant derived from NTBF (c,d).** Images are representative of three separate experiments and were taken using the 20 x dry objective lens (NA 0.50) of a confocal microscope.

After 12 hours, BFT-treated HT29 cells that were grown on glass and 5% gelatin hydrogels exhibited cell rounding and the loss of E-cadherin. This was visualised by the lack of green staining at the cell peripheries, as shown in Figures 4.26a and 4.26b. In contrast, HT29 cells treated with supernatant derived from NTBF, that were grown on glass and 5% gelatin hydrogels, had the presence of E-cadherin staining at the cell peripheries after

12 hours of incubation (Fig. 4.26c and 4.26d). Nuclei were observed in the cytosol of all cells, as shown in Figures 4.26 and 4.26.

To better visualise the exact location of E-cadherin and nuclei in the HT29 cells that were treated with BFT and supernatant derived from NTBF for 12 hours, the E-cadherin and nuclear stain images were lay on top of the original bright field images. As shown in Figures 4.27a and 4.27b, BFT-treated HT29 cells on glass and 5% gelatin hydrogels did not show the presence of E-cadherin at the cell peripheries. In contrast, HT29 cells treated with supernatant derived from NTBF, that were grown on glass and 5% gelatin hydrogels showed the presence of E-cadherin at the cell peripheries. This was confirmed by the location of the cell membranes in the bright field images, as shown in Figures 4.27c and 4.27d.

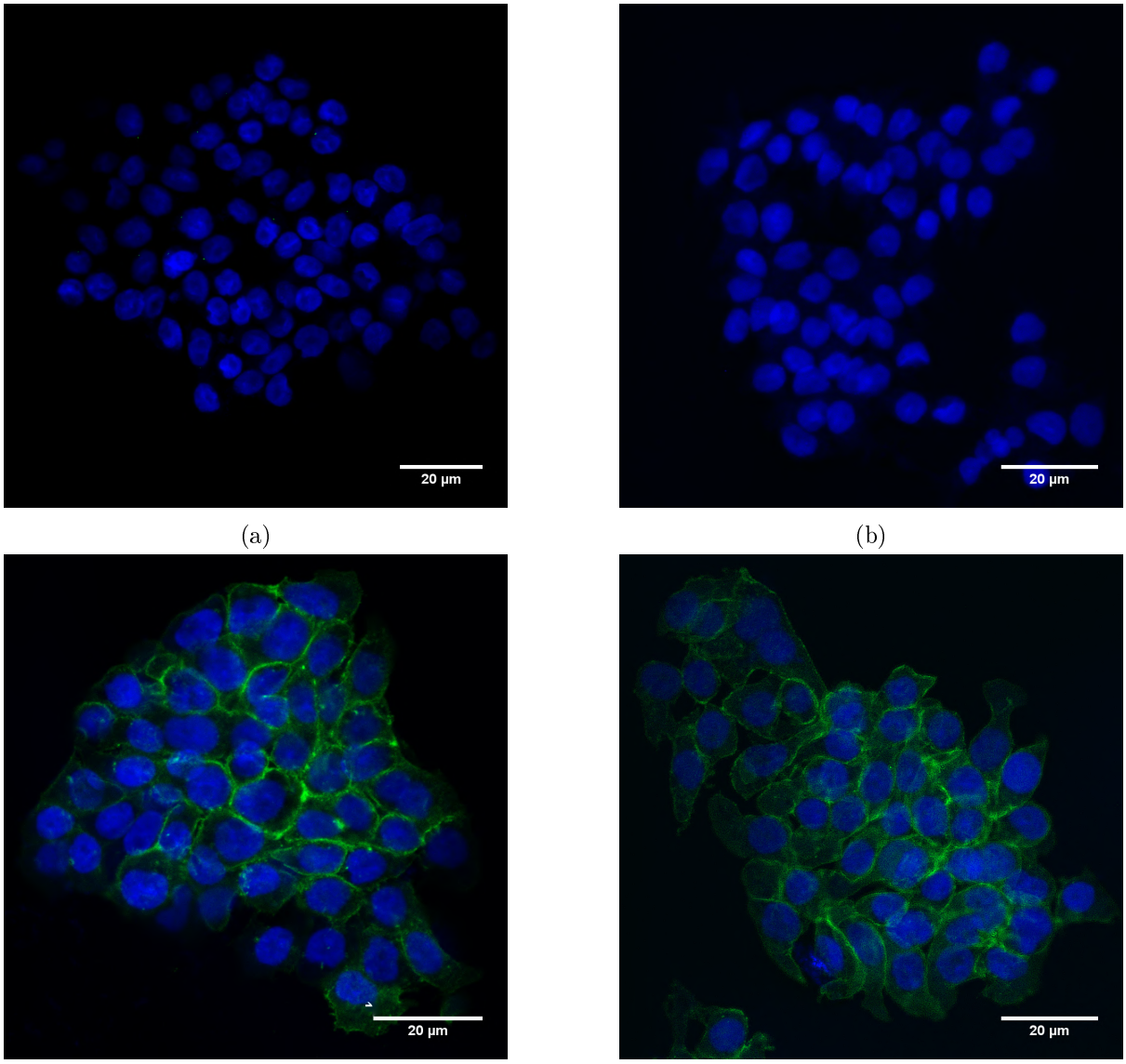

(a) (b)

(c) (d)

Figure 4.26: **After 12 hours, E-cadherin (green) was not present in BFT-treated HT29 cells grown on (a) glass and (b) a 5% gelatin hydrogel. E-cadherin was localised in HT29 cells grown on (c) glass and (d) 5% gelatin hydrogel, which were treated with concentrated supernatant derived from NTBF. Nuclei (blue) were observed to be present in the cytosol of cells treated with BFT (a,b) and concentrated supernatant derived from NTBF (c,d).** Images are representative of three separate experiments and were taken using the 20 x dry objective lens (NA 0.50) of a confocal microscope.

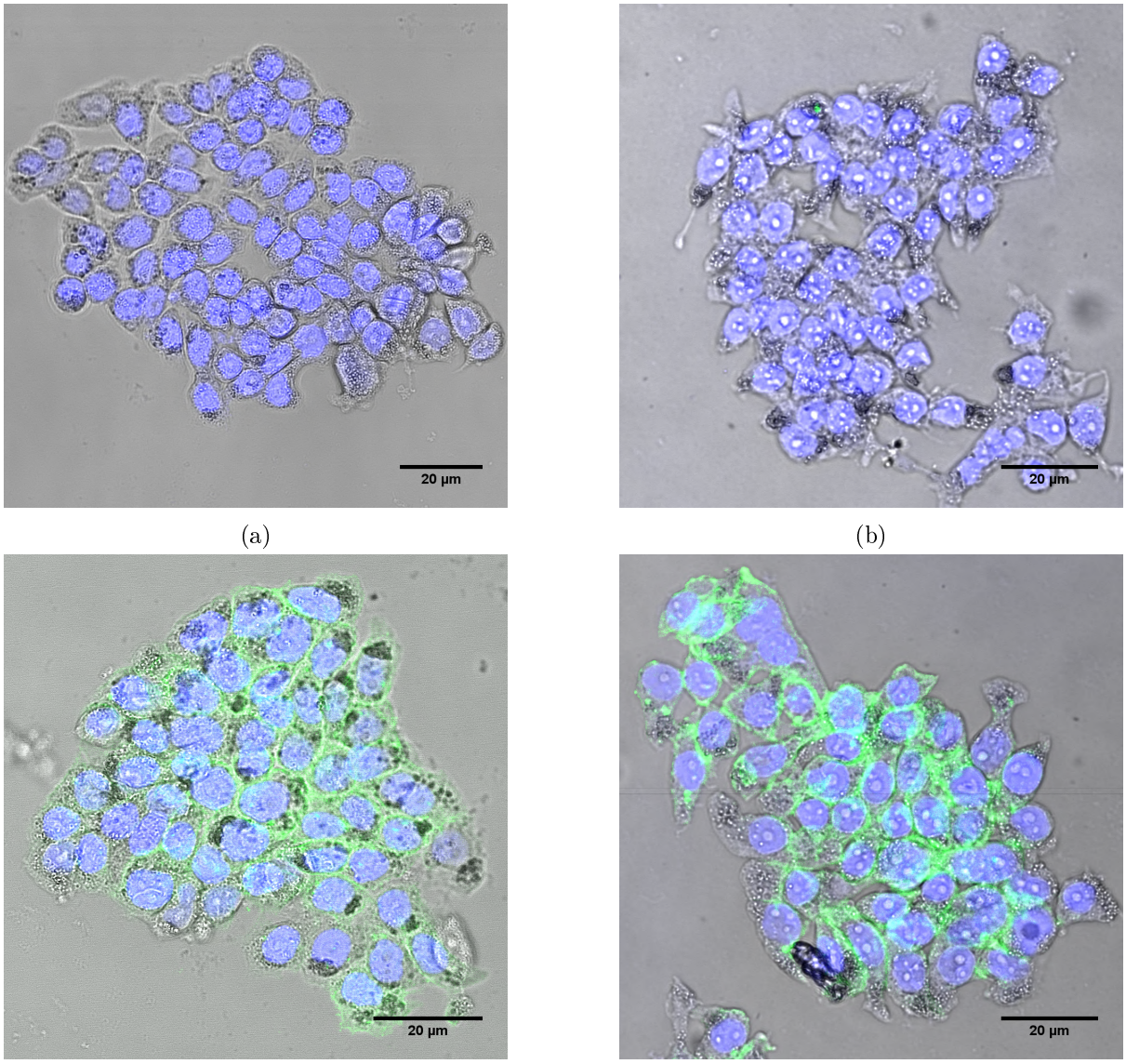

(a) (b)

(c) (d)

Figure 4.27: **After 12 hours, the localisation of E-cadherin (green) and nuclei (blue) were over-layed on the bright field images. E-cadherin was not present in BFT-treated HT29 cells grown on (a) glass and (b) a 5% gelatin hydrogel. E-cadherin was localised at the cell peripheries of HT29 cells grown on (c) glass and (d) 5% gelatin hydrogel, which were treated with concentrated supernatant derived from NTBF. Nuclei were observed in the cytosol of cells treated with BFT (a,b) and concentrated supernatant derived from NTBF (c,d).** Images are representative of three separate experiments and were taken using the 20 x dry objective lens (NA 0.50) of a confocal microscope.

Chapter 5

Discussion

5.1 Adherence and morphology of HT29 cells on polystyrene, PDMS and gelatin thin films

The adherence of HT29 cells was investigated on polystyrene (PS) well plates, PDMS, PS and PDMS coated with gelatin thin films. The aim was to identify whether gelatin could increase cellular adherence on both surfaces. Cell morphology was also analysed using the light microscope to identify whether cells were forming confluent layers after 24, 48 and 72 hours of incubation. All HT29 cells counted on PS after 72 hours were all adherent, as shown in Figure 4.1a, and exhibited normal cellular morphology and confluence, as shown in Figure 4.4a. This is consistent with previous literature, which showed that cells form adhesions to tissue culture treated PS surfaces, and formed confluent layers after at least 48 hours incubation, like the cells grown in the well plates used in this study [89, 90].

Cells grown on PDMS were non-adherent over the entire 72 hour incubation period, as shown in Figure 4.2a. This was expected as PDMS is inherently hydrophobic, which has been found to prevent cellular adhesion [91]. The cells also formed several three-dimensional clusters, suggesting that cells were adhering to each other, rather than to the PDMS surface (Fig. 4.5a). Several studies showed that surface treatment or modification of PDMS, such as plasma treatment, increased surface hydrophilicity and enhanced cellular adhesion [92, 93, 94]. Conventional oxygen plasma treatment in a vacuum chamber was found to decrease PDMS surface hydrophobicity and increase wettability, through

the removal of organic surface contaminants [95]. Fritz and Owen (1995) showed that after plasma treatment, low molecular weight material had diffused through the PDMS polymer matrix, which increase hydrophobicity and therefore led to an increase in contact angle [96]. Tan et al., (2010) showed that hydrophobic recovery of PDMS was prevented for weeks by storing the plasma treated PDMS in de-ionised water, which maintained hydrophilicity [97]. To increase hydrophilicity of the PDMS surface in this study, the PDMS could have been plasma treated prior to cell seeding, which may have increased cellular adhesion and promoted cells to form a confluent layer, rather than clusters as shown in Figure 4.5a. Hydrophilicity could have also been maintained over the 72 hour period as the PDMS was immersed in media the whole time.

Cells grown on the gelatin coated PS and PDMS plates showed no significant difference in the number of adhered and non-adhered cells after 72 hours of incubation, as shown in Figures 4.1b and 4.2b. Normal cellular morphology and confluence was observed prior to trypsinisation on the coated PS, as shown in Figure 4.4b. On the coated PDMS plate, cells had formed large three-dimensional clusters, suggesting that some cells had adhered to the gelatin surface and that other cells had grown on top of other cells to avoid the surface (Fig. 4.5b). PDMS is known to be porous, so the gelatin may have unevenly sunken in to the pores, leaving some areas of PDMS more exposed than others. This suggested that cells had formed clusters to avoid hydrophobic areas between the gelatin coating.

Cells were observed to remain adhered to the gelatin surface after trypsinisation, as shown in Figures 4.3a and 4.3b). Previous literature identified that gelatin aided cellular adhesion through linear arginine-glycine-aspartate (RGD) motifs [30] and that trypsin acted as a proteolytic enzyme which cleaved peptides on the C-terminal side or arginine or lysine. In this study, the cell count for adhered cells on PS and PDMS coated with gelatin may have been higher if the cells were trypsinised for a time period longer than ten minutes, as it would have allowed more time for the enzyme to cleave the RGD motifs adhering the cells to the gelatin thin films, therefore lifting more cells from the surface for counting [98]. The coated PDMS plate could have also been plasma treated prior to adding the gelatin thin film. This would have made the PDMS surface less porous,

preventing gelatin from unevenly sinking into it, thus forming an more even layer of gelatin on the PDMS surface for cells to adhere to. The cells may have then formed a confluent layer, similar to those seen in Figures 4.4b [96].

5.2 HT29 cellular morphology on collagen and gelatin hydrogels

Cells grown on 3%, 5% and 7% collagen hydrogels exhibited cell rounding and the formation of 3D clusters on the collagen gel surfaces. Previous literature showed that fibrillar collagen supports cellular adhesion through a subset of collagen-binding integrins [99]. Studies showed that HT29 cells were found to have high expression of the $\alpha 1\,\beta 1$ and $\alpha 2\,\beta 1$ integrins, and that $\alpha 2\,\beta 1$ specifically mediated adhesion of cells to type I collagen fibrils. The binding of $\alpha 2\,\beta 1$ may therefore possibly explain why cell clusters had adhered to the collagen surfaces in this study [100, 101, 102]. Haier et al., (1999) showed that HT29 cellular adhesion to components of the extracellular matrix was mediated by different integrins and was dependent on the substrate, such as type 4 collagen, laminin and fibronectin [103]. Another study by Haier et al., (1999) showed that other collagen-binding receptors, such as tyrosine kinases, affected and regulated intracellular signal transduction pathways, which in turn, regulated cell morphology and tumour growth of HT29 cells [102]. The activity of collagen-binding receptors in this study may possibly explain why the cells rounded up when grown on the three different concentration collagen hydrogels.

HT29 cells in this study exhibited normal morphology and confluence on 3%, 5% and 10% gelatin hydrogels after 72 hours incubation. These findings were consistent with previous literature, which identified that gelatin aids cellular adhesion through linear arginine-glycine-aspartate (RGD) motifs, as stated in Section 5.1 [30]. To further study HT29 cell confluence and morphology, integrin-mediated cell adhesion to the hydrogel surfaces could be investigated. Previous studies used immunocytochemistry to stain and localise different integrins, such as $\beta 1$, $\alpha 2$, 3 and 6, in HT29 cells grown on collagen and laminin [104, 103, 105]. Immunocytochemistry could therefore be used in the future to investigate HT29 cell adhesion on the different hydrogels, and potentially explain why cells rounded up on collagen hydrogels (Fig. 4.16) but not on gelatin hydrogels (Fig. 4.18).

Another reason for the observed cell morphologies on the hydrogels may have been due to the composition and cross-linking of the hydrogels. Previous literature showed that these factors affected integrin-mediated cell adhesion and had the potential to alter cellular binding and confluence across hydrogel surfaces [106]. Davidenko et al., (2016) showed that the availability of integrin binding sites for HT1080, C2C12 L3 and Rugli cells was strongly influenced by the extent of collagen hydrogel cross-linking. Davidenko et al., (2016) suggested that cross-linking can affect the number of cell recognition sequences that are important for cell-substrate interactions and binding. Other studies showed that HT29 cells grown on top of type I collagen hydrogels, or inside type I collagen hydrogel matrices, exhibited the formation of well-defined multi-cellular tumour spheroids, rather than 2D monolayers [13, 107]. The previous literature may therefore explain why HT29 cells formed 3D clusters on the collagen hydrogels in this study [106].

A limitation of investigating HT29 cell morphology on the different concentration collagen and gelatin hydrogels was that the hydrogel coatings in the bottom of the fluorodishes may not have had an even thickness in comparison to one another. Although 3 mL of each hydrogel was dispensed onto the bottom of each dish, as described in Section 3.8, the spreading of the hydrogels across the glass surfaces may not have been even in comparison to one another. This meant that there were likely some areas of hydrogel that were thicker than others, which in turn, may have affected cellular adhesion and morphology. Three different objective lenses were used to image cell morphology, as described in Section 3.8. This was because there were difficulties with focussing on clusters of HT29 cells on the different hydrogels, likely due to the differing thickness of the hydrogels in each dish. If this experiment were to be repeated, less hydrogel could be added to each fluorodish, which would possibly allow the use of the same objective lens for all of the imaging. The fluorodishes could also be placed on a tilt angle shaker to help spread the hydrogels evenly across the glass surfaces, before being incubated to complete cross-linking.

To further investigate HT29 cell morphology on gelatin hydrogels, dynamic mechanical analysis (DMA) could be carried out. DMA helps to identify the mechanical nature

of hydrogel samples and works by clamping a sample into a sample holder of a dynamical mechanical analyser machine. A sinusoidal force (stress) is then applied to the sample, followed by measurement of the displacement or deformation of the sample. Obtaining this information about the mechanical stress properties of the gelatin hydrogels would help to further characterise them. It would also allow for potential alteration of hydrogel composition to best mimic the composition of the human gut, which could potentially help to make the LOC devices more biologically relevant.

5.3 Contact angle of water on collagen and gelatin hydrogels

The hydrophobicity and hydrophilicity of water on the 3%, 5% and 10% gelatin hydrogels, and on the 3%, 5% and 7% collagen hydrogels was calculated by measuring the contact angle (CA) of water droplets on the surfaces. Hydrogels that have high concentrations of water show relatively low contact angles, indicating that the surfaces are hydrophilic [24]. It was therefore hypothesised that the 3% gelatin and collagen hydrogels would have the lowest measured mean CAs. The lowest mean CAs in this study were measured on the 5% gelatin ($\theta = 64.4°$) and 5% collagen ($\theta = 32.2°$) hydrogels, with the 3% gelatin ($\theta = 77.2°$) and collagen ($\theta = 34.9°$) hydrogels having higher CAs (Fig. 4.13 and 4.11). These results are consistent with those of Yasuda et al., (1994), which showed that the CA measurement of a 15% solid gelatin hydrogel was created due to the attractive force between the polymer molecules of the hydrogel sample and the sessile water droplets. They also showed that the CA resulted from the change in the configuration of the hydrogel surface molecules to reach equilibrium with the water droplet.

Hydrophobicity or hydrophilicity of hydrogels depends on the orientation of hydrophilic moieties toward the hydrogel-air interface [24, 108]. Holly and Refojo (1975) observed a low CA for water on the surface of a polyhydroxyethylmethacrylate hydrogel, by injecting an air bubble beneath the hydrogel surface immersed in water [109]. Their results suggested that at the hydrogel-water, interface the surface was hydrophilic, and at the the hydrogel-air interface, the surface was hydrophobic [109]. The groups were most likely

rotated and drawn into the mass of the hydrogel, thus lessening the number of hydrophilic moeities at the hydrogel-air interface and hence decreasing surface hydrophilicity [109]. Other studies support the findings of Holly and Refojo (1975), and have suggested that hydrogel exposure to air with low humidity can lead to the re-orientation of hydrophilic molecules in hydrogels with high water concentrations, leading to higher CA measurements than expected [24, 110].

With regards to the 3% gelatin and collagen hydrogels in this study, the polymer molecules within the gels may have been internally rotated toward the mass of the hydrogel disks, rather than facing toward the hydrogel-air interface. This likely meant that less hydrophilic molecules were present at the surface, possibly explaining why a high CA was measured for both gel types. If the CA measurements on the different gelatin and collagen hydrogel concentrations were carried out again, air humidity would be need to be taken into consideration. Measurements could be obtained in a temperature and humidity controlled room, where the air humidity could be moderated to prevent the re-orientation of hydrophilic molecules in the disks. Another approach would be controlling the exposure of the hydrogel surfaces to air. Rather than having all gel disk samples sitting on the bench when making single measurements, each sample could be kept in the fridge until a measurement needed to be made.

5.4 AlamarBlue assay of HT29 cell metabolism on collagen and gelatin hydrogels

The alamarBlue cell viability reagent was used to investigate the metabolic activity and health of HT29 cells grown on gelatin and collagen hydrogel surfaces over a 72 hour incubation period. Resazurin was the active reagent that was converted to resorufin by the reducing power of living cells [111]. Cell viability was then quantitatively measured by measuring the fluorescent wavelengths of the cell media after incubation with alamarBlue. HT29 cells grown on the PS controls, and on the 3%, 5% and 10% gelatin hydrogels showed a significant difference in cellular activity over the 72 hour incubation period, with a significant decrease in activity over 72 hours (Fig. 4.9). Similarly, cells grown on the PS controls and on the 3%, 5% and 7% collagen hydrogels showed a significant difference

in cellular activity over time, with an increase in activity after 72 hours of incubation, as shown in Figure 4.7. The hydrogel type and concentration had no significant effect on cellular activity over time, as shown in Figures 4.9 and 4.7.

AlamarBlue is known to act as an intermediate electron acceptor in the electron transport chain. Previous studies showed that NADPH, FADH and NADH acted as intermediate electron acceptors, which led to a conversion of resazurin to resorufin in living cells [112]. The results in this study are consistent with previous literature, which showed that an increase in cell-cell contacts of adherent 3T3 cells led to a decrease in ATP- and NAD-content, NAD-redox potential, lactate production, oxygen consumption, [113]. Hahn et al., (1998) showed that SV40T-3T3 cells at confluent densities exhibited low metabolic activity, with a decrease in NADH over time [113]. De Fries and Mitsuhashi (1995) showed that cell density of peripheral blood mononuclear cells (PBMC) led to a reduction in cellular metabolism. They observed a decrese in cellular proliferation when the cell density was too high, which led to less reduction of alamarBlue than expected [114]. This therefore supports the idea that in this study, the cells growing on the gelatin hydrogels became less metabolically active over time due to the formation of cell-cell contacts when the cells started to form confluent layers.

In this study, HT29 cells grown on the 3% and 7% collagen hydrogels formed small, 3D clusters after 72 hours of incubation, as shown in Figures 4.16a and 4.16c. HT29 cells grown on 5% collagen hydrogels formed 2D monolayers after 72 hours incubation, as shown in Figure 4.16b. The cluster formations observed were consistent with previous literature, which showed that cells grown in spheroids re-wired their metabolic networks to support the biosynthetic and energetic demands of spheroid / tumour growth [115]. The observed increase in metabolism of cells on the 5% hydrogel was possibly due to an increased energy demand over the 72 hour period, which was required for the migration of individual cells into a sheet and the formation of cell-cell junctions, such as E-cadherin.

If the alamarBlue assay for cell metabolism and health was carried out again, NADH could be used as a biomarker, and an NAD^+ and NADH in each well with cells could be quantified using a NAD / NADH colorimetric assay kit. Because NADH is a known

intermediate electron acceptor from resozurin [112], disseminating the amount of NADH in the samples over the 72 hour incubation period would help to provide further information about the metabolic activity of HT29 cells on the different hydrogels. A smaller incubation period, such as 48 hours could also be carried out, and alamarBlue measurements could be taken more frequently, such as every 8 to 12 hours, rather than every 20 hours. This may enable a more distinct metabolic trend to be disseminated and provide further information about HT29 cellular metabolism on the different hydrogels.

5.5 Seeding and growth of HT29 cells in LOC devices

Cells were seeded in the lumens of LOC devices at a density of $5\,\mathrm{x}\,10^{4}\,/\,\mathrm{mL}$. A total of $5\,\mu\mathrm{L}$ of cell suspension was pipetted into each lumen, so there was an approximate total of 50 cells seeded per $1\,\mu\mathrm{L}$ of cell suspension. The pump system was then set up at a flow rate of $5\,\mu\mathrm{L}$ per hour, which enabled the growing cells to access nutrients from fresh media, without being dislodged by sheer stress. The dimensions of the internal lumens within the LOC devices were measured to calculate how many cells would be required to coat the entire inner lumenal surface. The radius (r) of each lumen was 0.8 mm and the length (l) of each lumen was 10 mm. The total surface area (S_a) inside of the lumen was calculated using the equation, $S_a = 2\,\pi\,\mathrm{r}\,\mathrm{l}$. Surface area was calculated to be $50.3\,\mathrm{mm}^{2}$.

To calculate the area of a single HT29 cell which was in contact with the lumen surface, the cube root of the cell size was calculated using the equation, $\sqrt[3]{\text{cell size}}$. The known area of HT29 cells was $11\,\mu\mathrm{m}^{3}$, and cell size was calculated to be $2.2\,\mu\mathrm{m}^{2}$. To calculate the total number of cells required to coat the entire inner lumen surface, the total surface area of the lumen was divided by the area of a single cell in contact with the lumen surface.

Total number of cells was calculated to be:

$$\frac{50.3\mathrm{x}10^{6}}{2.2} = 22.9\mathrm{x}10^{6}\mathrm{cells}$$

.

The doubling time for HT29 cells was approximately 24 hours, and the cells in this study were sub-cultured when they had reached 80% to 90% confluence, or when the cell density was approximately 5×10^4 viable cells per cm^2. In this study, cells were seeded in the LOC devices at a density of 50 cells per μL, with a total volume of 5 μL. This meant it would have taken approximately 17 days for cells to coat the entire inner lumen surface. To coat the entire lumen surface with cells over a nine day period, 1 mL of the cell suspension left over from sub-culturing could have been centrifuged at 1000 G for three minutes to pellet the cells. The pellet would have contained approximately 50,000 cells, which could have been re-suspended in 5 μL of McCoy's media and then carefully seeded into the lumen of a LOC. At this seeding concentration, it would have taken approximately nine days to coat the entire inner lumen surface.

In this study, HT29 cells never fully coated the inner lumen surface because there were issues with the pump system. Specifically, the needle heads which were inserted into the holes of the LOC devices became slightly dislodged / disconnected over time, which led to media leakage and allowed air bubbles to get into the lumens. This in turn led to the lumens drying out over a short amount of time, which led to cell death. In microfluidics, there are three main approaches to form interconnections between LOC devices and tubing. These include the use of glue connectors on the LOC surfaces, the use of rubber O-rings, clamps or screws to form press-fit connections, and lastly, the direct insertion of tubes into LOC devices [116]. Wang et al., (2014) showed that a glued-tubing interface helped to prevent leakage of liquids from the channels within a PDMS LOC, which were then able to sustain inlet pressures of up to 600kPa [116].

Methodologically, Wang et al., (2014) applied a small amount of glue to the end of a plastic tube, which was then inserted into the LOC inlet. Following this, an uncured layer of PDMS was poured on top of the PDMS chip and was baked to solidify the PDMS [116]. In this study, HT29 cells were already adhered inside the lumens, and so the second layer of PDMS could not have been added and baked, as that would have dried out the hydrogel lumen and killed the cells. Wang et al, (2014) showed that at a flow rate of 10 mL per hour, leakage of coloured dye occurred from a micro-channel of a LOC which had been glued, but did not have the extra layer of PDMS added [116]. Their study

suggested that leakage from the needle inlets may not have occurred at far lower flow rate, such as the flow rate of 5 μL per hour which was used in this study. This suggests that to avoid media leakage in this study, the needle heads could have had glue applied to the ends before insertion into the LOC devices. Another reason why leakage may have occurred in this study was possible movement of the rigid Tefzel tubing which carried media from the reservoir into the LOC devices, and back out into the syringe. To prevent movement, the tubes could have been taped to the incubator shelf surface. This may have made it lessened tube movement and prevented slight dislodgement of the needles inserted in the LOC devices.

Future work will focus on applying BFT to HT29 cells grown inside the lumens of the LOC devices, through a passive pumping method. Immunostaining of E-cadherin, nuclei and actin could then be carried out, followed by immunofluorescent confocal microscopy, in order to detect and localise the aforementioned cell parts inside the LOC lumens. Future work could also focus on the E-cadherin / β-catenin complex, because it has been known to play a major role in tumour suppression. As seen in Figure 1.2, The intracellular domain of E-cadherin is bound to β-catenin. Several studies used western blotting and immunocytochemistry to show that loss of E-cadherin through the mechanism of BFT, led to the promotion of β-catenin release [117]. This has been associated with the facilitation of the epithelial-mesenchymal transition (EMT), which is known to play a role in cancer progression [117, 118].

5.6 E-cadherin localisation and effect of BFT on HT29 cells

HT29 cells grown on glass and 5% gelatin hydrogels were incubated with the non-toxigenic *Bacteroides fragilis* toxin (NTBF) control and BFT for three and a half hours. NTBF-treated HT29 cells on both the glass and hydrogel substrates exhibited no changes in morphology, as seen in Figure 4.23. BFT-treated cells grown on glass and hydrogel exhibited approximately 50% cell rounding after three and a half hours, as seen in Figure 4.22. HT29 cells on glass and hydrogel were then treated with NTBF and BFT for both 12 and 24 hours. During immunocytochemistry by immunofluorescent confocal microscopy,

the cells treated with NTBF exhibited the presence of cell nuclei (blue), which were localised in the cell cytosols, and E-cadherin (green), which were localised at the cell-cell interfaces, as observed in Figures 4.26c, 4.26d, 4.24c, 4.24d. These results are consistent with previous literature, which stated that NTBF was non-toxigenic, and showed that NTBF did not induce the loss of E-cadherin in HT29 cells [71, 66, 119].

The BFT-treated cells on glass and hydrogel exhibited the presence of cell nuclei (blue), which were localised in the cell cytosols. There was a clear loss of E-cadherin, because no green flourescence was observed at the HT29 cell-cell interfaces, as observed in Figures 4.26a, 4.26b, 4.24a, 4.24b. These results are consistent with previous literature, which showed that HT29 cells incubated with BFT lost the E-cadherin cell-cell junctions [72, 75, 120, 46]. Wu et al., (1998) treated HT29 / C1 cells with BFT (5 nM) for both 30 and 60 minutes, followed by cellular fixation with formaldehyde (10%), immunostaining of E-cadherin and immunofluorescent confocal microscopy (ICM) [72]. They showed that the BFT-treated cells exhibited cell rounding and had lost their E-cadherin junctions after both 30 and 60 minutes of incubation with BFT. A later study by Wu et al., (2003) also used ICM and showed that HT29 / C1 cells had become swollen and had lost E-cadherin junctions after treatment with BFT (100 ng / mL). They found that BFT rapidly cleaved E-cadherin and complete degradation was observed after one hour of incubation with BFT [75]. Koshy et al., (1996) showed that BFT (1 μg) stimulated a 10 to 25% increase in the cell volume of HT29 / C1 cells after 24 hours of incubation with BFT [121]. Other studies have used western blotting to show that cells treated with BFT lost the E-cadherin proteins [122, 46]. Hwang et al., (2013) treated HT29 / C1 cells with purified BFT (100 ng / ml) for 24 hours and western blotting showed that E-cadherin was not present [46].

A limitation of the staining process was that attempted actin microfilament staining did not work, which meant the distribution of actin before and after application of BFT could not be observed. Cellular fixation with 1% formaldehyde may have caused cellular contraction and changed the actin distribution in the cells. Future work will therefore focus on optimising the cellular fixation process and cell staining of actin, nuclei and E-cadherin. A previous study fixed HT29 cells with pre-cooled acetone and methanol (50 : 50

(v / v)) for 45 minutes, followed by immunostaining of E-cadherin and nuclei [123]. The use of acetone and methanol may have been gentler on the cells during fixation. In future, this may potentially preserve the cells better than the 1% formaldehyde solution used in this study. Another limitation was that only the 20 x dry objective lens (NA 0.50) of a confocal microscope was able to be used for imaging. This was likely because the 5% gelatin hydrogel surface in each fluorodish was unevenly spread, as described in Section 5.2, which meant that higher objective lenses were unable to see through the thicker parts of each hydrogel. As mentioned in Section 5.2, less hydrogel could be spread on the glass dish surface, which may have enabled the use of a higher magnification objective lens. This in turn would have provided higher resolution images of the E-cadherin and nuclei staining of HT29 cells treated with BFT and NTBF.

Chapter 6

Conclusions and Future Direction

Previous studies have identified a potential role of BFT in colon carcinogenesis, by which, the binding of BFT to a colonic epithelial cell receptor triggers an intracellular signalling cascade and induces cleavage of E-cadherin cell junctions in the intercellular space (Fig. 1.4). These in turn, lead to loss of cell polarity, cell rounding and eventually an increased risk of cancer formation [73, 75, 76]. In the present study, a lab-on-a-chip device was designed and fabricated, with the potential to model BFT as a possible driver of colon carcinogenesis. The HT29 colorectal cancer cell line was used in this study because cells exhibit a distinct change in cellular morphology after application of BFT. Cells grown on 5% gelatin hydrogels exhibited the loss of E-cadherin junctions after the application of BFT, supporting the role of BFT as a potential driver of colon carcinogenesis.

The LOC designed and fabricated in this study contained a hollow lumen inside, formed from a 5% gelatin hydrogel. The lumen shape mimicked the architecture of the human colon and provided a space for HT29 colorectal cancer cells to adhere to and grow in. The aim was for cells to form a fully confluent monolayer around the inner lumen surface. In this study, cells were found to adhere and grow inside the lumen; however, the initial seeding concentration was too low and the LOC had issues with leakage of media around the media inlet and outlet. Future work will focus on seeding HT29 cells at an optimum concentration, calculated in Section 5.5, so that the lumen would be fully coated within five to six days of incubation. Work will also aim to optimise the LOC devices so that they do not leak from around the inlet and outlet channels, possibly through the use of glue at the tubing-inlet interface, as described in Section 5.5.

In this study, the contact angle of three different concentration collagen and gelatin hydrogels were measured to identify hydrophobicity / hydrophilicty of the surfaces. Future work will focus on identifying the mechanical properties of the different hydrogels and focus on the optimisation of HT29 adherence and growth on the gelatin hydrogel surface used in the LOC devices. The morphology of HT29 cells grown on the hydrogels was also observed in this study to identify whether the hydrogels induced morphologies which were different to those observed on the polystyrene and glass controls, as seen in Figures 4.1a and 4.14. Future work will focus on integrin-mediated cell adhesion to the surfaces to identify how the HT29 cells specifically bind.

This study showed that BFT obtained from ETBF led to cell rounding and the cleavage E-cadherin cell-cell junctions in HT29 cells, which were grown on glass and 5% gelatin hydrogels (Section 5.6). This work gave proof of concept for the detection and localisation of the loss of E-cadherin and cell rounding on gelatin hydrogels, as seen in Figures 4.26b and 4.24b. Future work will focus on optimising and using the LOC device as a more biologically relevant platform to study carcinogenesis. As mentioned in Section 5.6, BFT could be applied to HT29 cells inside the lumen by passive pumping, which would mimic how liquid moves through the human gut. Immunocytochemistry could be also carried out to localise E-cadherin, nuclei and actin microfilaments within the cells grown inside of the lumens.

Lastly, the LOC devices could be modified to enable the formation of concentration gradients inside the lumens. Previous studies showed that the addition of an oxygen channel allowed for the diffusion of oxygen into the stream of liquid inside the lumen, which in turn mixed up the liquid and formed a concentration gradient from one end of the channel to the other [124]. As technologies for investigation of the mechanisms of cancer evolve, LOC devices appear to be an attractive options because they enable the creation of biologically relevant models which may be better than both 2D and 3D cell culture models. The LOC used in this study has great future potential to model and investigate carcinogenesis of the human gut, as well as modelling the effects of different toxins and drug treatments on different epithelial cancer cell lines.

Bibliography

[1] B. M. Baker and C. S. Chen. Deconstructing the third dimension – how 3d culture microenvironments alter cellular cues. *Journal of Cell Science*, 125(13):3015–3024, 2012.

[2] R. Edmondson, J. J. Broglie, A. F. Adcock, and L. Yang. Three-dimensional cell culture systems and their applications in drug discovery and cell-based biosensors. *ASSAY and Drug Development Technologies*, 12(4):207–218, 2014.

[3] K. Chitcholtan, E. Asselin, S. Parent, P. H. Sykes, and J. J. Evans. Differences in growth properties of endometrial cancer in three dimensional (3d) culture and 2d cell monolayer. *Experimental Cell Research*, 319(1):75–87, 2013.

[4] K. Kolind, K. W. Leong, F. Besenbacher, and M. Foss. Guidance of stem cell fate on 2d patterned surfaces. *Biomaterials*, 33(28):6626–6633, 2012.

[5] B. Nounamo, J. Liem, M. Cannon, and J. Liu. Myxoma virus optimizes cisplatin for the treatment of ovarian cancer in vitro and in a syngeneic murine dissemination model. *Molecular Therapy - Oncolytics*, 6:90–99, 2017.

[6] J. A. Holme. Xenobiotic metabolism and toxicity in primary monolayer cultures of hepatocytes. *NIPH annals*, 8(2):49—63, December 1985.

[7] M. R. Carvalho, D. Lima, R.L. Reis, J. M. Oliveira, and V. M. Correlo. Anti-cancer drug validation: the contribution of tissue engineered models. *Stem Cell Reviews and Reports*, 13(3):347–363, 2017.

[8] J. Fu, Y-K. Wang, M. T. Yang, R. A. Desai, X. Yu, Z. Liu, and C. S. Chen. Mechanical regulation of cell function with geometrically modulated elastomeric substrates. *Nature Methods*, 7:733, 2010.

[9] R. M. Ezzell, M. Toner, K. Hendricks, J. C. Y. Dunn, R. G. Tompkins, and M. L. Yarmush. Effect of collagen gel configuration on the cytoskeleton in cultured rat hepatocytes. *Experimental Cell Research*, 208(2):442–452, 1993.

[10] K. M. Mabry, S. Z. Payne, and K. S. Anseth. Microarray analyses to quantify advantages of 2d and 3d hydrogel culture systems in maintaining the native valvular interstitial cell phenotype. *Biomaterials*, 74:31–41, 2016.

[11] B. Glimelius, B. Norling, T. Nederman, and J. Carlsson. Extracellular matrices in multicellular spheroids of human glioma origin: Increased incorporation of proteoglycans and flbronectin as compared to monolayer cultures. *Apmis*, 96(1-6):433–444, 1988.

[12] H. Lu and M. H. Stenzel. Multicellular tumor spheroids (mcts) as a 3d in vitro evaluation tool of nanoparticles. *Small*, 14(13):1702858, 2018.

[13] M. Ranjbar-Mohammadi, M. Abbasian, E. Mousavi, and Z. Arab-Bafrani. Multicellular tumor spheroids formation of colorectal cancer cells on gelatin/plcl and collagen/plcl nanofibrous scaffolds. *European Polymer Journal*, 115:115–124, 2019.

[14] W. Y. Ho, S. K. Yeap, C. L. Ho, R. A. Rahim, and N. B. Alitheen. Development of multicellular tumor spheroid (mcts) culture from breast cancer cell and a high throughput screening method using the mtt assay. *PLOS ONE*, 7(9):e44640, 2012.

[15] L. A. Gurski, A. K. Jha, C. Zhang, X. Jia, and M. C. Farach-Carson. Hyaluronic acid-based hydrogels as 3d matrices for in vitro evaluation of chemotherapeutic drugs using poorly adherent prostate cancer cells. *Biomaterials*, 30(30):6076–6085, 2009.

[16] Y. Yamaguchi, D. Deng, Y. Sato, Y-T. Hou, R. Watanabe, K. Sasaki, M. Kawabe, E. Hirano, and T. Moringaga. Silicate fiber-based 3d cell culture system for anticancer drug screening. *Anticancer Research*, 33:5301–5310, 2013.

[17] S. Koga, A. Nakamura, H. Katayama, K. Okumura, K. Yoshimura, K. Shuzenji, T. Morinaga, and E. Hirano. Silicate fiber scaffold-based 3d perfusion cultures of the human colorectal cancer cell line ht-29 by using a microfluidic chip. *Alternatives to Animal Testing and Experimentation*, 20(2):57–65, 2015.

[18] R. H. Dosh, A. Essa, N. Jordan-Mahy, C. Sammon, and C. L. Le Maitre. Use of hydrogel scaffolds to develop an in vitro 3d culture model of human intestinal epithelium. *Acta Biomaterialia*, 62:128–143, 2017.

[19] A. Virgone-Carlotta, M. Lemasson, H. C. Mertani, J-J. Diaz, S. Monnier, T. Dehoux, H. Delanoë-Ayari, C. Rivière, and J-P. Rieu. In-depth phenotypic characterization of multicellular tumor spheroids: Effects of 5-fluorouracil. *PloS one*, 12(11):e0188100–e0188100, 2017.

[20] J. A. Jiménez-Torres, S. L. Peery, K. E. Sung, and D. J. Beebe. Lumenext: A practical method to pattern luminal structures in ecm gels. *Advanced healthcare materials*, 5(2):198–204, 2016.

[21] M. Rothbauer, H. Zirath, and P. Ertl. Recent advances in microfluidic technologies for cell-to-cell interaction studies. *Lab on a Chip*, 18(2):249–270, 2018.

[22] M. R. Carvalho, D. Barata, L. M. Teixeira, S. Giselbrecht, R. L. Reis, J. M. Oliveira, R. Truckenmüller, and P. Habibovic. Colorectal tumor-on-a-chip system: A 3d tool for precision onco-nanomedicine. *Science Advances*, 5(5):eaaw1317, 2019.

[23] V. C. Shukla, T-R. Kuang, A. Senthilvelan, N. Higuita-Castro, S. Duarte-Sanmiguel, S. N. Ghadiali, and D. Gallego-Perez. Lab-on-a-chip platforms for biophysical studies of cancer with single-cell resolution. *Trends in Biotechnology*, 36(5):549–561, 2018.

[24] T. Yasuda, T. Okuno, and H. Yasuda. Contact angle of water on polymer surfaces. *Langmuir*, 10(7):2435–2439, 1994.

[25] N. A. Peppas and E. W. Merrill. Poly(vinyl alcohol) hydrogels: Reinforcement of radiation-crosslinked networks by crystallization. *Journal of Polymer Science: Polymer Chemistry Edition*, 14(2):441–457, 1976.

[26] M. Hamidi, A. Azadi, and P. Rafiei. Hydrogel nanoparticles in drug delivery. *Advanced Drug Delivery Reviews*, 60(15):1638–1649, 2008.

[27] M. A. Daniele, A. A. Adams, J. Naciri, S. H. North, and F. S. Ligler. Interpenetrating networks based on gelatin methacrylamide and peg formed using concur-

rent thiol click chemistries for hydrogel tissue engineering scaffolds. *Biomaterials*, 35(6):1845–1856, 2014.

[28] S-Y. Jeong, J-H. Lee, Y. Shin, S. Chung, and H-J. Kuh. Co-culture of tumor spheroids and fibroblasts in a collagen matrix-incorporated microfluidic chip mimics reciprocal activation in solid tumor microenvironment. *PLOS ONE*, 11(7):e0159013, 2016.

[29] A. Paguirigan and D. J. Beebe. Gelatin based microfluidic devices for cell culture. *Lab on a Chip*, 6(3):407–413, 2006.

[30] A. Ito, A. Mase, Y. Takizawa, M. Shinkai, H. Honda, K-I. Hata, M. Ueda, and T. Kobayashi. Transglutaminase-mediated gelatin matrices incorporating cell adhesion factors as a biomaterial for tissue engineering. *Journal of Bioscience and Bioengineering*, 95(2):196–199, 2003.

[31] G. A. Di Lullo, S. M. Sweeney, J. Körkkö, L. Ala-Kokko, and J. D. San Antonio. Mapping the ligand-binding sites and disease-associated mutations on the most abundant protein in the human, type i collagen. *The Journal of Biological Chemistry*, 277(6):4223–4231, 2002.

[32] G. Pitingolo, A. Riaud, C. Nastruzzi, and V. Taly. Gelatin-coated microfluidic channels for 3d microtissue formation: On-chip production and characterization. *Micromachines*, 10(265):1–11, 2019.

[33] I. Van Nieuwenhove, A. Salamon, K. Peters, G-J. Graulus, J. C. Martins, D. Frankel, K. Kersemans, F. De Vos, S. Van Vlierberghe, and P. Dubruel. Gelatin- and starch-based hydrogels. part a: Hydrogel development, characterization and coating. *Carbohydrate Polymers*, 152:129–139, 2016.

[34] P. Louis, G. L. Hold, and H. J. Flint. The gut microbiota, bacterial metabolites and colorectal cancer. *Nature Reviews Microbiology*, 12:661, 2014.

[35] I. I. Ivanov and D. R. Littman. Modulation of immune homeostasis by commensal bacteria. *Current Opinion in Microbiology*, 14(1):106–114, 2011.

[36] C. L. Sears. A dynamic partnership: Celebrating our gut flora. *Anaerobe*, 11(5):247–251, 2005.

[37] C-J. Chang, C-S. Lin, J. Martel, D. M. Ojcius, W-F. Lai, C-C. Lu, Y-F. Ko, J. D. Young, and H-C. Lai. Modulation of host immune response by *Bacteroides fragilis* polysaccharides: a review of recent observations. *Journal of Biomedical and Laboratory Sciences*, 28(1):1–6, 2016.

[38] S. Franzenburg, J. Walter, S. Künzel, J. Wang, J. F. Baines, T. C. G. Bosch, and S. Fraune. Distinct antimicrobial peptide expression determines host species-specific bacterial associations. *Proceedings of the National Academy of Sciences of the United States of America*, 110(39):E3730–E3738, 2013.

[39] U. Cavallaro and E. Dejana. Adhesion molecule signalling: not always a sticky business. *Nature Reviews Molecular Cell Biology*, 12:189, 2011.

[40] G. Bazzoni and E. Dejana. Endothelial cell-to-cell junctions: Molecular organization and role in vascular homeostasis. *Physiological Reviews*, 84(3):869–901, 2004.

[41] T. J. C. Harris and U. Tepass. Adherens junctions: from molecules to morphogenesis. *Nature Reviews Molecular Cell Biology*, 11:502, 2010.

[42] J. M. Halbleib and W. J. Nelson. Cadherins in development: cell adhesion, sorting, and tissue morphogenesis. *Genes & development*, 20(23):3199–3214, 2006.

[43] E. Kohfeldt, P. Maurer, C. Vannahme, and R. Timpl. Properties of the extracellular calcium binding module of the proteoglycan testican. *FEBS letters*, 414(3):557–561, 1997.

[44] M. El-Bahrawy, S. R. Poulsom, A. J. Rowan, I. T. Tomlinson, and M. R. Alison. Characterization of the e-cadherin/catenin complex in colorectal carcinoma cell lines. *International Journal of Experimental Pathology*, 85(2):65–74, 2004.

[45] C. P. Chen, S. Posy, A. Ben-Shaul, L. Shapiro, and B. H. Honig. Specificity of cell–cell adhesion by classical cadherins: critical role for low-affinity dimerization through β-strand swapping. *Proceedings of the National Academy of Sciences*, 102(24):8531–8536, 2005.

[46] S. Hwang, S-Y. Gwon, Sook K. M., S. Lee, and K-J. Rhee. *Bacteroides fragilis* toxin induces il-8 secretion in ht29/c1 cells through disruption of e-cadherin junctions. *Immune network*, 13:213–7, 2013.

[47] T. S. Jou, D. B. Stewart, J. Stappert, W. J. Nelson, and J. A. Marrs. Genetic and biochemical dissection of protein linkages in the cadherin-catenin complex. *Proceedings of the National Academy of Sciences of the United States of America*, 92(11):5067–5071, 1995.

[48] S. A. Kim, K. Inamura, M. Yamauchi, R. Nishihara, K. Mima, Y. Sukawa, T. Li, M. Yasunari, T. Morikawa, K. C. Fitzgerald, C. S. Fuchs, K. Wu, A. T. Chan, X. Zhang, S. Ogino, and Z. R. Qian. Loss of cdh1 (e-cadherin) expression is associated with infiltrative tumour growth and lymph node metastasis. *British Journal Of Cancer*, 114:199, 2016.

[49] A. C. Daulagala, M. C. Bridges, and A. Kourtidis. E-cadherin beyond structure: A signaling hub in colon homeostasis and disease. *International journal of molecular sciences*, 20(11):2756, 2019.

[50] C. L. Sears. Enterotoxigenic *Bacteroides fragilis*: a rogue among symbiotes. *Clinical Microbiology Reviews*, 22(2):349–369, 2009.

[51] M. Plunkett, M. Murray, F. Frizelle, Lo. Teague, and M. Hinder, V.and Findlay. Colorectal adenocarcinoma cancer in new zealand in those under 25 years of age (1997–2007). *ANZ Journal of Surgery*, 84(5):371–375, 2014.

[52] M. Arnold, M. S. Sierra, M. Laversanne, I. Soerjomataram, A. Jmal, and F. Bray. Global patterns and trends in colorectal cancer incidence and mortality. *Gut*, 66(4):683–691, 2017.

[53] E. R. Fearon. Molecular genetics of colorectal cancer. *Annual Review of Pathology: Mechanisms of Disease*, 6(1):479–507, 2011.

[54] D. M. Flood, N. S. Weiss, L. S. Cook, J. C. Emerson, S. M. Schwartz, and J. D. Potter. Colorectal cancer incidence in asian migrants to the united states and their descendants. *Cancer Causes & Control: CCC*, 11(5):403–411, 2000.

[55] M. A. Azcárate-Peril, M. Sikes, and J. M. Bruno-Bárcena. The intestinal microbiota, gastrointestinal environment and colorectal cancer: a putative role for probiotics in prevention of colorectal cancer? *American Journal of Physiology-Gastrointestinal and Liver Physiology*, 301(3):G401–G424, 2011.

[56] T. Norat, A. Lukanova, P. Ferrari, and E. Riboli. Meat consumption and colorectal cancer risk: Dose-response meta-analysis of epidemiological studies. *International Journal of Cancer*, 98(2):241–256, 2002.

[57] A. Richardson, J. Hayes, C. Frampton, and J. Potter. Modifi able lifestyle factors that could reduce the incidence of colorectal cancer in new zealand. *New Zealand Medical Journal*, 129(1447), 2016.

[58] Y. Yamada and H. Mori. Pre-cancerous lesions for colorectal cancers in rodents: a new concept. *Carcinogenesis*, 24(6):1015–1019, 2003.

[59] D. Barata, C. van Blitterswijk, and P. Habibovic. High-throughput screening approaches and combinatorial development of biomaterials using microfluidics. *Acta Biomaterialia*, 34:1–20, 2016.

[60] J. Allen, S. Hao, C. L. Sears, and W. Timp. Epigenetic changes induced by *Bacteroides fragilis* toxin. *Infection and Immunity*, 87(6):e00447–18, 2019.

[61] F. A. Uzal, B. L. Plattner, and J. M. Hostetter. Chapter 1 - alimentary system. In M. Grant Maxie, editor, *Jubb, Kennedy & Palmer's Pathology of Domestic Animals: Volume 2 (Sixth Edition)*, pages 1–257.e2. W.B. Saunders, 2016.

[62] M. Pop, J. N. Paulson, S. Chakraborty, I. Astrovskaya, B. R. Lindsay, S. Li, H. C. Bravo, C. Harro, J. Parkhill, A. W. Walker, R. I. Walker, D. A. Sack, and O. C. Stine. Individual-specific changes in the human gut microbiota after challenge with enterotoxigenic escherichia coli and subsequent ciprofloxacin treatment. *BMC Genomics*, 17(1):440, 2016.

[63] R. Smits, P. Ruiz, S. Diaz–Cano, A. Luz, S. Jagmohan–Changur, C. Breukel, C. Birchmeier, W. Birchmeier, and R. Fodde. E-cadherin and adenomatous polyposis coli mutations are synergistic in intestinal tumor initiation in mice. *Gastroenterology*, 119(4):1045–1053, 2000.

[64] D. Pinto and H. Clevers. Wnt, stem cells and cancer in the intestine. *Biology of the Cell*, 97(3):185–196, 2005.

[65] F. Corini, G. Tomasello, A. Jurjus, A. Geagea, S. Al Kattar, P. Damiani, E. Sinagra, F. Rappa, S. David, F. Cappello, M. Mazzola, and A. Leone. Colorectal cancer and

inflammatory bowel diseases: Effects of diet and antioxidants. *Journal of biological regulators and homeostatic agents*, 31:149–153, 07 2017.

[66] C. L. Sears, A. L. Geis, and F. Housseau. *Bacteroides fragilis* subverts mucosal biology: from symbiont to colon carcinogenesis. *The Journal of Clinical Investigation*, 124(10):4166–4172, 2014.

[67] S. K. Mazmanian, J. L. Round, and D. L. Kasper. A microbial symbiosis factor prevents intestinal inflammatory disease. *Nature*, 453:620, 2008.

[68] R. R. Vines, S. S. Perdue, J. S. Moncrief, D. R. Sentz, Lisa A. Barroso, R. L. Wright, and T. D. Wilkins. Fragilysin, the enterotoxin from *Bacteroides fragilis*, enhances the serum antibody response to antigen co-administered by the intranasal route. *Vaccine*, 19(6):655–660, 2000.

[69] M. J. Avila-Campos, C. Liu, Y. Song, M-C. Rowlinson, and S. M. Finegold. Determination of bft gene subtypes in *Bacteroides fragilis* clinical isolates. *Journal of Clinical Microbiology*, 45(4):1336–1338, 2007.

[70] E. B. Troy and D. L. Kasper. Beneficial effects of *Bacteroides fragilis* polysaccharides on the immune system. *Frontiers in bioscience : a journal and virtual library*, 15:25–34, 2010.

[71] A. Boleij, E. M. Hechenbleikner, A. C. Goodwin, R. Badani, Ellen M. Stein, M. G. Lazarev, B. Ellis, K. C. Carroll, E. Albesiano, E. C. Wick, E. A. Platz, D. M. Pardoll, and C. L. Sears. The *Bacteroides fragilis* toxin gene is prevalent in the colon mucosa of colorectal cancer patients. *Clinical Infectious Diseases*, 60(2):208–215, 2015.

[72] S. Wu, K-C. Lim, J. Huang, R. F. Saidi, and C. L. Sears. *Bacteroides fragilis* enterotoxin cleaves the zonula adherens protein, e-cadherin. *Proceedings of the National Academy of Sciences of the United States of America*, 95(25):14979–14984, 1998.

[73] R. V. Purcell, J. Pearson, A. Aitchison, L. Dixon, F. A. Frizelle, and J. I. Keenan. Colonization with enterotoxigenic *Bacteroides fragilis* is associated with early-stage colorectal neoplasia. *PLOS ONE*, 12(2):e0171602, 2017.

[74] G. Christofori and H. Semb. The role of the cell-adhesion molecule e-cadherin as a tumour-suppressor gene. *Trends in Biochemical Sciences*, 24(2):73–76, 1999.

[75] S. Wu, P. J. Morin, D. Maouyo, and C. L. Sears. *Bacteroides fragilis* enterotoxin induces c-myc expression and cellular proliferation. *Gastroenterology*, 124:392–400, 2003.

[76] N. U. Toprak, A. Yagci, B. M. Gulluoglu, M. L. Akin, P. Demirkalem, T. Celenk, and G. Soyletir. A possible role of *Bacteroides fragilis* enterotoxin in the aetiology of colorectal cancer. *Clinical Microbiology and Infection*, 12(8):782–786, 2006.

[77] K. S. Viljoen, A. Dakshinamurthy, P. Goldberg, and J. M. Blackburn. Quantitative profiling of colorectal cancer-associated bacteria reveals associations between fusobacterium spp., enterotoxigenic *Bacteroides fragilis* (etbf) and clinicopathological features of colorectal cancer. *PLOS ONE*, 10(3):e0119462, 2015.

[78] Jacqueline I. Keenan, Alan Aitchison, Rachel V. Purcell, Rosie Greenlees, John F. Pearson, and Frank A. Frizelle. Screening for enterotoxigenic *Bacteroides fragilis* in stool samples. *Anaerobe*, 40:50–53, 2016.

[79] J. Fogh and G. Trempe. New human tumor cell lines. In Jørgen Fogh, editor, *Human tumor cell in vitro*, pages 115–159. Springer, New York, 1975.

[80] L. M. Mundy and C. L. Sears. Detection of toxin production by *Bacteroides fragilis*: Assay development and screening of extraintestinal clinical isolates. *Clinical Infectious Diseases*, 23(2):269–276, 1996.

[81] R. F. Saidi, K. Jaeger, M. H. Montrose, S. Wu, and C. L. Sears. *Bacteroides fragilis* toxin alters the actin cytoskeleton of ht29/c1 cells in vivo qualitatively but not quantitatively. *Cell Motility ans the Cytoskeleton*, 37:159–165, 1997.

[82] Amy L. Paguirigan and David J. Beebe. Protocol for the fabrication of enzymatically crosslinked gelatin microchannels for microfluidic cell culture. *Nature Protocols*, 2:1782, 2007.

[83] Y. Tamada and Y. Ikada. *Cell Attachment to Various Polymer Surfaces*, volume 34. Springer US, 1986. Polymers in Medicine II.

[84] A. A. Franco, A. Goodman, and C. L. Sears. Modulation of bft expression by the *Bacteroides fragilis* pathogenicity island and its flanking region. *Molecular Microbiology*, 45(5):1067–1077, 2002.

[85] H. J. Windle and D. Kelleher. Identification and characterization of a metalloprotease activity from helicobacter pylori. *Infection and Immunity*, 70(5):2463–2471, 1997.

[86] S. Wu, L. A. Dreyfus, A. O. Tzianbos, C. Hayashi, and C. L. Sears. Diversity of the metalloprotease toxin produced by enterotoxigenic *Bacteroides fragilis*. *Infection and Immunity*, 70(5):2463–2471, 2002.

[87] M. F. Graham, R. F. Diegelmann, C. O. Elson, W. J. Lindblad, N. Gotschalk, S. Gay, and R. Gay. Collagen content and types in the intestinal strictures of crohn's disease. *Gastroenterology*, 94:257–265, 1988.

[88] S. Munshi, R. C. Twining, and R. Dahl. Alamar blue reagent interacts with cell-culture media giving different fluorescence over time: Potential for false positives. *Journal of Pharmacological and Toxicological Methods*, 70(2):195–198, 2014.

[89] J. C. Olson, J. E. Fraylick, E. M. McGuffie, K. M. Dolan, T. L. Yahr, Dara W. F., and T. S. Vincent. Interruption of multiple cellular processes in ht-29 epithelial cells by *Pseudomonas aeruginosa* exoenzyme s. *Infection and Immunity*, 67(6):2847–2854, 1999.

[90] M. J. Lerman, J. Lembong, S. Muramoto, G. Gillen, and J. P. Fisher. The evolution of polystyrene as a cell culture material. *Tissue Engineering Part B: Reviews*, 24(5):359–372, 2018.

[91] D. Bodas and C. Khan-Malek. Hydrophilization and hydrophobic recovery of pdms by oxygen plasma and chemical treatment—an sem investigation. *Sensors and Actuators B: Chemical*, 123(1), 2007.

[92] E. Leclerc, Y. Sakai, and T. Fujii. Cell culture in 3-dimensional microfluidic structure of pdms (polydimethylsiloxane). *Biomedical Microdevices*, 5(2):109–114, 2003.

[93] M-H. Wu. Simple poly(dimethylsiloxane) surface modification to control cell adhesion. *Surface and Interface Analysis*, 41(1):11–16, 2009.

[94] Z. Qian, D. Ross, W. Jia, Q. Xing, and F. Zhao. Bioactive polydimethylsiloxane surface for optimal human mesenchymal stem cell sheet culture. *Bioactive materials*, 3(2):167–173, 2018.

[95] D. Bodas and C. Khan-Malek. Formation of more stable hydrophilic surfaces of pdms by plasma and chemical treatments. *Microelectronic Engineering*, 83(4):1277–1279, 2006.

[96] J. L. Fritz and M. J. Owen. Hydrophobic recovery of plasma-treated polydimethylsiloxane. *The Journal of Adhesion*, 54(1-4):33–45, 1995.

[97] S. H. Tan, N-T. Nguyen, Y. C. Chua, and T. G. Kang. Oxygen plasma treatment for reducing hydrophobicity of a sealed polydimethylsiloxane microchannel. *Biomicrofluidics*, 4(3):032204, 2010.

[98] M. A. Brown, C. S. Wallace, C. C. Anamelechi, E. Clermont, W. M. Reichert, and G. A. Truskey. The use of mild trypsinization conditions in the detachment of endothelial cells to promote subsequent endothelialization on synthetic surfaces. *Biomaterials*, 28(27):3928–3935, 2007.

[99] S. R. Caliari and J. A. Burdick. A practical guide to hydrogels for cell culture. *Nature methods*, 13(5):405–414, 2016.

[100] S. Hamaia and R. W. Farndale. Integrin recognition motifs in the human collagens. In Donald Gullberg, editor, *I Domain Integrins*, pages 127–142. Springer Netherlands, Dordrecht, 2014.

[101] C. Zeltz and D. Gullberg. The integrin–collagen connection – a glue for tissue repair? *Journal of Cell Science*, 129(4):653–664, 2016.

[102] J. Haier, M. Nasralla, and G. L. Nicolson. Influence of phosphotyrosine kinase inhibitors on adhesive properties of highly and poorly metastatic ht-29 colon carcinoma cells to collagen. *International Journal of Colorectal Disease*, 14(2):119–127, 1999.

[103] J. Haier, M. Nasralla, and G. L. Nicolson. Different adhesion properties of highly and poorly metastatic ht-29 colon carcinoma cells with extracellular matrix com-

ponents: role of integrin expression and cytoskeletal components. *British Journal of Cancer*, 80(12):1867–1874, 1999.

[104] C. Schreiner, J. Bauer, M. Margolis, and R. L. Juliano. Expression and role of integrins in adhesion of human colonic carcinoma cells to extracellular matrix components. *Clinical & Experimental Metastasis*, 9(2):163–178, 1991.

[105] Maxime Lehmann, Assou El Battari, Brigitte Abadie, Jean-Michel Martin, and Jacques Marvaldi. Role of αvβ5 and αvβ6 integrin glycosylation in the adhesion of a colonic adenocarcinoma cell line (ht29-d4). *Journal of Cellular Biochemistry*, 61(2):266–277, 1996.

[106] N. Davidenko, C. F. Schuster, D. V. Bax, R. W. Farndale, S. Hamaia, S. M. Best, and R. E. Cameron. Evaluation of cell binding to collagen and gelatin: a study of the effect of 2d and 3d architecture and surface chemistry. *Journal of materials science. Materials in medicine*, 27(10):148–148, 2016.

[107] T. Magdeldin, V. López-Dávila, C. Villemant, G. Cameron, R. Drake, U. Cheema, and M. Loizidou. The efficacy of cetuximab in a tissue-engineered three-dimensional in vitro model of colorectal cancer. *Journal of tissue engineering*, 5:2041731414544183–2041731414544183, 2014.

[108] H. Yasuda, Ashok K. Sharma, and Takeshi Yasuda. Effect of orientation and mobility of polymer molecules at surfaces on contact angle and its hysteresis. *Journal of Polymer Science: Polymer Physics Edition*, 19(9):1285–1291, 1981.

[109] F. J. Holly and M. F. Refojo. Wettability of hydrogels i. poly(2-hydroxyethyl methacrylate). *Journal of Biomedical Materials Research*, 9(3):315–326, 1975.

[110] P. Eftimov, N. Yokoi, N. Peev, and G.A. Georgiev. Impact of air exposure time on the water contact angles of daily disposable silicone hydrogels. *International Journal of Molecular Sciences*, 20(1313), 2019.

[111] J. O'Brien, I. Wilson, T. Orton, and F. Pognan. Investigation of the alamar blue (resazurin) fluorescent dye for the assessment of mammalian cell cytotoxicity. *European Journal of Biochemistry*, 267(17):5421–5426, 2000.

[112] B. Page, M. Page, and C. Noel. A new fluorometric assay for cytotoxicity measurements in vitro. *International Journal of Oncology*, 3:473–476, 1993.

[113] J. Bereiter-Hahn, A. Munnich, and P. Woiteneck. Dependence of energy metabolism on the density of cells in culture. *Cell Structure and Function*, 23(2):85–93, 1998.

[114] R. De Fries and M. Mitsuhashi. Quantification of mitogen induced human lymphocyte proliferation: Comparison of alamarbluetm assay to 3h-thymidine incorporation assay. *Journal of Clinical Laboratory Analysis*, 9(2):89–95, 1995.

[115] M. Roy and S. D. Finley. Metabolic reprogramming dynamics in tumor spheroids: Insights from a multicellular, multiscale model. *PLOS Computational Biology*, 15(6):e1007053, 2019.

[116] J. Wang, W. Chen, J. Sun, C. Liu, Q. Yin, L. Zhang, Y. Xianyu, X. Shi, G. Hu, and X. Jiang. A microfluidic tubing method and its application for controlled synthesis of polymeric nanoparticles. *Lab Chip*, 14:1673–1677, 2014.

[117] P. Savagner. Leaving the neighborhood: molecular mechanisms involved during epithelial-mesenchymal transition. *BioEssays*, 23(10):912–923, 2001.

[118] M. P. Rastaldi. Epithelial-mesenchymal transition and its implications for the development of renal tubulointerstitial fibrosis. *Journal of nephrology*, 19(4):407–412, 2006.

[119] C. Lucas, N. Barnich, and H. T. T. Nguyen. Microbiota, inflammation and colorectal cancer. *International Journal of Molecular Sciences*, 18(6):1310, 2017.

[120] S. Wu, K-J. Rhee, M. Zhang, A. Franco, and C. L. Sears. *Bacteroides fragilis* toxin stimulates intestinal epithelial cell shedding and γ-secretase-dependent e-cadherin cleavage. *Journal of Cell Science*, 120(11):1944–1952, 2007.

[121] S. S. Koshy, M. H. Montrose, and C. L. Sears. Human intestinal epithelial cells swell and demonstrate actin rearrangement in response to the metalloprotease toxin of *Bacteroides fragilis*. *Infection and immunity*, 64(12):5022–5028, 1996.

[122] K-J. Rhee, S. Wu, X. Wu, D. L. Huso, B. Karim, A. A. Franco, S. Rabizadeh, J. E. Golub, L. E. Mathews, J. Shin, R. B. Sartor, D. Golenbock, A. R. Hamad,

C. M. Gan, F. Housseau, and C. L. Sears. Induction of persistent colitis by a human commensal, enterotoxigenic *Bacteroides fragilis*, in wild-type c57bl/6 mice. *Infection and Immunity*, 77(4):1708–1718, 2009.

[123] J. Swan. Aspirin's role in preventing e-cadherin cleavage by the carcinogenic *Bacteroides fragilis* toxin. *University of Otago Honours Thesis*, pages 1–59, 2018.

[124] L. Orcheston-Findlay, A. Hashemi, A. Garrill, and V. Nock. A microfluidic gradient generator to simulate the oxygen microenvironment in cancer cell culture. *Microelectronic Engineering*, 195:107–113, 2018.